Function of the Aryl hydrocarbon Receptor Repressor during polymicrobial and parasitic infections

Inaugural-Dissertation

zur Erlangung des Doktorgrades

der Mathematisch-Naturwissenschaftlichen Fakultät

der Heinrich-Heine-Universität Düsseldorf

vorgelegt von

Jessica Daniela König

aus Bonn

Düsseldorf, November 2016

aus dem Life and Medical Science Institut (LIMES),
Abteilung Immunologie und Umwelt
der Rheinischen Friedrich-Wilhelms-Universität Bonn

Gedruckt mit der Genehmigung der
Mathematisch-Naturwissenschaftlichen Fakultät der
Heinrich-Heine-Universität Düsseldorf

Referentin:	Prof. Dr. rer. nat. Irmgard Förster Abteilung Immunologie und Umwelt Rheinische Friedrich-Wilhelms-Universität Bonn
Korreferent:	Prof. Dr. rer. nat. Johannes H. Hegemann Funktionelle Genomforschung der Mikroorganismen Heinrich-Heine-Universität Düsseldorf

Tag der mündlichen Prüfung: 31. Januar 2017

Eidesstattliche Versicherung

In versichere an Eides statt, dass die Dissertation selbstständig und ohne unzulässige fremde Hilfe unter Beachtung der „Grundsätze zur Sicherung guter wissenschaftlicher Praxis an der Heinrich-Heine-Universität Düsseldorf“ erstellt worden ist.

Ich habe bisher keine erfolglosen Promotionsversuche unternommen und habe diese Dissertation in vorliegender oder ähnlicher Form in keiner anderen Institution eingereicht.

Teile dieser Arbeit (Figure 16A, Figure 17 and Figure 18B) wurden in ähnlicher Form bereits veröffentlicht:

Olga Brandstätter, Julia Vorac, Oliver Schanz, Jessica König, Tetsushi Mori, Toru Maruyama, Markus Korkowski, Thomas Haarmann-Stemmann, Dorthe von Smolinski, Joachim L. Schultze, Josef Abel, Charlotte Esser, Haruko Takeyama, Heike Weighardt and Irmgard Förster; “Balancing intestinal and systemic inflammation through cell type-specific expression of the aryl hydrocarbon receptor repressor”; *Scientific reports*, *vol. 6, p. 26091,* May 2016

Datum Jessica König

Table of contents

1. Introduction

1.1. The immune system

All organisms are faced with a constant threat by an enormous variety of pathogens. These pathogens, such as bacteria, viruses, parasites or fungi, are detected and distinguished from self-molecules by the organism's immune system. Invertebrates possess a so called innate immune response and even unicellular organisms own a simple and rudimentary immune system. In mammalian species this protection is mediated by an innate and an adaptive immune system. The latter can also be divided into a humoral and a cell-mediated immunity.

Before pathogens are recognized by the innate and subsequently the adaptive immune system, they have to overcome a set of barriers, which can be mechanical, chemical or biological. In mammalian species, these first layers of defense are made up of physical barriers, such as the epidermal layer of the skin and the mucous membranes of the respiratory, gastrointestinal and urogenital tracts. An acidic pH on skin, in stomach and in genital tracts, represents a chemical barrier, mediating protection of the mammalian organism against pathogens. Moreover, antimicrobial peptides (AMPs) are able to eliminate pathogens by targeting their membranes or interfering with the pathogen's protein synthesis [1]. Commensal bacteria, which reside in a symbiotic relationship with the mammalian host, are mainly found on the skin and in the gastrointestinal tract. They represent a biological barrier as they prevent the colonization of pathogens to protect their own living space. However, if pathogens successfully breach the first layers of defense, they encounter cells, molecules and mechanisms of the innate immune system, followed by the activation of the antigen-specific adaptive immunity.

1.1.1. Innate immune system

The innate immune system is a rather non-specific, broad line of defense against different classes of pathogens. The components of the innate immune system can act immediately after the physical, chemical and biological barriers are penetrated, as they are always in *stand-by* mode. This allows a rapid response within minutes and often leads to a successful elimination of the pathogen. The innate immune system includes humoral components, such as the complement cascade, a complex of proteolytic proteins facilitating the detection, opsonisation and lysis of pathogens, as well as a variety of immune cells, which are recruited by cytokines and chemokines to the site of infection.

The innate immune response is mediated by the quick recognition of evolutionarily conserved, structural features of the pathogens, known as pathogen-associated molecular patterns (PAMPs). Likewise it recognizes danger-associated molecular patterns (DAMPs), which can be stress signals like alarmins that are passively released by necrotic cells (reviewed in [2]). PAMPs and DAMPs are identified by special receptors known as pattern recognition receptors (PRRs) [3]. The different families of PRRs can be expressed on the cell surface or intracellularly and upon PAMP recognition a variety of signaling pathways are triggered, leading to the synthesis and release of a broad range of pro-inflammatory cytokines and chemokines [4], [5].

Toll-like receptors (TLRs) are the most extensively described PRRs and are expressed on a variety of cells, including leukocytes and non-immune cells, such as epithelial and endothelial cells (reviewed in [6]). Upon activation, TLR signaling initiates the secretion of pro-inflammatory cytokines and Type I interferons [4]. The name Toll-like receptor is derived from the *toll* gene discovered in *Drosophila melanogaster* by Christiane Nüsslein-Volhard in 1985. Since the identification of the first human TLR in 1994 [7] and the discovery of the link between the now known TLR4 and the human immune system in 1997 [8], the TLR family has been studied intensively. The different TLRs recognize a great range of PAMPs, such as TLR1, TLR2, TLR4, and TLR6, which detect lipopeptides,

lipoproteins, peptidoglycans, LPS and mannan among others, whereas TLR3, TLR7, TLR8, and TLR9 identify nucleic acids [4] and TLR5, which recognizes flagellin [5], [9].

In addition to the TLRs, there are several cytoplasmic PRR families, such as retinoic acid-inducible gene I (RIG-I)-like receptors (RLRs), which are able to sense cytoplasmic RNA [10] and nucleotide-binding oligomerization domain (NOD)-like receptors (NLRs), which are able to detect intracellular microbes and danger signals [11].

In summary, PRR signaling leads to the induction of cytokines and chemokines [12]. Furthermore, it leads to the recruitment of leukocytes to the site of infection and it even establishes a link between innate and adaptive immunity, for instance by playing a role in TLR-mediated maturation of dendritic cells (DCs) [6].

The cellular components of the innate immune system predominantly originate from the myeloid lineage (Figure 1). They consist of phagocytes, including macrophages, neutrophils and DCs as well as granulocytes, including basophils and eosinophils (Figure 1). In addition to cells of the myeloid lineage, the innate immune system comprises γδ T lymphocytes, cytotoxic natural killer (NK) cells and innate lymphoid cells (ILCs), which originate from the lymphoid lineage (Figure 1) (reviewed in [13], [14]). Important to note is that certain cells, such as DCs or γδ T cells can bridge the innate to the adaptive immune system (reviewed in [15]).

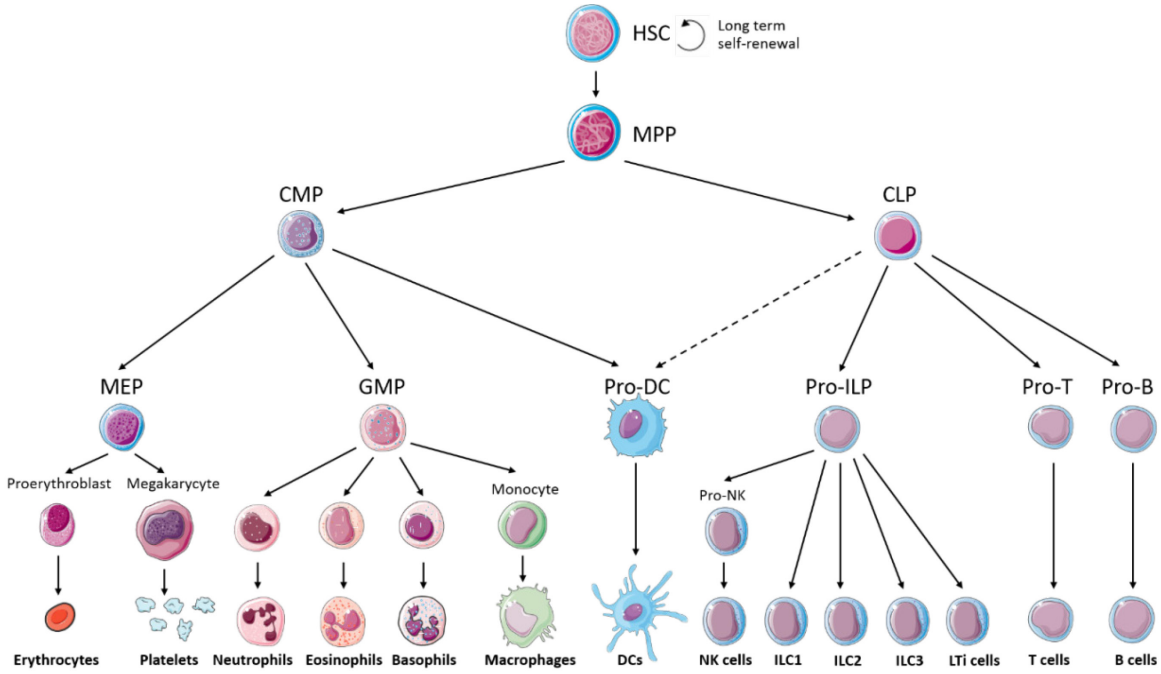

Figure 1 – Diagram of hematopoietic development. HSC, which reside in the bone marrow, give rise to several different blood and immune cell types. Numerous steps of differentiation generate erythrocyte (MEP), myeloid (GMP) and lymphoid (CLP) precursor cells, which differentiate to specialized cell populations, such as erythrocytes and platelets, granulocytes (neutrophils, eosinophils and basophils), macrophages, myeloid derived and lymphoid derived dendritic cells (DCs), innate lymphoid cells (ILC, including natural killer (NK) cells, group 1, 2 and 3 ILCs and lymphoid tissue inducer (LTi) cells), T cells and B cells. HSC: Hematopoietic stem cell, owning long term self-renewing capacities; MPP: multipotent progenitors with limited self-renewal capabilities; CMP: common myeloid progenitor; CLP: common lymphoid progenitor; MEP: megakaryocyte/erythroid progenitor; GMP: granulocyte/macrophage progenitor. Adapted from [14], [16] and Servier Medical Art

In general, phagocytes patrol the mammalian body searching for pathogens. In addition, diverse populations of organ resident macrophages are located throughout the body, such as Kupffer cells, which are found in the liver, microglia in the brain or alveolar macrophages found in the lung. Macrophages use the release of reactive oxygen species (ROS), a mechanism known as respiratory burst, to eliminate engulfed pathogens. Neutrophils are also able to induce respiratory burst in order to eliminate pathogens. Neutrophils represent a large population of leukocytes and usually serve as an early indicator for an infection, since they are one of the first responding inflammatory immune cells. Another cell type belonging to the phagocytes are DCs, which play a pivotal role in immunity and link the innate with the adaptive immune system. The adaptive immune system is activated and primed by the innate immune system through a mechanism

named antigen presentation, which is characterized by the recognition of "non-self" antigens. This mechanism is mediated by antigen presenting cells (APCs). Pathogens are phagocytosed by APCs, lysed and processed. The processed antigens are presented to T cells on major histocompability complex (MHC) molecules, leading to T cell activation.

1.1.2. Adaptive immune system

Compared to innate immunity, the adaptive immune system acts more specific and adjusts to immune responses. It uses a wide range of molecules and cells, which have the ability to recognize processed antigens of distinct pathogens, whereas the innate immune system recognizes evolutionarily conserved molecules on pathogens. Most prominent cellular members of the adaptive immune system include B and T cells, which own high affinity antigen receptors, known as B cell receptors (BCR) and T cell receptors (TCR), respectively. Both receptors can be expressed in a wide variety to ensure vast specificity. However, unlike the BCR, which can also occur in a soluble form known as antibodies, the TCR is membrane-bound. With the help of somatic recombination, B and T cells have the ability to generate a nearly endless repertoire of BCRs and TCRs, owning different specificities against pathogens, during their development.

The adaptive immunity is induced by immature DCs, which sample antigens throughout the body in search of pathogens and can be found in all peripheral tissues. Upon pathogen encounter through PRRs, the pathogen is phagocytosed and processed, leading to the maturation of the DC. The cells migrate to draining lymph nodes (LN) in order to interact with T cells by presenting their antigens. The TCR identifies the epitope bound to the MHC molecule, while a secondary signal between co-stimulatory molecules, for instance CD80/CD86 on the APC and CD28 on the T cell, leads to clonal proliferation. T cells can be divided into two subsets by their accessory molecule or co-receptor. Either they own cluster of differentiation (CD)-4 and are known as $CD4^+$ helper T cells or they express CD8 and are known as $CD8^+$ cytotoxic T cells. MHC molecules can also be divided into two classes. MHC class I (MHC-I) is found on the cell surface of all nucleated cells, while MHC class II (MHC-II) is only found on DCs, macrophages, B cells and specialized

epithelial cells. Intracellular antigens are presented on MHC-I to $CD8^+$ cytotoxic T cells, while extracellular antigens are presented on MHC-II to $CD4^+$ helper T cells. These pathways can be referred to as the classical antigen presentation pathways. In addition, there is another pathway termed cross-presentation, where exogenous antigens can be presented on MHC-I to $CD8^+$ cytotoxic T cells. This pathway is very beneficial for the immune system, as it allows protection against intracellular infectious organisms that do not infect APCs.

Upon antigen presentation and activation, cytotoxic T cells release cytotoxins, such as perforin, which can create pores in plasma membranes, followed by granulysin inducing apoptosis. Helper T cells on the other hand do not own cytotoxic activities, but are able to influence other cells, such as enhancing the microbial function of macrophages or the activity of cytotoxic T cells and upregulation of co-stimulatory molecules, which can promote B cell maturation. Naïve $CD4^+$ T cells can differentiate into different effector helper T cell populations, which secrete cytokines. Furthermore, they can differentiate to regulatory T cells (T_{reg} cells), which act immunosuppressive, as well as memory helper T cells. Effector helper T cells are subdivided into several different types, for instance Type 1 helper T cells (T_h1), T_h2 cells, T_h17 cells and T_h22 cells among others. T_h1 cells secrete IFNγ, which is especially effective against intracellular pathogens by activating macrophages. Their differentiation is triggered by IL-12 (reviewed in [17], [18]). Parasites however can be eliminated by T_h2 cells secreting IL-4, IL-5 and IL-13. IL-4 promotes T_h2 differentiation. T_h2 cells are able to interact with eosinophils, basophils, mast cells as well as B cells, in which the IgE antibody production is stimulated (reviewed in [17]–[19]). IL-17 production defines T_h17 cells, which are necessary for the elimination of extracellular pathogens especially in mucosal barriers. TGFβ and IL-6 lead to T_h17 differentiation *in vitro* [20]–[22]. They are most abundant in the lamina propria (LP) of the small intestine [22]. T_h22 cells secrete IL-22, which protects against bacterial and fungal infections at mucosal surfaces (reviewed in [23], [24]) and plays a role in the maintenance of the epithelial barrier of the small intestine (reviewed in [25]). Forkhead box protein P3 (FoxP3) expressing T_{reg} cells can be differentiated *in vitro* using only TGFβ, while the addition of IL-6 leads to suppression of FoxP3 expression and thus inhibits T_{reg} differentiation [26]. T_{reg} cells act immunosuppressive by the secretion of IL-10 and TGFβ

and are particularly important for the establishment of tolerance towards commensal bacteria in the gastrointestinal tract (reviewed in [27]).

Furthermore, helper T cells have been described to induce B cell proliferation. B cells, which induce humoral immunity, are another well-known member of the cellular adaptive immune system. After stimulation by a helper T cell, B cells clonally proliferate into antibody secreting plasma cells. Initially, B cells secrete antibodies belonging to the class M (immunoglobulin M, IgM). However, upon encounter with different helper T cell subsets, B cells undergo antibody class switching in order to be able to produce IgG, IgA or IgE. This class switch is regulated by the recognition and binding of cytokines specific to the different helper T cell subsets. T_h1 cells can induce a class switch from IgM to IgG2a and IgG3, while T_h2 cells promote the production of IgE and IgG1 and T_{reg} cells lead to a class switch to IgA and Ig2b [28]. These secreted antibodies circulate through the body in the blood, patrolling for pathogens to which they can bind, marking them for elimination by the complement cascade or phagocytes. Beyond the existing immune response during an infection, a certain number of B and T cells turn into memory cells, allowing a quick recognition and adaptive response against the re-occurrence of the same pathogen.

1.2. The gut-associated lymphoid tissue

The gastrointestinal tract represents the largest physical barrier next to the skin, separating the internal body from the surrounding environment. In addition to the obvious function of digestion and uptake of nutrients, the gastrointestinal tract and its immune system, termed gut-associate lymphoid tissue (GALT), play an important role in the detection and defense against pathogens and the establishment of tolerance towards harmless food components, along with the maintenance of the gut barrier. The GALT is part of the mucosa-associated lymphoid tissue (MALT) and consists of several types of organized lymphoid tissues, such as cryptopatches (CP), isolated lymphoid follicles (ILF), Peyer's patches (PP), and mesenteric lymph nodes (mLN), as well as more diffusely distributed lymphoid tissues, such as the lamina propria (LP) and the follicle-associated epithelium (FAE) [29], [30].

The LP is located underneath the epithelium and consists of loose connective tissue, smooth muscle fibers and fibroblasts. In addition, the LP is infiltrated with immune cells, such as lymphocytes, especially IgA-secreting B cells, plasma cells and APCs. Furthermore, small clusters of lymphoid cells, termed cryptopatches (CP), firstly described in 1996 by Kanamori *et al.* [31], are randomly distributed in the basal area of the LP [32]. They are made up of DCs mostly and lineage-negative cells expressing c-kit, named lymphoid tissue inducer (LTi) cells [31]. Besides CP, isolated lymphoid follicles (ILF) can be found in the LP. In addition, Peyers's patches (PP) are also located in the LP of the mucosa extending into the submucosa. PPs were discovered in 1977 and named after the Swiss pathologist Johann Conrad Peyer (reviewed in [30]). They can be easily identified macroscopically when analyzing the small intestine. Morphologically, PPs are organized similar to LN, containing T cells, B cells, DCs, macrophages and germinal center (GC) with proliferating B cells, accounting for their arched appearance and dome-like structure. They are surrounded by the follicle-associated epithelium (FAE), which contains specialized epithelial cells termed microfold cells (M cells). M cells received their name due to a great number of tiny folds on their cell surface, leading to an increase in surface area, which facilitates and enhances antigen uptake [33]. M cells have been described to take up antigens located in the intestinal lumen by endocytosis and enable the trans-epithelial transport to the underlying immune cells by exocytosis [34]. After antigen encounter, these immune cells, such as DCs, migrate to naïve T or B cells located in the PP in order to stimulate them by antigen presentation. ILFs are structurally and functionally comparable to PPs, and especially exhibit similarities to the B cell follicles in PPs, and have been firstly described in the murine intestine in 2002 by Hamada *et al.* [35]. Additionally, lymphatic vessels and capillaries traverse the LP, allowing trafficking of immune cells along the gastrointestinal tract and to the mLN (Figure 2). Immune cells enter the mLNs in order to initiate adaptive immune responses. Antigen-loaded APCs enter the LNs via the afferent lymphatics and present the antigens to T cells located in the paracortex. Activated T cells differentiate and proliferate, and in case of helper T cells migrate to B cells in the cortex or in case of effector T cells and plasma cells leave the LN via the efferent lymphatics or the blood stream (Figure 2). Directed migration of these effector cells is enabled by homing receptors [36].

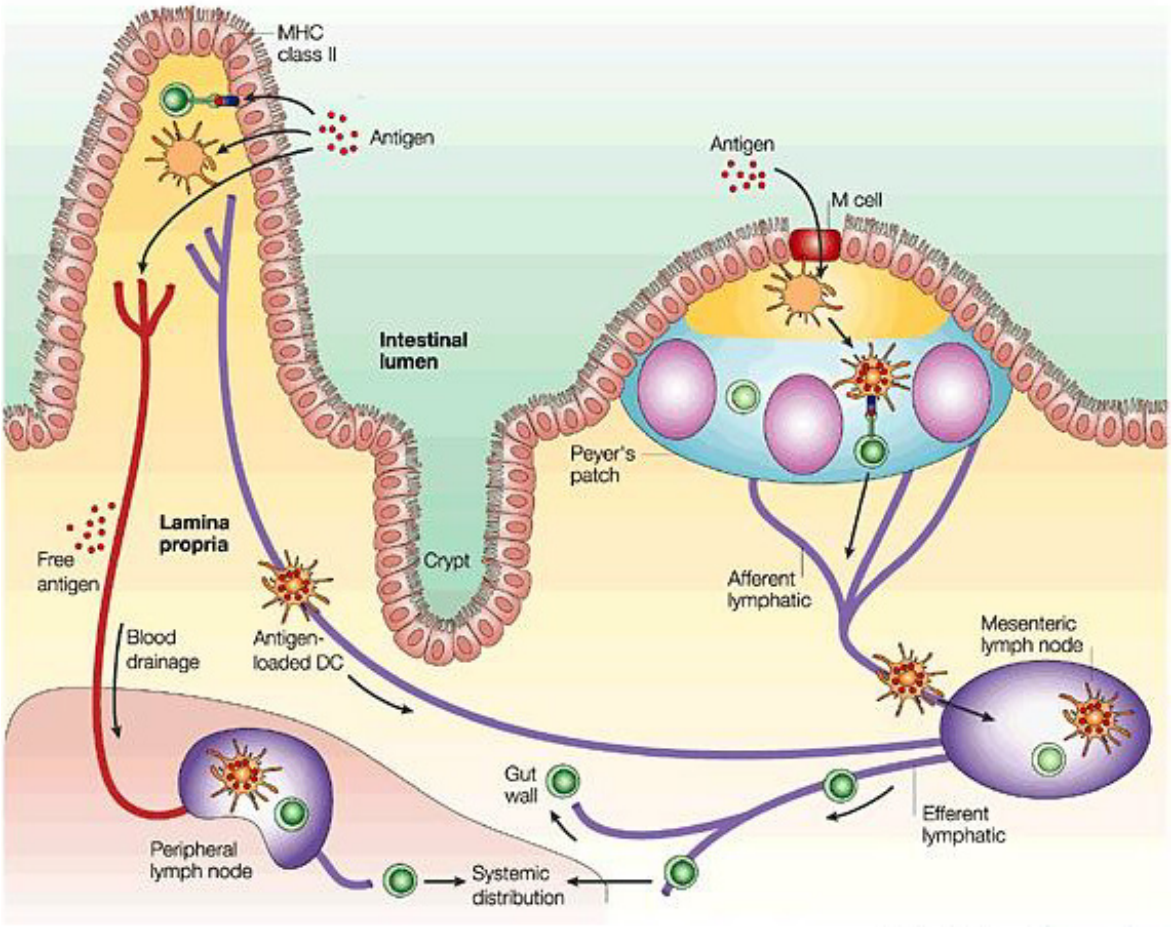

Figure 2 – Scheme of antigen uptake in gut-associated lymphoid tissue. Antigens can be taken up by microfold (M) cells, which reside in the follicle-associated epithelium (FAE). After the antigen has been transferred by exocytosis to underlying APCs (orange), located in Peyer's patches (PP), it can either be directly presented to T cells (green) or the antigen-loaded APCs migrate to the mesenteric lymph node (mLN). Alternatively, antigens can enter through the epithelium, and either be presented by MHC-II^{+} enterocyte or pass through and be taken up by an APC, which executes antigen presentation. Adapted from [37]

1.3. The Aryl hydrocarbon Receptor

The Aryl hydrocarbon Receptor (AhR) is a ligand-activated transcription factor, whose activity is controlled by binding to environmental toxins, promoting their detoxification through the induction of xenobiotic metabolizing enzymes. Originally, the AhR was investigated as a receptor that confers toxicity of 2,3,7,8-tetrachlorodibenzo-p-dioxin (TCDD) [38]. TCDD was found to be responsible for chloracne, which is known for instance

from an industrial accident in 1976 in Seveso in Italy, leading to 196 chloracne cases, as well as the assassination attempt on Viktor Yushchenko in 2004. Furthermore, TCDD has been described to lead to progressive liver failure, renal failure and myocardial degeneration among many other health problems (reviewed in [39]). TCDD and other related halogenated aromatic hydrocarbons (HAHs) have been described to exhibit a great binding affinity to the AhR [40], [41]. Well-studied examples include polychlorinated dibenzo-p-dioxins (PCDDs), generated for example during paper bleaching using chlorine, and polychlorinated biphenyl (PCB), which is used as a coolant fluid in transformers, capacitors and electric motors (reviewed in [42]). Next to HAHs, polycyclic aromatic hydrocarbons (PAHs), such as Benzo(a)pyrene and 3-methylcholanthrene (3MC), have also been described to bind and activate the AhR, however, with a lower affinity [43]. PAHs are byproducts of industrial processes, generated from the incomplete pyrolysis of organic materials and can be found in cigarette smoke, in fumes of combustion engines, and also in forest fires.

The AhR is a member of the Per-Arnt-Sim (PAS) protein superfamily of basic helix-loop-helix (bHLH) transcription factors [44], [45]. Other members of the bHLH-PAS superfamily include hypoxia inducible factors (HIFs), which regulate responses to decreases in oxygen levels in the cellular environment [44]. The PAS domain is also found in the *Drosophila melanogaster* genes *Period* (Per) [46] and *Single-minded* (Sim) [47] and the mammalian AhR nuclear translocator (ARNT, also known as HIF-1β) protein [45], [48]. The PAS domain functions as the binding site, while the bHLH motif facilitates the dimerization between two bHLH-PAS proteins (Figure 3) [39], [45], [49]. Furthermore, the AhR functional domain also contains a Q-rich domain, which is required for transactivation potential [50].

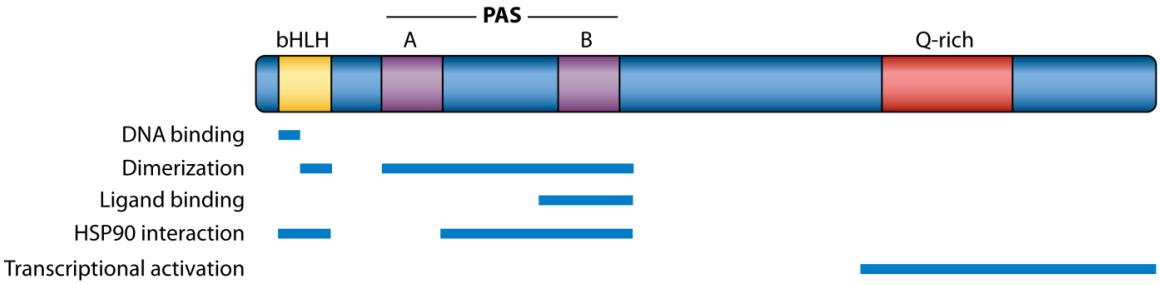

Figure 3 – Scheme of AhR functional domains. The bHLH motif is found in many transcription factors and allows DNA binding and dimerization between two bHLH-family members, such as the AhR and ARNT. The AhR contains two PAS domains, facilitating ligand binding. Both, the bHLH motif and the PAS domain are required for protein-portein interactions. The glutamine-rich (Q-rich) domain is incorporated within the transcriptional activation domain. bHLH: basic helix-loop-helix; PAS: Per-Arnt-Sim [39].

In 1994 Li *et al.* found that the AhR is constitutively expressed in several mammalian tissues, such as lung, heart, liver, thymus, brain, placenta and to a lesser extent in spleen, kidney and muscle tissue [51]. The generation of AhR knock out mutant mice in three independent working groups, namely Fernandez-Salguero *et al.* in 1995, Schmidt *et al.* in 1996 and Mimura *et al.* in 1997, revealed that the AhR plays a role in growth, differentiation, liver development and physiology besides xenobiotic metabolism [52]–[55]. AhR-deficient mice exhibit abnormalities in vascular development, reduced liver size, portal fibrosis and steatosis, lower life expectancy and impaired fertility in female mice [52], [56]–[58]. More recently, the AhR has been identified as an immune regulator and sensor of endogenous low molecular weight chemicals (reviewed in [59]).

These novel insights lead to the search for additional AhR ligands, and the finding that in addition to exogenous chemicals, the AhR also recognizes endogenous ligands, such as dietary flavones, polyphenols and tryptophan-derivatives; some of which act as antagonists [60]. Many naturally occurring ligands belong to secondary plant products, for instance flavonoids, which are polyphenolic compounds and are ingested in significant amounts by humans and animals, as they can be found in almost all plants [60]. Prominent examples are curcumin, which serves as a dietary supplement, spice or food coloring, quercetin found in many fruits and vegetables, such as apples, berries and onions, or indol-3-carbinol (I3C), which is produced by the breakdown of glucobrassicin found in cruciferous vegetables, for instance broccoli, Brussels sprouts and cauliflower.

Other reports describe heme metabolites, such as bilirubin [61], and arachidonic acid and its related structures [62] as AhR ligands. However, none of these ligands have been shown to own a binding affinity comparable to TCDD or 3MC, most of them having been tested *in vitro* in competitive binding assays (reviewed in [55]). Nevertheless, in 1987 Rannug *et al.* identified two tryptophan photoproducts, 6-formylindolo(3,2-b)carbazole (FICZ) and 6,12-diformylindolo(3,2-b)carbazole (dFICZ), as high-affinity AhR ligands equivalent to TCDD [55], [63].

The AhR is located in the cytosol in an inactive complex with chaperones, such as heat shock protein (Hsp) 90, AhR-interacting protein (AIP)-1 (also known as ARA9) and p23 [64]–[66]. AhR ligands can enter the cytosol by diffusion. Upon ligand binding the AhR undergoes conformational changes and translocates to the nucleus, where it dissociates from its chaperones and forms a complex with ARNT and thus becomes activated. This interaction allows the AhR to bind as a heterodimer with ARNT to promoters containing xenobiotic response elements (XREs, or also known as dioxin responsive elements, DREs) (Figure 4) [67]. The best studied downstream targets of AhR activation are the xenobiotic metabolizing mono-oxygenases of the cytochrome P450 family, such as CYP1A1, CYP1A2 and CYP1B1 [38], [44], [67], [68]. The AhR/ARNT dimer can also bind to genes responsible for the regulation of cell cycle and cell growth [69].

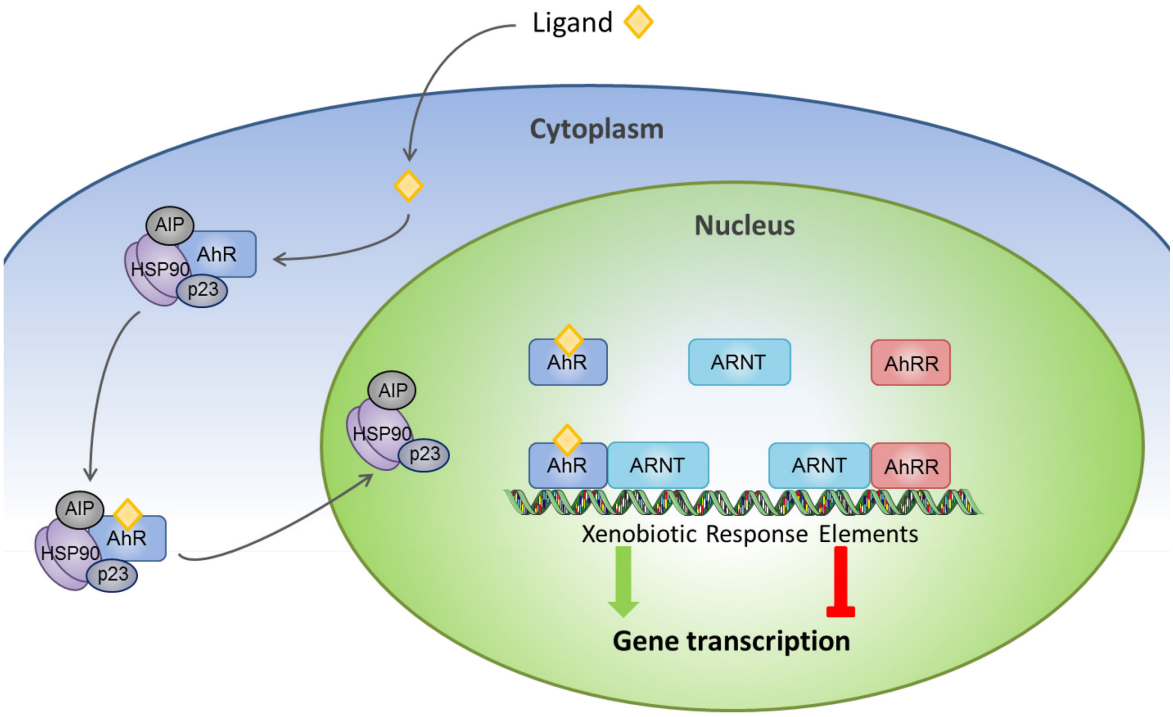

Figure 4 – Scheme of the AhR/AhRR signaling pathway. AhR ligands diffuse across the cell membrane. Ligands can bind to the AhR, which is located in a complex with AIP, Hsp90 and p23 in the cytoplasm. This leads to conformational changes and translocation into the nucleus. In the nucleus, the AhR dissociates from the stabilizing chaperones, then dimerizes with ARNT and binds to XRE sites to initiate gene transcription. The AhR is regulated in a negative feedback loop by the AhRR, which competes with the AhR for dimerization with ARNT and binding to the XRE sites. The AhRR/ARNT complex does not induce transcription. Adapted from [39]

Apart from this canonical pathway, other pathways have been shown to be involved in AhR signal transduction. In 1992 Barker *et al.* identified a link between the NF-κB pathway and the AhR based on the suppressive effects of IL-1β and TNF on TCDD-mediated induction of CYP1A1 and CYP1A2 in studies performed in primary hepatocytes [70]. This notion was reinforced by the demonstration of a direct interaction between AhR and NF-κB subunit RelA [71] and physical interactions between RelB and the AhR [72].

1.4. The Aryl hydrocarbon Receptor Repressor

The AhR also induces the expression of the AhRR, which in turn regulates the activity of the AhR in a negative feedback loop by competing with the AhR for dimerizing with ARNT and binding to XREs [73]. The AhRR/ARNT-dimer however, does not act as a transcriptional activator (Figure 4). *In vitro* experiments demonstrated that the AhRR inhibits AhR transcription [73]. Furthermore it was shown that, in contrast to the AhR, the interaction between the AhRR and ARNT is ligand-independent [73]. Also, the AhRR does not have binding capacity to chaperones and seems to be expressed and localized in the nucleus [73].

Similar to the AhR, the AhRR belongs to the bHLH-PAS superfamily and the *ahrr* gene displays a high homology with the *ahr* gene (Figure 5).

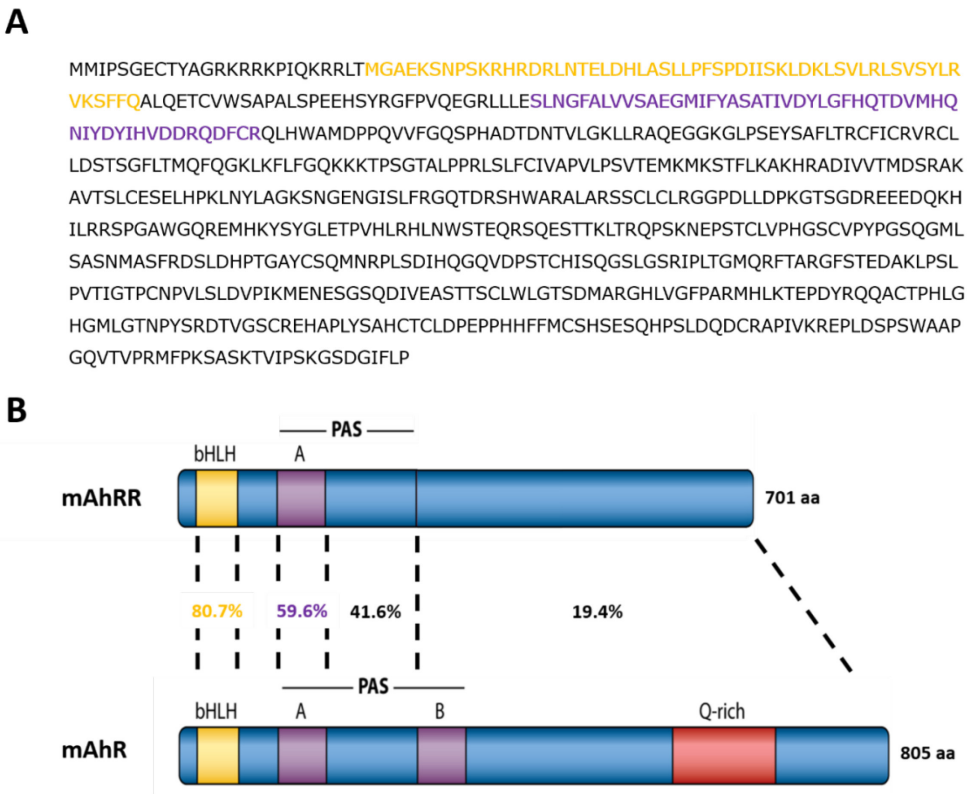

Figure 5 – Murine AhRR primary structure and scheme of functional domains. (**A**) Predicted amino acid sequence of mAhRR, in single-letter symbols. bHLH (26–82 amino acids) in yellow and PAS-A regions (116–167) in purple. (**B**) Functional domains of AhRR in comparison with AhR. Matches are indicated as percentages. Adapted from [39], [73]

Baba *et al.* were able to show that the chromosomal location of the AhRR is at chromosome 13C2 in the mouse genome, in the rat at chromosome 1p11 and in humans at chromosome 5p15.3 [74]. Moreover, by promotor analysis, they were able to show that the *ahrr* gene contains XRE sequences, as well as GC boxes and NF-κB-binding sites [74]. In 2008 Hosoya *et al.* generated AhRR knock out mice by homologous recombination. These mice did not display growth defects and were fertile [75]. Additionally, when AhRR knock out mice were challenged with 3MC intraperitoneally (i.p.), Hosoya *et al.* were able to measure elevated levels of the AhR target gene CYP1A1 in spleen, stomach and skin compared to wild-type mice. Other tissues however, such as lung and heart showed no significant increase in CYP1A1 expression [75]. Our group was able to demonstrate that the AhRR was expressed in immune cells in the skin and intestine using an AhRR-reporter mouse line, expressing the enhanced green fluorescent protein (EGFP) under the control of the AhRR promotor [76]. More specifically, in skin AhRR/EGFP expression was found in epidermal Langerhans cells (LC) and to a lesser extent in keratinocytes (KC), as well as in dermal fibroblasts [76]. AhRR/EGFP expression was also detected in intestinal $CD45^+$ cells, such as APCs and certain T cell populations, in PPs along with the LP in the small intestine and in the colon [76].

1.5. The role of the AhR and AhRR in the immune system

The AhR and AhRR are widely expressed in different organs of the body. While the AhR is ubiquitously expressed, AhRR expression can be mainly found in immune cells located at barrier sites and is often restricted to specific subsets [76].

Using microarray analysis, AhR expression was identified in myeloid cells, such as macrophages and DCs [77]. Nguyen *et al.* were able to show that LPS and CpG activate AhR expression in bone marrow-derived DCs (BMDC), and induce indoleamine 2,3-dioxygenase (IDO) expression, which catabolizes tryptophan into kynurenine (Kyn) [78]. Furthermore, it was shown that LPS treatment of peritoneal macrophages from AhR knock out mice leads to enhanced inflammatory responses, such as increased IL-6 and TNF production [79].

Another cell type influenced by AhR expression are intestinal innate lymphoid cells (ILC), more precisely ILC3 and lymphoid tissue inducer (LTi) cells, which are responsible for the differentiation of lymphatic tissue as well as the control of immune and inflammatory responses by producing IL-22 [80]. Kiss *et al.* showed that the postnatal expansion of these RORγt expressing cells and the formation of isolated lymphoid follicles (ILFs) is regulated by the AhR. Furthermore, AhR-deficient mice are more susceptible to an infection with *Citrobacter rodentium* [81]. *Citrobacter rodentium* infection is often used as a rodent infection model because of its similarity to human enterohaemorrhagic *Escherichia coli* (EHEC) infections. In the gastrointestinal tract, AhR deficiency leads to impaired numbers of ILCs and intraepithelial lymphocytes (IEL) resulting in reduced IL-22 production along with the disruption of colonic crypts and a disturbed intestinal commensal population [81], [82]. Therefore, the AhR may contribute to the maintenance of the gut barrier. In addition, these studies propose a link between AhR dietary ligands and intestinal immunity [81], [82] (reviewed in [83]). Furthermore, the influence of AhR on ILC3 in response to mucosal infection with *Toxoplasma gondii* was investigated. *Toxoplasma gondii* infection led to reduced frequencies of ILCs and AhR deficiency resulted in a higher susceptibility as revealed by increased weight loss [84].

In skin, almost all cells express the AhR, such as keratinocytes (KC), melanocytes and Langerhans cells (LC), in the epidermis and fibroblasts, DCs and T cells, such as T_h17 and γδ T cells, in the dermis [39], [85], [86]. It has been described that the AhR promotes KC differentiation, regulates the function of LCs and enhances wound healing through an interplay between fibroblasts and KC, thus controlling skin homeostasis resulting in an intact barrier [85], [87]–[89].

Kimura *et al.* discovered that the AhR in T cells inhibits Stat1 phosphorylation during culture conditions and facilitates *in vitro* T_h17 differentiation, resulting in the blockade of potential T_h1 differentiation and thus further supporting T_h17 polarization [90]. Induction of RORγt, the key transcription factor promoting naïve T cell differentiation into pro-inflammatory T_h17 cells, is enabled by the AhR, too, leading to a strengthened T_h17 polarization, but also to the production of IL-22 [91], [92]. High tryptophan levels in the culture medium, or the addition of the AhR ligand FICZ lead to an increase in T_h17 differentiation [93]. T_{reg} cells on the other hand show only a marginal AhR expression

[91], [94]. Quintana *et al.* reported that FICZ is not only able to induce T_h17 differentiation during experimental autoimmune encephalomyelitis (EAE), but also inhibits T_{reg} cell polarization, whereas AhR activation by TCDD boosted T_{reg} development leading to a suppression of EAE [94]. Another T cell subset, the type 1 regulatory T cells (T_r1) have been described to express AhR. These cells are characterized by the secretion of high levels of IL-10, interactions with c-Maf and only a transient expression of FoxP3 [95]–[97]. In contrast, AhR expression cannot be detected either in naïve T cells, or in T_h1 or T_h2 cells [91].

Compared to T cells, less is known about the regulation of the AhR in B cells. AhR expression has been detected in *ex vivo* isolated B cells and in marginal zone B cells [39]. Furthermore, B cells are also targets for TCDD, which causes a suppression of the IgM response [98], [99].

In contrast to the AhR, the influence and function of the AhRR still remains to the most part unknown. In our group AhRR-deficient mice were described to be protected against LPS-induced septic shock [76], whereas AhR-deficient mice exhibited a high susceptibility [100]. In contrast, both AhR- and AhRR-deficient mice are very sensitive to DSS-induced colitis, indicating that both molecules might be necessary to control intestinal inflammation [76], [101], [102]. In addition, AhRR deficiency leads to increased IL-1β production in the gut, supporting the importance of the AhRR for the maintenance of colonic homeostasis [76]. Furthermore, during intestinal inflammation caused by 5% DSS, AhRR-deficiency leads to diminished frequency of IFNγ producing T_h1 cells, as well as increased T_h17 differentiation [76].

1.6. Inflammatory bowel diseases

The gastrointestinal tract serves as a barrier to the surrounding environment, in which an interplay between microbial and dietary signals as well as immune cells can take place. Any disturbances in this homeostasis can have detrimental effects, such as enhanced susceptibility to infections, the development of inflammatory bowel diseases (IBD) or even the induction of cancer. IBD comprises a group of inflammatory diseases of the

gastrointestinal tract, for example Morbus Crohn or Colitis ulcerosa. Morbus Crohn can affect any part of the digestive system, whereas Colitis ulcerosa is restricted to the colon and rectum. Both Morbus Crohn and Colitis ulcerosa show high incidences in Europe. Ulcerative colitis occurs in 505 per 100000 persons and Crohn's disease has been diagnosed in 322 per 100000 persons [103]. Histopathological, ulcerative colitis exhibits neutrophil infiltration within the LP and a decrease in goblet cell numbers [104]. Crohn's disease on the other hand is characterized by an accumulation of macrophages and, even though the whole gastrointestinal tract can be affected, inflammatory pathology is more obvious in ileum and PPs [104]. Furthermore, in contrast to ulcerative colitis, Crohn's disease is characterized by a patchy inflammation, leaving parts of the intestine less damaged [104].

The establishment of IBD appears to be facilitated by a dysregulation of the intestinal epithelial barrier, in which immune cells of the GALT become activated by commensal bacteria or by the loss of T_{reg} induced tolerance (reviewed in [105]). Fuss *et al.* were able to show that the mucosa of patients with ulcerative colitis is dominated by T_h2 cells producing IL-5 and TGFβ, but not IL-4, whereas the mucosa of patients suffering from Crohn's disease has increased numbers of T_h1 cells producing IFNγ and IL-2 [106].

Causes for IBD are not entirely clear and seem to be a combination of genetic predisposition and influence from microbes and the environment. In 2001 the *nucleotide-binding oligomerization domain-containing protein (NOD) 2* (also known as CARD15 and IBD1) gene has been identified as a susceptibility gene associated with Crohn's disease [107], [108]. Several more susceptibility genes have been identified and some are even linked to autoimmune disorders [104]. Antibiotic treatment in IBD patients identified the interplay between microorganisms and the host defense system as a possible cause [104], [109]. Furthermore, increased incidence of Crohn's disease has been associated with smoking [110] and hormonal contraceptives [111]. Ulcerative colitis appears to be connected to an increased intake of unsaturated fats [112] and alcohol consumption [113]. It is important to mention that the AhR and its dietary ligands have been linked to IBD (reviewed in [114]). Additionally, as mentioned before, murine experimental models revealed that AhR deficiency leads to increased susceptibility in DSS-induced colitis [101] and *Toxoplasma gondii*-induced ileitis comparable to Crohn's disease.

1.7. Infections with *Toxoplasma gondii*

Toxoplasma gondii is an obligate intracellular parasite, discovered in 1908 by Nicolle and Manceaux in a rodent in North Africa. Besides rodents, the parasite can infect any warm-blooded animal including humans. Felines however, are the only known definitive hosts, in which the parasite can sexually reproduce. Estimations show that approximately 30% to 50% of the world population is infected with *Toxoplasma gondii* [115]. Interestingly, underdeveloped countries show higher infection rates compared to developed countries (reviewed in [116]).

The main or best described pathway of infection occurs through ingestion of infected food, such as raw or undercooked meat, or water contaminated with tissue cysts or oocytes (Figure 6) [117]. Other possibilities are infections through blood products, as well as congenital transmission, when a previously seronegative mother suffers from an acute toxoplasmosis and the tachyzoites cross from the mother's blood to the placenta and infect the unborn child (Figure 6) [118]. A primary infection during the first trimester of a pregnancy can lead to spontaneous abortion or to neurological defects of the fetus (reviewed in [116]). Most commonly, in healthy immunocompetent adults, an infection progresses inapparent, without any recognizable symptoms, apart from mild, flu-like symptoms. However, an infection with *Toxoplasma gondii* in immunocompromised adults and children can lead to toxoplasmosis, displaying seizures, poor coordination skills and even encephalitis.

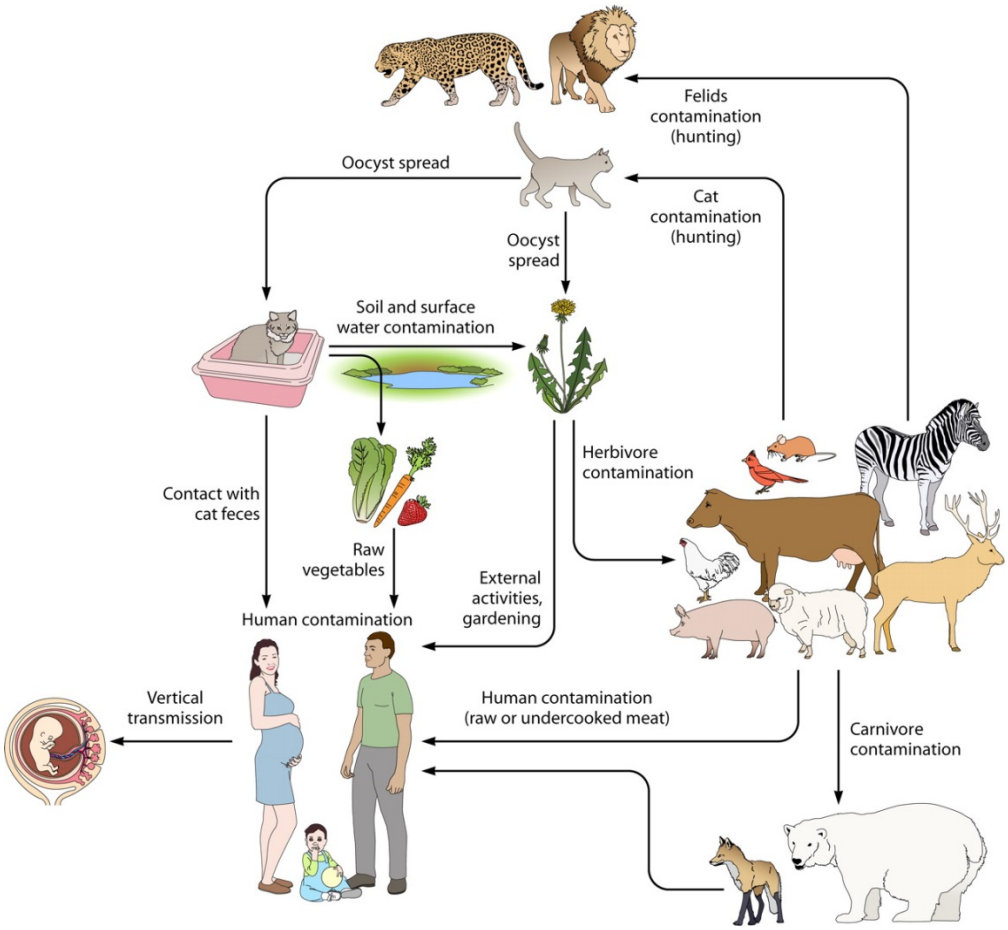

Figure 6 – Scheme of *Toxoplasma gondii* infection pathways in humans. Different sources of contaminated food and water, as well as congenital (vertical) transmission are depicted [119]**.**

Toxoplasma gondii can be infectious in three different stages of its life-cycle: sporozoites, tachyzoites and bradyzoites (Figure 7) [120]. Oocysts are a resilient form of the *Toxoplasma gondii* sexual reproduction, produced in the intestine of domestic cats or any other felidae and can be found in the feces of infected cats. Once they leave the feline intestine, they mature to infectious sporulated oocysts. After ingestion by intermediate hosts they develop to tachyzoites. Tachyzoites are the fastest replicating life stage and they are able to circulate in the blood and infect any nucleated cells. Their replication occurs during a 6- to 8-hour cycle in a protective parasitophorous vacuole, which avoids fusion with endo-lysosomes, until the tachyzoites exit the cell to infect neighboring cells [121], [122]. Tachyzoites eventually differentiate into bradyzoites, a slower replicating form. However, if bradyzoites are ingested, they also able to convert back to tachyzoites,

allowing quick replication and distribution. This is known as stage conversion. Bradyzoites also replicate in a vacuole, which matures into a cyst reaching diameters of up to 100 µm [123]. These cysts can persist for years and are located primarily in the brain and muscle tissue, but can also be located in the lung, liver or kidney [116], [120].

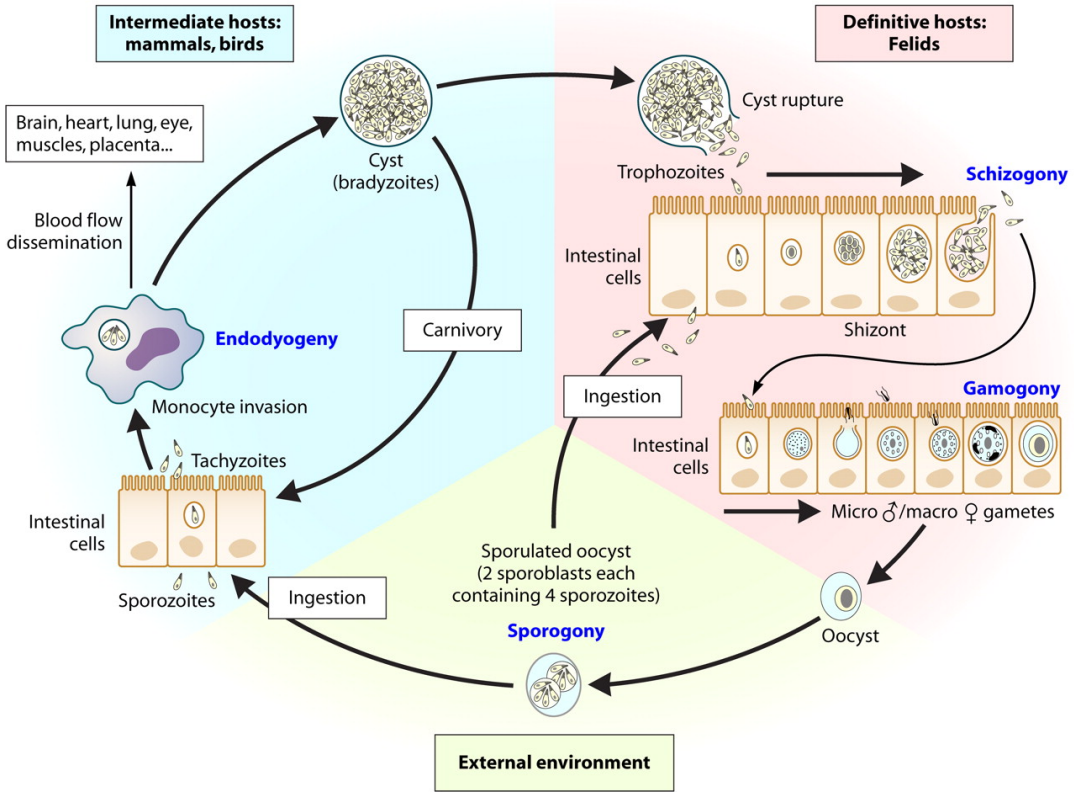

Figure 7 – Schematic of *Toxoplasma gondii* life-cycle. Depicted are the different infectious stages and replication forms depending on the host [119].

The population of *Toxoplasma gondii* found in Europe and North Amerika can be divided into three different strains, which are termed Type 1, Type 2 and Type 3. Infections of humans and animals in Europe are predominantly caused by Type 2 (such as ME49) [124], [125]. The different types are characterized by their virulence in mice. Type 1 strain parasites exhibit a very high virulence, leading to a mortality rate of 100% after an infection with less than 10 parasites [125], [126]. Parasites of the Type 2 strain have been described to show a lethal dose $(LD)_{50}$ of more than 10^3 parasites [125], [127]. Type 3 strain parasites show a LD_{50} of more than 10^5 parasites [125], [128]. An intact competent

immune system however, is able to eliminate the parasite from the body within a few weeks [116].

In experimental mouse models, the genetic background has been shown to play a role in eliminating the infection. C57BL/6 mice in comparison to Balb/c mice have been described to be more susceptible, exhibiting necrosis of the villi in the ileum caused by the spreading parasites, but also by large quantities of IFNγ indicating T_h1-type immunopathology similar to Crohn's disease [129]. Therefore, *Toxoplasma gondii* infection has been used as a model to mimic and study Crohn's disease in the murine system [129]. It has been described that both the innate and the adaptive immune system are involved in the elimination of a *Toxoplasma gondii* infection (Figure 8) (reviewed in [130]).

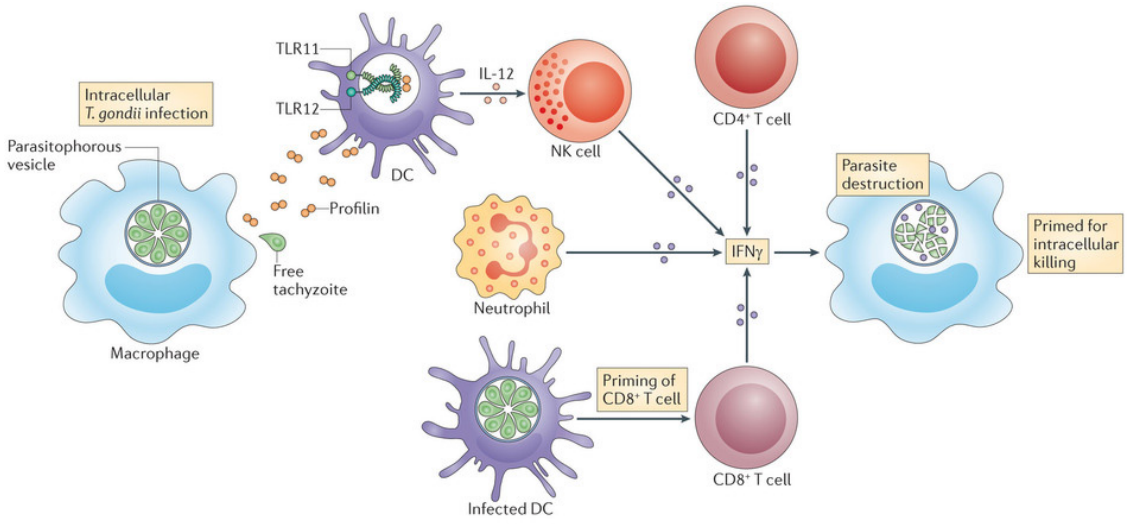

Figure 8 – Innate and adaptive immune cells involved in elimination of *Toxoplasma gondii* infection through IFNγ production. *Toxoplasma gondii* is recognized and taken up by macrophages and dendritic cells (DC). DC can induce IFNγ production in natural killer (NK) cells as well as prime $CD8^+$ T cells via cross presentation. Additionally, neutrophils and $CD4^+$ T cells produce IFNγ**,** which leads to parasite elimination in macrophages [130].

In the early phase of infection, infected cells secrete chemokines, thereby attracting innate immune cells. NK cells play an important role by secreting large amounts of IFNγ. They are triggered by DCs and neutrophils, which produce IL-12 and IL-18 leading to the activation of NK cells. Additionally, DCs activate $CD8^+$ T cells via cross presentation, as well as IFNγ producing T_h1 cells, which are essential to control the parasitic burden (Figure 8)

[116], [129]. IFNγ-activated macrophages play an important part in the disruption of parasitophorous vacuoles [131]. Fibroblasts, epithelial and endothelial cells also get stimulated by IFNγ to induce anti-parasitic activity, such as the induction of indoleamine 2,3-dioxygenase (IDO), an enzyme involved in tryptophan metabolism, leading to the depletion of tryptophan and increases in reactive oxygen species [132]. On the downside, this potent immune response can lead to inflammation and intestinal tissue damage if anti-inflammatory signals, such as IL-10 and TGFβ, are impaired.

1.8. Sepsis

Sepsis in humans is a very severe and usually life-threatening disease commonly caused by a systemic bacterial infection, which leads to dysregulation of the host's own immune response resulting in the injury of tissue and organs. Estimations of annual worldwide sepsis cases lie by 31.5 million, resulting to approximately 5.3 million deaths per year [133]. In the human system, sepsis proceeds in two phases. The systemic inflammatory response (SIRS), involving pro-inflammatory cytokines, such as TNF, IL-1, IL-6 and IL-12, is followed by the compensatory anti-inflammatory response (CARS), including the production of anti-inflammatory mediators, such as IL-4, IL-10, IL-13 and TGFβ (Figure 9A) [134], [135]. A dysbalance of these two pathways leads to irreversible tissue damage by harming endothelial, epithelial and immune cells and finally to multiple organ failure (Figure 9).

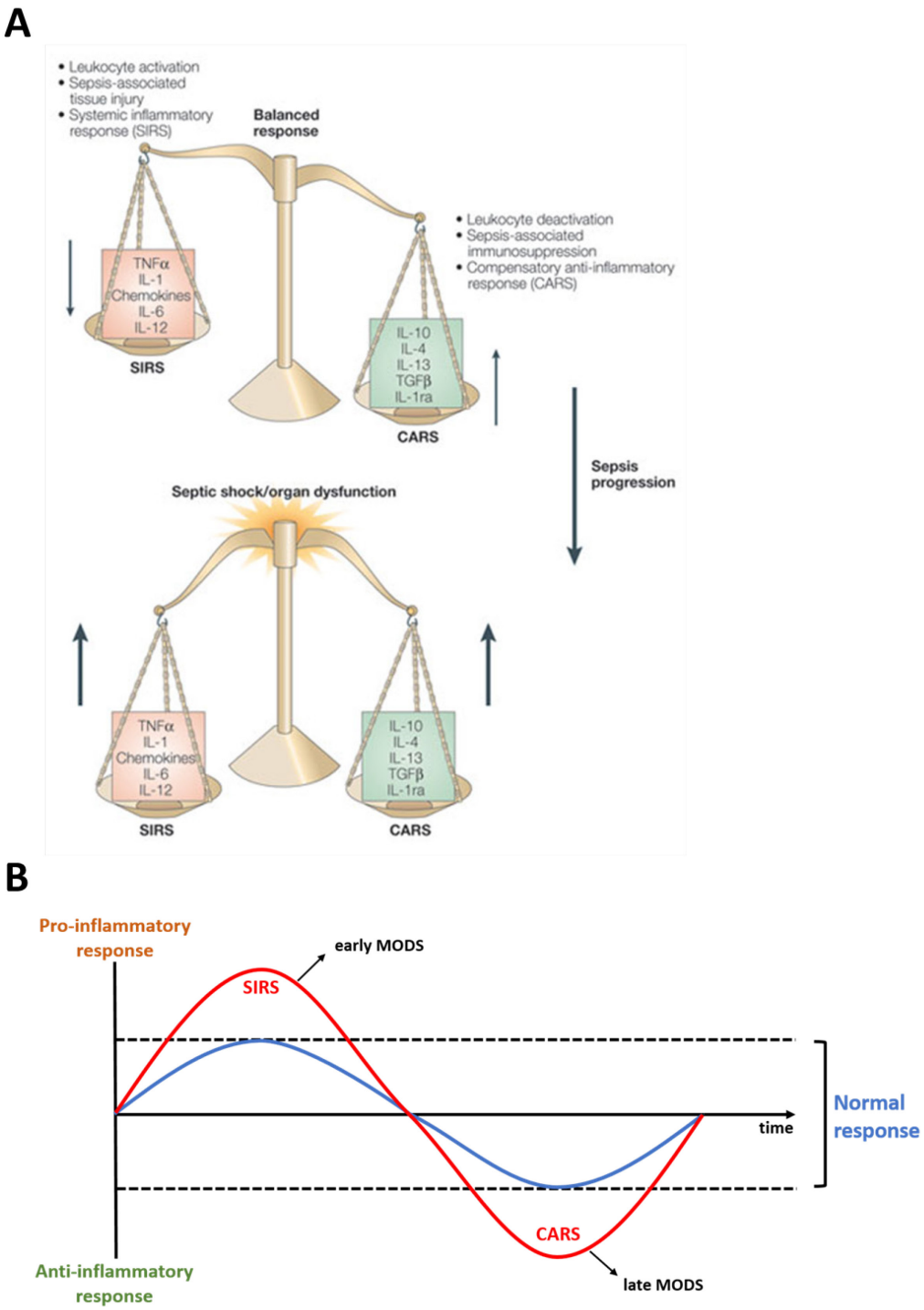

Figure 9 – Balance of systemic inflammatory response (SIRS) and compensatory anti-inflammatory response (CARS) in sepsis. (**A**) SIRS is characterized by leukocyte activation and involves cytokine production, such as tumour-necrosis factor (TNF), IL-1, IL-6 and IL-12, leading to the activation of the host's inflammatory system. This phase is followed and de-activated through the expression of CARS mediators, such as IL-4, IL-10, IL-13 and TGFβ. During sepsis, regulation of SIRS and CARS mediators is lost, leading to dysbalance and organ dysfunction [135]. (**B**) Scheme of the dynamic changes in SIRS and CARS beyond normal responses. MODS: multiple organ dysfunction syndrome. Adapted from [136], [137]

Treatment of sepsis includes intravenous fluid resuscitation and antibiotics, carried out in an intensive care unit. Furthermore, removal of the source of infection is of utmost importance, thereby clearing the septic focus. Failure of surgical clearance of the septic focus leads to increased mortality [138]. If severe damage has occurred to kidney or lungs, dialysis and mechanical ventilation will additionally be performed. However, if multiple organ failure starts progressing, treatment is very much restricted.

One of the main players in sepsis and often used in animal models to study septic shock symptoms, is lipopolysaccharide (LPS), also referred to as endotoxin. LPS is an abundant cell wall component of all gram-negative bacteria. Experimental setups in animals can include intraperitoneal injection or infusion of LPS or gram-negative bacteria, leading to a LPS-induced septic shock dependent on the dosage and genetic background (reviewed in [139]). Also, repeated challenges with endotoxin enable the investigation of possible tolerance to the second LPS stimulation [140]–[143]. The toxicity of gram-negative bacteria is thought to be attributed to lipid A, a component of LPS, which is released upon the destruction of the outer membrane of the bacteria. In 1998 Bruce Beutler described that LPS is recognized by the innate immune system via TLR4 [144]. TLR4 recognizes LPS together with its co-receptor CD14 and a secreted adaptor protein termed myeloid differentiation factor (MD-2), prompting cytokine synthesis and secretion [145], [146]. Apart from TLR3, all other TLRs, including TLR4, signal via the adaptor molecule myeloid differentiation primary response gene (MyD) 88. TLR3 signals through the TIR-domain-containing adaptor-inducing interferon-β (TRIF) molecule. For complete TLR4 signaling however, both adaptor molecules are necessary (reviewed in [147], [148]). The signaling cascade leads to the activation of the transcription factor NF-κB, which translocates into the nucleus initiating the transcription of pro-inflammatory genes, such as TNF, IL-6, IL-10, IL-12 and IFNγ (reviewed in [149]). It has been described that during an endotoxin-induced septic shock, TNF production reaches a peak already 1.5 hours after the endotoxin challenge [148], [150]. Many different cell types, such as macrophages, DCs, monocytes and B cells, can detect LPS and induced signaling leads to cytokine secretion and can cause a detrimental cytokine storm (reviewed in [148]).

Many therapeutic targets that were discovered and shown to be effective in animal studies, however, proved to be rather unsuccessful in human clinical trials [135], [151].

Consequently, animal models needed to be more multifaceted, establishing more complexity than the mere administration of a single PAMP, such as LPS. In 1998 Zantl *et al.* established an animal model used to study sepsis pathophysiology named colon ascendens stent peritonitis (CASP) model, a rodent model, which can be used to induce a polymicrobial sepsis [152]–[154]. In this model, a small stent is surgically inserted into the ascending colon of mice, creating a continuous connection between the intestinal lumen and the peritoneal cavity resulting in a septic peritonitis (Figure 10). The severity of the infection can be controlled by the diameter of the inserted stent.

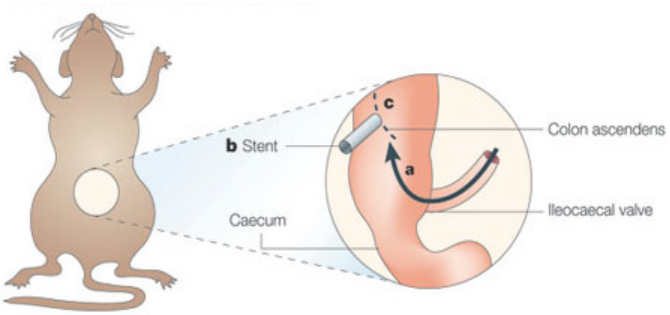

Figure 10 – Scheme of the colon ascendens stent peritonitis (CASP) model. The CASP model is an animal model used to study sepsis. A continuous connection is created by surgically inserting a small stent into the colon ascendens, allowing flow of faecal material from the colon into the peritoneal cavity leading to polymicrobial infection [135].

2. Aims of this thesis

The AhR is a well-studied ligand-activated transcription factor, which has been described to play a role in xenobiotic metabolism [38], [59], [73], as well as in immune regulation, linking it to essential regulatory functions in immunity, such as intestinal homeostasis [59], [60]. AhR activity is regulated by the AhRR in a negative feedback mechanism. Using AhRR-EGFP-reporter mice our working group showed that the AhRR is mainly expressed in immune cells of the intestine and skin. AhRR-deficient mice are protected from LPS-induced septic shock and display reduced pro-inflammatory cytokine production in comparison to wild-type mice. In contrast, AhRR-deficient mice are more susceptible in a DSS induced colitis model [76]. In this thesis, the function and influence of the AhRR in systemic and intestinal infections was addressed:

1. The influence of AhRR deficiency and the expression pattern of the AhRR was characterized in the different helper T cell subsets.
2. The role of the AhRR in intestinal infection was analyzed by performing an ileitis model caused by oral infection with the parasite *Toxoplasma gondii* resembling the pathology of Morbus Crohn. The influence of AhRR deficiency on survival in AhRR-deficient mice and wild-type littermate control mice was investigated, as well as parasite burden, cytokine production and histological evaluation.
3. Using the Colon Ascendens Stent Peritonitis (CASP) model, which leads to polymicrobial sepsis, the influence of the AhRR in systemic infection was addressed in both male and female mice to exclude gender influences. A possible role for the AhRR, as well as for the AhR, in endotoxin tolerance was also explored.
4. Additionally, to further analyze the expression of the AhRR *in vivo*, AhRR-dsRed-reporter mice were generated, in which the second exon of the *ahrr* locus was replaced by a dsRed-cassette.

3. Materials and methods

3.1. Materials

3.1.1. Technical equipment

Equipment	Manufacturer
Accu-jet® pro	Brand, Wertheim
Balance 440-35N	Kern, Balingen
BD flow cytometer FACS Aria	BD Biosciences, Heidelberg
BD flow cytometer FACS Canto II	BD Biosciences, Heidelberg
ChemiDoc™ MP Imaging system	BioRad, Munich
Centrifuge 5415 R	Eppendorf, Hamburg
Centrifuge 5810 R	Eppendorf, Hamburg
Centrifuge Allegra® X-15R	Beckman Coulter, Krefeld
Cryopreservation 800 series-190 MVE	Thermo Scientific, Braunschweig
Cryostat CM3050S	Leica, Nussloch
Electroporator Gene pulser Xcell™	BioRad, Munich
Feeding needle	AgnTho, Lidingö, Schweden
Fridges and freezers	Bosch
Gel documentation	Biostep GmbH, Jahnsdorf
Gel electrophoresis equipment	BioRad, Munich
Hemocytometer Neubauer improved	Marienfeld Superior, Lauda-Königshofen
Incubator 37°C Binder	Binder, Tuttlingen
Incubator 37°C, 1% O_2 HERA cell 150	Thermo Scientific, Braunschweig
Keyence BZ-9000 digital microscope	Keyence Deutschland GmbH, Neu-Isenburg
Magnetic stirrer C-MAG HS 4	IKA®, Staufen
Microscope Eclipse TS 100	Nikon, Düsseldorf
Microtome RM2255	Leica, Nussloch
Multichannel pipette	Abimed, Langenfeld

NanoDrop 1000	Peqlab, Erlangen
Odyssey, infrared imager	LI-COR, Bad Homburg
Oven	Tri-Star, Texas, USA
Pipettes	Starlab GmbH, Hamburg
Precellys 24 homogenizer	Peqlab, Erlangen
Precision balance	Kern, Balingen
Real-Time System CFX96	BioRad, Munich
Semi-dry blotting/transfer cell	BioRad, Munich
Spectrometer (ELx 800)	BioTek Instruments, Bad Friedrichshall
Steril bench BDK	BDK, Sonnenbühl-Gerkingen
Steril bench S@feflow 1.2	Nunc, New York, USA
T1 thermocycler	Biometra, Göttingen
Tissue processor, TP 1020	Leica, Nussloch
ThermoShaker Ts1	Biometra, Göttingen
QuadroMACS™ Separation Unit & MACS MultiStand	Miltenyi Biotec, Bergisch Gladbach
Vortex Genie 2	Scientific Industries, New York, USA

3.1.2. Laboratory materials

Item	**Manufacturer**
Biosphere® Filter Tips	Sarstedt, Nümbrecht
Cell culture plates Cellstar (6, 12, 24, 48 and 96 Well)	Greiner Bio-One, Frickhausen
Cell strainers (100 µm, 70 µm)	BD Biosciences, Heidelberg
Cover slips (24 x 60 mm)	Roth, Karlsruhe
CryoPure Tube	Sarstedt, Nümbrecht
Disposable hypodermic needles, Sterican®	Braun, Melsungen
ELISA plates, 96-well, half area	Greiner Bio-One, Frickhausen
Flow Cytometry tubes	Sarstedt, Nümbrecht
Glas beads (Ø 1,25-1,65 mm)	Roth, Karlsruhe
ImmEdge pen	Vector Lab. Inc., Burlingame, USA
Low profile microtome blades	Leica, Nussloch
Microseal® B seal	BioRad, Munich

Microscope slides superfrost plus	Thermo Scientific, Braunschweig
Nitrocellulose Blotting Membrane, Amersham™ Protran™ 0.45 µm NC	GE Healthcare, Freiburg
PCR Plates Hard-Sell®, 96-well, thin-wall	BioRad, Munich
Reaction tubes (Falcons, 15 ml, 50 ml)	Greiner Bio-One, Frickhausen
Reaction tubes (0.5 ml, 1 ml, 2 ml)	Sarstedt, Nümbrecht
Sterile applicators	Böttger, Bodenmais
Surgical suture, nylon, DSM 11	Resorba, Nürnberg
Surgical suture, nylon, DSM 13	Resorba, Nürnberg
Syringes, single-use, Injekt®	Braun, Melsungen
Tissue-Tek® Cryomolds Intermediate/Standard	Sakura, California, USA
Vein catheter, BD Venflon™ (14 gauge, 16 gauge)	BD Biosciences, Heidelberg
Whatmanpaper GB005 200 x 200 mm	GE Healthcare, Freiburg

3.1.3. Chemicals, enzymes and reagents

Description	Manufacturer
2-Propanol	Roth, Karlsruhe
Absolute qPCR Sybr Green ROX Mix	Thermo Scientific, Braunschweig
Acetone	VWR, Darmstadt
Acrylamide (30%)	Sigma-Aldrich, Munich
Agarose	PeqLab, Darmstadt
APS (Ammonium persulfate)	Roth, Karlsruhe
β-mercaptoethanol	Sigma-Aldrich, Munich
Brefeldin A Solution (1000x)	eBioscience, Frankfurt am Main
BSA (Albumin bovine fraction)	Serva, Heidelberg
DABCO (1,4-Diazabicyclo[2.2.2]octan)	Roth, Karlsruhe
DAPI (4'-6-Diamidino-2-phenylindole)	Sigma-Aldrich, Munich
Dextran Sulfate	Sigma-Aldrich, Munich
DMEM medium (BHK-21)	Invitrogen, Carlsbad, USA
DMSO (Dimethyl sulfoxide)	Merck, Darmstadt
dNTP (deoxynucleotides)	Thermo Scientific, Braunschweig
DTT (Dithiothreitol)	Promega, Fitchburg, USA

EDTA (Ethylenediaminetetraacetic acid)	Sigma-Aldrich, Munich
Entellan	Roth, Karlsruhe
Eosin Y solution (alcoholic)	Sigma-Aldrich, Munich
EtOH (Ethanol)	Roth, Karlsruhe
Euparal	Roth, Karlsruhe
FCS (Fetal Bovine Serum)	PAN Biotech, Aidenbach
Ficoll-Paque™ PLUS (density 1.077 g/ml)	GE Healthcare, Freiburg
FICZ (6-Formylindolo(3,2-b)carbazole)	Enzo Life Sciences, Lörrach
Fixable Viability Dye eFluor® 780	eBioscience, Frankfurt am Main
Formaldehyde	Merck, Darmstadt
Gelatine	Roth, Karlsruhe
Geneticin® Selective Antibiotic (G418 Sulfate), Powder	Invitrogen, Carlsbad, USA
Glycerol	Roth, Karlsruhe
Hemalum solution (Mayer's)	Merck, Darmstadt
HEPES (4-(2-hydroxyethyl)-1-piperazineethanesulfonic acid)	Roth, Karlsruhe
HCl (Hydrogen chloride)	Roth, Karlsruhe
IMDM medium Gibco™	Life Technologies, Carlsbad, USA
Ionomycin calcium salt from *Streptomyces conglobatus*	Sigma-Aldrich, Munich
Isoflurane (Forene)	Abbvie, Ludwigshafen
KCl (Potassium chloride)	Merck, Darmstadt
L-Glutamine 200 mM (100x)	Invitrogen, Carlsbad, USA
Lipopolysaccharides from *Escherichia coli* 0111:B4	Sigma-Aldrich, Munich
Lipopolysaccharides from *Escherichia coli* 055:B5	Sigma-Aldrich, Munich
Methanol	Roth, Karlsruhe
Milk powder, skim	Roth, Karlsruhe
Monensin Solution (1000x)	BioLegend, Fell
Mouse serum	Sigma-Aldrich, Munich
Mowiol	Roth, Karlsruhe
MyTaq™ HS Red DNA Polymerase (Polymerase & buffer)	Bioline, Luckenwalde
NaCl (Sodium chloride)	Roth, Karlsruhe
NaOH (Sodium hydroxide solution, 4 N)	Roth, Karlsruhe
Non-essential amino acids (100x)	Invitrogen, Carlsbad, USA
Oligo(dt)18 primer	Thermo Scientific, Braunschweig

Paraformaldehyde	Merck, Darmstadt
PBS (Phosphate buffered saline)	Merck, Darmstadt
Penicillin/Streptomycin	Invitrogen, Carlsbad, USA
PMA (Phorbol 12-myristate 13-acetate)	Sigma-Aldrich, Munich
Ponceau S	Roth, Karlsruhe
Precision Plus Protein™ Dual Color Standard	BioRad, Munich
Proteinase K, recombinant	Roche, Mannheim
Proteinase inhibitor (10x)	Roche, Mannheim
Rat serum	Sigma-Aldrich, Munich
Restriction enzyme *DraI*	New England Biolabs, Frankfurt
Retinoic acid	Sigma-Aldrich, Munich
RevertAid reverse transcriptase	Thermo Scientific, Braunschweig
RiboLock RNase Inhibitor	Thermo Scientific, Braunschweig
Ripa puffer (10x)	Cell Signaling, Frankfurt am Main
RPMI 1640 medium	PAN Biotech, Aidenbach
RT Reaction buffer (5x)	Thermo Scientific, Braunschweig
Salmon sperm DNA	Sigma-Aldrich, Munich
Saponin	Sigma-Aldrich, Munich
SDS (Sodium dodecyl sulfate)	Sigma-Aldrich, Munich
Sodium pyruvate (100 mM)	Invitrogen, Carlsbad, USA
SSC (Saline sodium citrate)	Sigma-Aldrich, Munich
Sucrose	Sigma-Aldrich, Munich
Sulfonic acid (H_2SO_4), 25%	Roth, Karlsruhe
Sybr Safe DNA gel stain	Life Technologies, Carlsbad, USA
TAE buffer (10x)	Invitrogen, Carlsbad, USA
TEMED	Roth, Karlsruhe
Tissue freezing medium®	Leica, Nussloch
TMB Plus 2 (Peroxidase substrate)	BioTrend, Köln
Tris	Roth, Karlsruhe
Tris-HCl	Roth, Karlsruhe
Tris-Ultra	Roth, Karlsruhe
Trypan blue solution	Sigma-Aldrich, Munich
Trypsin-EDTA 0.25% (1x)	Life Technologies, Carlsbad, USA
Tween®20	Roth, Karlsruhe
Vectashield Hard Set Mounting Medium with DAPI	Biozol, Eching

Xylol	Roth, Karlsruhe

3.1.4. Solution, media and buffers

Description	Dissolved in	Composition
ACT buffer	Aqua dest.	0.16 M NH4Cl Tris base pH 7.65 Stored at RT
Antibody diluent (WB)	TBST	2,5% skim milk powder Stored at 4°C
Blocking buffer (WB)	TBST	5% skim milk powder
Blocking buffer (Histology)	PBS	1% FCS 1% mouse serum 1% rat serum Stored at -20°C
Blotting buffer (WB)	Aqua dest.	25 mM Tris, pH 8-10 192 mM Glycerol 20% Methanol Stored at RT
Complete IMDM medium	IMDM medium	10% FCS 1% L-glutamine 1% Penicillin (10000 U/ml)/Streptomycin (10000 U/ml) β-mercaptoethanol Stored at 4°C
Complete RPMI 1640 medium	RPMI medium	10% FCS 1% L-glutamine 1% Penicillin (10000 U/ml)/Streptomycin (10000 U/ml) β-mercaptoethanol Stored at 4°C
Complete ES cells medium	DMEM medium	20% FCS 10% LIF 1% L-glutamine 1% Sodium pyruvate 1% Non-essential amino acids 1% Penicillin (10000 U/ml)/Streptomycin (10000 U/ml) β-mercaptoethanol Stored at 4°C
GM-CSF	RPMI medium	Supernatant of transfected X63Ag8-653-cells [155] Stored at -20°C

ELISA washing buffer	PBS	0,5% Tween®20 Stored at RT
Formaldehyd	PBS	2% Formaldehyd Stored at RT
Hybridization buffer	PBS	1 M NaCl 10% Dextran Sulfate 50 mM Tris-HCL, pH 7,5 1x SDS Stored at 4°C 200 µg/ml salmon sperm DNA was added prior using the buffer 10 min on 90°C, followed by 10 min on ice
Laemmli buffer (WB)		40% Glycerol 1 M Tris, pH 6.8 4% SDS 0.5% Bromophenol blue 20% β-mercaptoethanol Stored at 4°C
Lysis buffer	Aqua dest.	10 mM Tris-HCL, pH 8.5 5 mM EDTA, pH 8.0 0,2% SDS 200 mM NaCl Stored at RT 0.1 mg/ml Proteinase K was added prior using the buffer
M-CSF	RPMI medium	Supernatant of L929 fibroblasts Stored at -20°C
Mowiol solution		2.4 g Mowiol 6 g Glycerol 6 ml Aqua dest. ON stirring 12 ml 0.2 Tris, pH 8.5 10 min stirring at 50°C Centrifugation 15 min at 5000 x g 2.5% DABCO to supernatant Stored at -20°C
Paraformaldehyde	PBS	4% PFA Stored at RT
PBS	Aqua dest.	13.7 mM NaCl 2.7 mM KCl 80.9 mM Na_2HPO_4 1.5 mM KH_2PO_4, pH 7.4 Stored at RT
Permeabilisation buffer	PBS	0.5% Saponin 0.5% BSA
Ponceau S	Aqua dest.	0.1% Ponceau S 5% Acetic acid

Running buffer (WB)	Aqua dest.	25 mM Tris, pH 8.3-8.8 192 mM Glycerol 0.1% SDS Stored at RT
Separating gel (WB)	Aqua dest.	1.5 mM Tris, pH 8.8 Acrylamid (30%) SDS (10%) APS (10%) TEMED
Stacking gel (WB)	Aqua dest.	1.5 mM Tris, pH 6.8 Acrylamid (30%) SDS (10%) APS (10%) TEMED
TBST (WB)	Aqua dest.	7.7 mM Tris-HCl, pH 7.5 150 mM NaCl 0.05% Tween 20 Stored at RT
TE buffer (genotyping)	Aqua dest.	10 mM Tris-HCl, pH 8.0 1 mM EDTA Stored at RT
Toluidine blue stock	70% EtOH	1% Toluidine blue Stored at RT
Toluidine blue working solution		1 part Toluidine blue stock 9 parts 1% Sodium chloride solution, pH 2.3 Stored at RT
Trypan blue working solution	PBS	0.25% Trypan blue Stored at RT

3.1.5. Commercial kits

Description	Company/Manufacturer
$CD4^+$ $CD62L^+$ T cell Isolation Kit II, mouse	Miltenyi Biotec, Bergisch Gladbach
CD8a (Ly-2) MicroBeads, mouse	Miltenyi Biotec, Bergisch Gladbach
DNA ladder, 100 bp, 1 kb	New England Biolabs, Frankfurt
ELISA DuoSet development kits (IL-1β, IL-4, IL-10, IL-12 p70, IL-22, IL-23, IFNγ, TGFβ, TNF)	R&D Systems, Wiesbaden
ELISA MAX™ Standard Mouse IL-17A	BioLegend, Fell

Foxp3 / Transcription Factor Fixation/Permeabilization Concentrate and Diluent	eBioscience, Frankfurt am Main
Ladderman™ Labelling Kit	TaKaRa Bio Inc., Japan
MagniSort™ Mouse CD4 T cell Enrichment Kit	eBioscience, Frankfurt am Main
MyTaq™ HS Red DNA Polymerase	Bioline, Luckenwalde
Pan T Cell Isolation Kit II, mouse	Miltenyi Biotec, Bergisch Gladbach
RNeasy fibrous tissue mini kit	Qiagen, Hilden
Qiagen® Plasmid Midi Kit	Qiagen, Hilden

3.1.6. Cytokines

Description	Source	Company/Manufacturer
Recombinant Murine IL-2	*E. coli*	PeproTech, Hamburg
Recombinant Murine IL-4	*E. coli*	PeproTech, Hamburg
Recombinant Murine IL-6	*E. coli*	PeproTech, Hamburg
Recombinant Murine IL-12 (p70)	CHO cells	PeproTech, Hamburg
Recombinant Human IL-23	(BTI-Tn-5B1-4) Hi-5 Insect cells	PeproTech, Hamburg
Recombinant Human IL-27	HEK293 cells	PeproTech, Hamburg
Recombinant Murine TNF	*E. coli*	PeproTech, Hamburg
Recombinant Human TGF-β1	HEK293 cells	PeproTech, Hamburg

3.1.7. Antibodies

3.1.7.1. Flow cytometry antibodies

Antibody	Conjugate	Clone	Dilution/ Concentration	Company/Manufacturer
CD3ε	FITC	145-2C11	1:200	BioLegend, Fell
CD3ε	LEAF™ Purified	145-2C11	3 µg/ml	BioLegend, Fell

CD4	APC-Cy7; PE-Cy7	RM4-5	1:200	BioLegend, Fell
CD8a	PerCP	53-6.7	1:200	BioLegend, Fell
CD11c	APC-Cy7	N418	1:200	BioLegend, Fell
CD11b	PerCP; APC	M1/70	1:200	BioLegend, Fell
CD25	PE-Cy7; APC	PC61	1:200	BioLegend, Fell
CD28	LEAF™ Purified	37.51	1 µg/ml	BioLegend, Fell
CD44	PE	IM7	1:200	BioLegend, Fell
CD62L	APC	MEL-14	1:200	BioLegend, Fell
FoxP3	PE	FJK-16s	1:100	eBioscience, Frankfurt am Main
GFP, rabbit IgG Fraction	Purified	Polyclonal	1:1000	Life Technologies, Carlsbad, USA
Goat anti-rabbit IgG (H+L)	Alexa Fluor® 488	Polyclonal	1:500	Life Technologies, Carlsbad, USA
IFNγ	PE	XMG1.2	1:100	BD Pharmingen, Heidelberg
IFNγ	LEAF™ Purified	R4-6A2	10 µg/ml	BioLegend, Fell
IL-4	PE	11B11	1:100	BioLegend, Fell
IL-4	LEAF™ Purified	11B11	10 µg/ml	BioLegend, Fell
IL-10	PE	JES5-16E3	1:100	BioLegend, Fell
IL-17A	PE	eBio17B7	1:100	eBioscience, Frankfurt am Main
IL-22	PE	1H8PWSR	1:100	eBioscience, Frankfurt am Main
MHCII	APC; PE-Cy7	M5/114.15.2	1:2000	BioLegend, Fell
RFP, rabbit IgG	Purified	Polyclonal	1:1000	Rockland, Pennsylvania, USA
TruStain fcX™ (CD16/32)	Purified	93	1:100	BioLegend, Fell

3.1.7.2. Western Blot antibodies

Antibody	Conjugate	Clone	Dilution	Company/Manufacturer
RFP, rabbit IgG	Purified	Polyclonal	1:1000	Rockland, Pennsylvania, USA
GAPDH, mouse IgG	Purified	Monoclonal	1:5000	Acris Antibodies, Herford
IRDye® 680RD Donkey anti-Mouse IgG (H+L)	IRDye 680RD	Polyclonal	1:10000	LI-COR, Bad Homburg vor der Höhe
IRDye® 800CW Goat anti-Rabbit IgG (H+L)	IRDye 800CW	Polyclonal	1:10000	LI-COR, Bad Homburg vor der Höhe

3.1.7.3. Antibodies for immunohistology

Antibody	Conjugate	Clone	Dilution	Company/Manufacturer
Toxoplasma gondii, rabbit (antiserum)			1:300	Dr. Ingrid Reiter-Owona, Bonn [156], [157]
Goat anti-rabbit IgG (H+L)	Alexa Fluor® 594	Polyclonal	1:500	Life Technologies, Carlsbad, USA
RFP, rabbit IgG	Purified	Polyclonal	1:500	Rockland, Pennsylvania, USA
Goat anti-rabbit IgG (H+L)	Alexa Fluor® 488	Polyclonal	1:500	Life Technologies, Carlsbad, USA

3.1.8. Primer

3.1.8.1. qRT-PCR primer

Description	Forward primer	Reverse primer
Toxoplasma gondii ME49 B1 gene	CGC TGC AGG GAG GAA AGT TG	CGC TGC AGA CAC AGT GCA TCT GGA TT
GAPDH	CAT ATT TCT CGT GGT TCA CAC C	GAG CCA AAC GGG TCA TCA
RPS6	ATT CCT GGA CTG ACA GAC AC	GTT CTT CTT AGT GCG TTG CT

3.1.8.2. PCR primer for genotyping

Description	Forward primer	Reverse primer
AhR-WT	GGA TTT GAC TTA ATT CCT TCA GCG G	TCT TGG GCT CGA TCT TGT GTC AGG AAC AGG
AhR-Neo	ACT TAG TCT GCG TGA GAA GAC	TCG TCC TGC AGT TCA TTC AG
AhRR-EGFP-WT	CAT AGT GGA AGT CCA GCA CAT AGA	TCC TTG AAG TCG ATG CCC TT
AhRR-EGFP	CAT AGT GGA AGT CCA GCA CAT AGA	TCC TTC TCT TCC TAC CGG CG
AhRR-dsRed-WT	ATG GGC CTG TGG GTG CAA GA	GAT CTC CAG CAA CTC CAG CC
AhRR-dsRed	ATG GGC CTG TGG GTG CAA GA	CGC CCT CGA TCT CGA AGT AG

3.1.9. Parasites

Parasite	Strain	Source of supply
Toxoplasma gondii, type II	ME 49	Prof. Dr. Klaus Pfeffer, Düsseldorf

3.1.10. Computer Software

Software	Producer/distributor
Argus X1	Biostep GmbH, Jahnsdorf
BD FACSDiva™ version 6.0	BD Biosciences, Heidelberg
BZ-II Analyser	Keyence Deutschland GmbH, Neu-Isenburg
BZ-II Viewer	Keyence Deutschland GmbH, Neu-Isenburg
Citavi 5.2	Citavi Swiss Academic Software GmbH, Wädenswil, Switzerland
FlowJo version 10	FlowJo LLC Data Analysis Software, Ashland, USA
Gen5	BioTek Instruments, Bad Friedrichshall
Graphpad Prism version 6.04	GraphPad Software, California, USA
ImageJ	ImageJ, U.S. National Institutes of Health, Bethesda, USA
Microsoft Office	Microsoft, Redmond, USA
NanoDrop 1000 V3.8.1	Thermo Fischer Scientific, Wilmington, USA

3.2. Methods

3.2.1. Laboratory mice and housing conditions

AhRR-EGFP-reporter mice (AhRR-reporter mice ($AhRR^{E/+}$), AhRR-deficient mice ($AhRR^{E/E}$) and wild-type littermate control mice ($AhRR^{+/+}$)) were previously described [76]. They express Enhanced Green Fluorescent Protein (EGFP) under the control of the *ahrr* promoter. The mice were backcrossed for nine generations to C57BL/6J wild-type background. Female CD1 outbred mice were purchased from *Charles River Laboratories, Research Models and Services, Germany GmbH,* Schweinfurt. Furthermore, C57BL/6J wild-type mice and AhR knock out mice (AhR-deficient mice ($AhR^{-/-}$) [158] and wild-type littermate control mice ($AhR^{+/+}$)) were bred at the *Genome Resource Centre (GRC)* of the *Life and Medical Sciences (LIMES) institute*, Bonn. All mice were bred under specific pathogen free (SPF) conditions in individually ventilated cages (IVC) (Tecniplast Deutschland GmbH, Hohenpeißenberg). Food (*LASQCdiet® Rod16* from *LASvendi*, Soest) and water were available *ad libitum*. The mice were 6 to 18 weeks of age. For initial *Toxoplasma gondii* infection studies, mice (AhRR-deficient mice and wild-type littermate control mice) were bred at the animal facility of the *Leibniz Research Institute for Environmental Medicine (IUF)*, Düsseldorf and transferred to the S2 area in the animal facility of the *Heinrich-Heine University of Düsseldorf*. All experiments were performed in accordance with institutional, state, and federal guidelines and with the permission of the state government of North-Rhine-Westphalia, Germany.

3.2.2. Genotyping of laboratory mice

All genetically modified mice received an individual earmark between the age of 4 to 6 weeks. The genotype of each mouse was determined by PCR. Tail biopsies were taken and lysed at 56°C in *Lysis buffer* supplemented with *proteinase K*. Thereafter, the samples

were centrifuged for 10 min at 13000 rpm, the supernatant was decanted into a reaction tube and the DNA was precipitated by adding the same volume 100% 2-propanol. The sample was inverted several times before centrifugation at 13000 rpm for 10 min. The supernatant was discarded, the DNA pellet was washed by adding 70% EtOH, centrifuged at 13000 rpm for 5 min, dissolved in 200 µl *TE buffer* for 30 min at 50°C and stored at 4°C.

The isolated tail biopsy DNA was then analyzed with the corresponding PCR using the same sample reaction setup (Table 1) with a specific set of primers and PCR protocol (Table 2). The PCR products were loaded on a 1% TAE-agarose gel supplemented with *Sybr Safe DNA gel stain* to determine the band size using a *100 bp DNA ladder*.

Table 1 - General PCR reaction setup.

Reagent	1 PCR reaction
A. dest	13.0 µl
MyTaq™ HS Red Reaction buffer	4 µl
Primer fwd	0.7 µl
Primer rev	0.7 µl
MyTaq™ HS Red DNA Polymerase	0.05 µl
Genomic DNA	1.5 µl
Total	20 µl

Table 2 – Expected band sizes and PCR-cycle protocol.

Mouse line	Gene/ allele	Band size	Denaturing	Melting	Annealing	Elongation	End
AhR	AhR-WT	800 bp	94°C	94°C	61°C	72°C	72°C
	AhR-Neo	900 bp	3 min	30 sec	1 min	1 min	1 min
AhRR	AhRR-WT	450 bp	94°C	94°C	55°C	72°C	72°C
	AhRR-EGFP	800 bp	3 min	1 min	1 min	1.5 min	5 min

3.2.3. Serum preparation

Blood was collected in a reaction tube using the submandibular bleeding method [159] and coagulated erythrocytes were separated from the serum by a two-fold centrifugation at 13000 rpm for 15 min. The serum was transferred into a reaction tube and stored at -20°C until analysis by ELISA.

3.2.4. Determination of cell numbers using Trypan blue vital stain

The cell numbers of BMDCs, BMMϕs or splenic T cells were determined using a hemocytometer. Prior to cell counting, the cell suspension was diluted 1:10 with Trypan blue, which is a vital stain that selectively colours dead cells blue. Live cells, which own an intact cell membrane, cannot take up the stain and therefore remain uncoloured. Approximately 10 µl of the solution were loaded on the hemocytometer and analyzed under the microscope. The cell numbers in all 4 large squares were counted, the average was determined and the cell number per ml was calculated by multiplying by the dilution factor and chamber factor (10^4).

3.2.5. Enzyme-linked Immunosorbent Assay

The Enzyme-Linked Immunosorbent Assay (ELISA) is an antibody-based method to detect and quantify proteins. To determine the concentration of cytokines in serum samples or in supernatants of cell or organ cultures, a sandwich-ELISA in half-area 96-well plates was performed. This was achieved by coating the ELISA plates with a *capture* antibody against the relevant cytokine according to manufacturer´s guidelines O/N either at RT or at 4°C depending on the manufacturer. On the following day, the plate was washed three times with ELISA *washing buffer*. In the next step unspecific binding sites were blocked for 1 h

at RT using the manufacturer´s recommended blocking buffer. After a three-fold washing step, serum samples or supernatants as well as an eight point standard curve using a two-fold serial dilution of recombinant cytokine in a specific diluent were added to the plate. The standard and if possible the samples were assayed in duplicates. Additionally, at least two wells were filled only with diluent to serve as blanks. The plate was incubated for 2 h at RT. Subsequently the plate was washed three times and a biotinylated *detection* antibody against the same cytokine was added and incubated for 2 h at RT. After another three-fold washing step, streptavidin-conjugated-HRP was added and incubated for 20 min at RT in the dark. Finally after washing the plate three times, the substrate solution *TMB Plus 2* was added yielding a blue colour, indicating the turnover of the substrate by HRP. As soon as the different standard dilutions were distinguishable, the reaction was stopped by the addition of 2N H_2SO_4, leading to a colour change to yellow. Using a spectrophotometer, the optical density was measured at 450/570 nm and with the help of the standard curve and normalization against the blanks, the concentration of the cytokine were calculated using the *Gen5* program.

3.2.6. Western blot analysis

3.2.6.1. Protein sample preparation

BMDC were lysed in *RIPA buffer* supplemented with *protease inhibitors* for 15 min on ice followed by centrifugation at 13000 rpm for 15 min at 4°C. The protein concentration in the supernatant was then measured using a *NanoDrop.* The sample volumes were adjusted to match the concentrations, then supplemented with 5x *Laemmli buffer*, denatured for 5 min at 95°C and then either loaded directly on a SDS-gel or stored at -20°C.

3.2.6.2. Sodium Dodecyl Sulfate Polyacrylamide Gel Electrophoresis and semi-dry Western blot

To separate proteins of different sizes efficiently, acrylamide can be used in various concentrations, which results in altered pore sizes. The concentration of the separating gel used was 15%. Electrophoresis was performed at 120 V for approximately 1 h. Then the gel was transferred to a *nitrocellulose* membrane and blotted for 90 min at 100 mA by semi-dry blotting method. The membrane was then blocked for 1 h in *blocking buffer*, followed by an O/N incubation at 4°C with the primary antibody diluted in *antibody diluent*. On the following day, the membrane was washed 3 times for 10 min in TBST. Next, the secondary antibody diluted in *antibody diluent* was added and incubated O/N at 4°C. Finally, the membrane was washed again 3 times for 10 min in TBST and then analyzed using the *Odyssey infrared imager*.

3.2.7. Southern blot

This method is used for the detection of specific DNA sequences by probe hybridization after DNA fragments have been separated by electrophoresis and transferred to a *nitrocellulose* membrane. Genomic DNA from ES cells transfected with AhRR-dsRed-vector was isolated using *Lysis buffer* supplemented with *Proteinase K* O/N at 56°C. The DNA was centrifuged, resuspended in 100% EtOH/NaCl and incubated for 30 min shaking at RT. Next, the pellet was washed three times with 70% EtOH, dried and cut into fragments using the restriction endonuclease *DraI* O/N at 37°C. The DNA fragments were separated by electrophoresis on an 0.8% TAE-agarose gel at 35 V O/N. The agarose gel was then alkalized for 15 min in 0.25 N HCl solution, followed by a two-fold incubation for 15 min in 0.4 N NaOH solution. In order to transfer the DNA fragments from the gel to the *nitrocellulose* membrane, the gel was placed on the membrane on top of a large stack of paper towels and covered with *whatmanpaper* soaked in 0.4 N NaOH solution. Pressure was applied by placing a weight on top of the *whatmanpaper*. The *whatmanpaper* was

placed in two containers containing 0.4 N NaOH solution on either side in order to create capillary forces to move the DNA from the gel onto the membrane. The transfer was performed O/N. The membrane was then incubated for 15 min in 0.5 M Tris-Ultra/0.6 M NaCl solution. Next, the membrane was backed at 80°C for 2 h and washed in 2x SSC. Before probe hybridization, the membrane was incubated in *hybridization buffer* for 2 h at 60°C in a rotator. Meanwhile the probe was radioactively labelled with 50 µCi ^{32}p-dCTP using the *Ladderman™ Labelling Kit* from *TaKaRa*. Using *MicroSpin Columns S 200 HR* excess nucleotides were removed. The hybridization probe was denatured at 95°C for 5 min and cooled on ice for 10 min and then added to the *hybridization buffer*. The membrane was incubated in the *hybridization buffer* supplemented with the probe at 60°C on a rotator O/N. The following day, the membrane was washed three times with 2x SSC at 50°C for 10 min. The pattern of hybridization was visualized and analyzed on X-ray film by autoradiography.

3.2.8. Histology

3.2.8.1. Frozen sections

In order to histologically analyze different tissues, the samples, such as skin, ear or intestine were fixed in 4% PFA for at least 4 h at RT or O/N at 4°C in order to preserve cell structures and avoid loss of EGFP. The organs were dehydrated in a sucrose gradient (5%, 10% and 20% sucrose in PBS) for 1 h at RT respectively. The tissue samples were then embedded in cryomolds using tissue freezing medium on dry ice and stored at -80°C. With the help of a *Leica* cryostat the tissue samples were cut into 7 µm sections at approximately -19°C working temperature. Typically, three sections were then transferred onto microscope slides and dried. Subsequently, the sections were fixed in ice cold acetone for 10 min, dried shortly and stored at -80°C.

3.2.8.2. Paraffin sections

Paraffin sections were generated to achieve a more preserved intestinal tissue structure. The samples were fixed in 4% PFA for at least 4 hours at RT or O/N at 4°C. Thereafter, the samples were placed in embedding cassettes and transferred into the *tissue processor*, where they were dehydrated by undergoing two incubation steps in 70% EtOH, two steps in 80% EtOH, twice in 95% EtOH, two incubation steps in 100% EtOH, three steps in xylol and lastly paraffin wax for 30 min. Subsequently, the tissue samples were cut into appropriate length and embedded into paraffin blocks, left to harden and stored at RT. Using a *Leica* microtome the tissue samples were cut into 5 µm sections and transferred in a water bath (45°C). The sections were placed on a glass slide, dried and stored at RT.

3.2.8.3. Immunohistology

Frozen sections were stained with different immunofluorescent antibodies, which allow the detection of specific antigens. Single sections on a glass slide were surrounded with a hydrophobic pen (*ImmEgde* pen) to create a barrier around each section. Subsequently, the slides were rehydrated in PBS for 5 min. The slides were placed in a darkened humidified chamber for all following steps. To prevent unspecific antibody binding, the sections were treated with *blocking buffer* for 1 h at RT. Thereafter, they were washed 3 times in PBS for 5 min. The primary antibody was diluted in *blocking solution* and added to the sections on the slides. The slides were incubated for 2 h at RT or O/N at 4°C and then washed three times in PBS for 5 min. The appropriate secondary antibody was diluted in PBS and added to the sections on the slides. The slides were incubated for additional 2 h at RT or O/N at 4°C. Finally, the sections were counterstained with 0.2 µg/ml *DAPI* diluted in PBS for nucleus staining, incubated for 5 min at RT, washed three times for 5 min in PBS, dried and mounted with *Mowiol*. Alternatively, the sections were covered with a DAPI containing mounting medium (*Vectashield*). In both cases the

slides were dried O/N at RT. The stained sections on the slides were analyzed using the digital fluorescence microscope *Keyence BZ-9000* and *BZ-II Viewer and Analyser* software.

3.2.8.4. Hematoxylin and Eosin staining

The Hematoxylin and Eosin staining of paraffin sections allows a more precise assessment of the tissue structure and morphology. Hematoxylin is a positively charged molecule that binds to negatively charged compounds. Therefore, Hematoxylin is used to stain DNA and RNA leading to a dark violet stain of the nuclei. Eosin on the other hand stains eosinophilic structures in a pink colour, such as proteins and is therefore used as a counterstain of the cytoplasm. To perform H&E staining, the paraffin sections were deparaffinized twice in xylol for 10 min. Thereafter, they were incubated twice in 100% EtOH for 5 min. Next, they were transferred to 95% EtOH for 2 min, 70% EtOH for 2 min and rehydrated in Aqua dest. for 1 min. Subsequently, the sections were incubated for 3 min in *Mayer´s Hemalum solution* and then dipped for 2 sec in aqueous hydrochloric acid (0.1%). Next, the slides were rinsed under running tap water for 3 min and then incubated for 3 min in *alcoholic Eosin Y solution,* which was acidified with 2 drops acetic acid just prior to use. Then the slides were shortly rinsed under running tap water for 30 sec, followed by a two-fold incubation in 95% EtOH for 10 sec. Lastly, the slides were incubated twice for 10 sec in 100% EtOH and twice for 5 min in xylol. The slides were immediately mounted in *Entellan*, dried ON at RT and the sections were analyzed using the digital fluorescence microscope *Keyence BZ-9000* and *BZ-II Viewer and Analyser* software. The histological scores were calculated by classifying epithelial changes in the mucosa and submucosa, such as erosions, ulcerations or necrosis, and changes in the mucosal architecture, such as the distortion of villous structure [160].

3.2.9. Flow cytometry and Fluorescence Activated Cell Sorting

Flow cytometry is a laser-based analysis, which can be used to quantify and qualify specific cell populations according to their size, granularity, surface markers or intracellular antigens. The phenotypic characterization of cells in a heterogeneous mixture can be achieved by the differences in light scattering and fluorescence. The cells are suspended in a stream of fluid which carries them through a thin capillary, aligning them so that they pass individually by an optical system equipped with lasers. The scattering of light provides information about the size or volume of the cell, which is measured and depicted in the *forward scatter* (FSC), whereas the *side scatter* (SSC) correlates with the granularity of the cell. Additionally, cells can be further analyzed by their expression of surface markers or intracellular antigens using specific monoclonal or polyclonal antibodies either directly coupled to fluorochromes or indirectly by the use of secondary antibodies coupled to fluorescent molecules. These fluorochromes are excited by the laser beams leading to the emission of different wave lengths. The different signals were depicted and analyzed using the *BD FACSDiva™* program and further assessed with *FlowJo*.

Fluorescence Activated Cell Sorting (FACS) functions similar to flow cytometry, but allows the sorting and collection of specific cells from mixed suspensions beyond the characterization and analysis of these cells.

3.2.9.1. Extracellular staining for flow cytometry

Single cell suspensions were transferred into FACS tubes, washed in 1 ml PBS per tube and centrifuged for 5 min at 1200 rpm. To avoid unspecific staining, the cells were treated with *TruStain FcX™ (α-CD16/32)* block diluted in PBS for 5 min at 4°C. The antibodies used for staining were added to the cells without performing a washing step and incubated for 20 min at 4°C in the dark. The excess antibodies were washed away by adding 1 ml PBS

and centrifuging 5 min at 1200 rpm. The cell pellet was resuspended in PBS and the samples were analyzed by flow cytometry.

3.2.9.2. Intracellular staining for flow cytometry

In order to perform an intracellular staining, while maintaining the cellular structure and EGFP signals, the cells were pelleted by centrifugation for 5 min at 1200 rpm, resuspended in 2% PFA and fixed for 20 min at RT in the dark. Next, the cells were washed in PBS, centrifuged 5 min at 1200 rpm, resuspended in *permeabilisation buffer* and incubated for 10 min at RT. Thereafter, the cells were washed with *permeabilisation buffer* and centrifuged 5 min at 1200 rpm. The previously in *permeabilisation buffer* diluted antibodies were added to the cells and incubated O/N at 4°C. The following day, the cells were washed with *permeabilisation buffer*, centrifuged for 5 min at 1200 rpm and either resuspended in PBS and analyzed by flow cytometry or stained with secondary antibodies diluted in *permeabilisation buffer* for 1 h at 4°C, followed by a washing step and resuspended in PBS prior to flow cytometry analysis.

3.2.10. Culturing bone marrow-derived dendritic cells and macrophages

3.2.10.1. Isolation and generation

Tibia and *femur* were separated from each other by cutting the knee joint at the *patella* without exposing the bone marrow and then transferred to a petri dish containing 70% EtOH. Then the bones were transferred to a petri dish containing sterile PBS. Next the *epiphyses* of each bone were cut off and the exposed bone marrow was flushed out into a falcon tube using a sterile syringe (26 gauge needle) with cold PBS. This was repeated until the bone was white and translucent. The cells were washed in PBS by centrifugation at 1200 rpm for 5 min at 4°C. The supernatant was discarded, the pellet

was resuspended in *complete RPMI medium*, the cell number was determined and 10 ml cell suspension with a concentration of 5 x 10^5 cells/ml were plated in 10 cm petri dishes. For BMDC differentiation, 2% supernatant of GM-CSF transfected X63Ag8-653-cells was added to the cell cultures and for BMMϕ differentiation, 10% M-CSF-containing supernatant of L929 fibroblasts was supplemented to the cell cultures. On the third day the same volume of *complete RPMI medium* and corresponding supplement was added to the cell cultures. On the sixth day, BMMϕs were harvested using trypsin/EDTA and used for *in vitro* stimulation in an endotoxin tolerance assay. The supernatant of the BMDCs cultures was discarded. BMDCs were harvested from the dishes by adding 10 ml pre-warmed 5 mM EDTA/PBS and incubated for 15 to 20 min at 37°C in the incubator. The cell suspension was collected and used for *in vitro* stimulation for flow cytometry or Western blot analysis. Cells that did not detach from the dish after this procedure were discarded as they probably belonged to the macrophage lineage.

3.2.10.2. *In vitro* stimulation of BMDC and BMMϕ

Prior to each stimulation assay, the cell number was determined using a Trypan blue vital stain and a hemocytometer.

For flow cytometry analysis BMDCs were plated in a concentration of 1 x 10^6 cells/ml in *complete RPMI medium* in a 6-well plate. The cells were left to settle for 2 h before stimulating them O/N with or without 100 ng/ml LPS (0111:B4) at 37°C and 5% CO_2. Thereafter the cells were harvested by scraping, washed with PBS, centrifuged at 1200 rpm for 5 min and extracellularly stained with fluorophore conjugated antibodies against specific surface markers for 20 min at 4°C, washed with PBS and analyzed by flow cytometry.

For Western blot analysis, BMDCs were plated in a concentration of 2 x 10^6 cells/ml in *complete RPMI medium* in a 6-well plate, left to settle for 2 h and stimulated O/N with 100 ng/ml LPS (0111:B4) or left untreated at 37°C. Following, they were harvested by scraping, washed with PBS, centrifuged at 1200 rpm for 5 min, supernatant was discarded

and the pellet was resuspended in 200 µl *RIPA buffer* supplemented with *protease inhibitors* and stored at -20°C.

For the assessment of endotoxin tolerance, BMMϕs were seeded at a concentration of 1 x 10^6 cells/ml in *complete RPMI medium* in a 96-well plate. The cells were left to settle for 2 h before stimulating cell duplicates for 20 h with or without 1, 10 or 20 ng/ml LPS (0111:B4) at 37°C and 5% CO_2. Next the 96-well plate was centrifuged shortly and the supernatants were carefully discarded. The cells were washed once with fresh RPMI medium, centrifuged shortly and after discarding the supernatants, resuspended in 200 µl *complete RPMI medium* per well and stimulated for 6 h with 1, 10 or 20 ng/ml LPS (0111:B4) or left untreated at 37°C. The supernatants were carefully transferred to a new 96-well plate after a short centrifugation to pellet the cells and stored at -20°C until measurement of TNF levels by ELISA.

3.2.11. *In vitro* helper T cell differentiation assay

3.2.11.1. Isolation of naïve $CD4^+$ T cells

Spleens were transferred to a sterile 100 µm cell strainer, moistened with 1 ml ice cold PBS and pressed through the mesh. The meshed tissue was collected and the strainer was washed with ice cold PBS. The cell suspension was centrifuged at 1500 rpm for 10 min at 4°C. The supernatant was discarded; the cell pellet was resuspended in *ACT buffer* and incubated for 5 min at 37°C to lyse erythrocyte. The reaction was stopped with ice cold PBS. The suspension was filtered through a 70 µm cell strainer, the cell number was determined and the suspension was centrifuged at 1500 rpm for 10 min at 4°C. $CD4^+$ splenic T cells were thereafter enriched using *MACS Pan T cell Isolation Kit* and *CD8a (Ly-2) MicroBeads* from *Miltenyi Biotec* or alternatively *MagniSort™ Mouse CD4 T cell Enrichment Kit* from *eBioscience* according to the manufacturer´s guidelines. Subsequently, the cells were extracellularly stained for at least 30 min at 4°C using antibodies against CD3 (FITC), CD4 (APC-Cy7), CD8 (PerCP), CD44 (PE), CD62L (APC) and CD25 (PE-Cy7). Naïve $CD4^+$ T cells ($CD3^+CD4^+CD8^-CD44^{lo}CD62L^{hi}CD25^-$) were then purified

by FACS sorting using the *FACS Aria.* During the establishment of the assay, $CD4^+$ splenic T cells were isolated using *$CD4^+$ $CD62L^+$ T cell Isolation Kit II* from *Miltenyi Biotec* according to the manufacturer´s guidelines.

3.2.11.2. Differentiation protocol

T cells were cultured in triplicates at a concentration of 1 x 10^5 cells/ml in 200 µl *complete IMDM medium* per well supplemented with various amounts of antibodies and cytokines and activated with plate-bound anti-CD3 (3 µg/ml) and soluble anti-CD28 (1 µg/ml) in 96-well round bottom culture plates for 5 days at 37 °C, 5% CO_2 either under normoxic or hypoxic (1% O_2) conditions. A combination of different cytokines and antibodies was added to the culture to achieve helper T cell differentiation in T_h0, T_h1, T_h2, T_h17, T_h22 and regulatory T cell (T_{reg}) and Type I regulatory T cell (T_r1) populations. In the following Table 3 the antibody and cytokine cocktail for each subset is depicted.

Table 3 – Additives for naïve T cell cultures to achieve different helper T cell polarization.

Helper T cell subset	Cytokines and additives	Antibodies
T_h0		α-IFNγ (10 µg/ml) α-IL-4 (10 µg/ml)
T_h1	IL-12 (20 ng/ml)	α-IL-4 (10 µg/ml)
T_h2	IL-4 (100 ng/ml)	α-IFNγ (10 µg/ml)
T_h17	IL-6 (100 ng/ml) TGFβ (5 ng/ml) FICZ (300 nM)	α-IFNγ (10 µg/ml) α-IL-4 (10 µg/ml)
T_h22	IL-6 (40 ng/ml) IL-23 (20 ng/ml) TNF (50 ng/ml) FICZ (300 nM)	
T_{reg}	TGFβ (5 ng/ml) Retinoic acid (2,5 ng/ml)	
T_r1	TGFβ (2 ng/ml) IL-27 (25 ng/ml) FICZ (100 nM)	

3.2.11.3. Validation of differentiation

Secreted cytokines were measured after 5 days by ELISA in the supernatants, namely IFNγ for T_h1, IL-4 for T_h2, IL-17 for T_h17, IL-22 for T_h22, IL-10 for T_r1 and TGFß for T_{reg} cells. For extra- and intracellular cytokine staining, cells were re-stimulated for 4 h at 37 °C in *complete IMDM medium* containing *PMA* (50 ng/ml), *ionomycin* (1 µg/ml), *monensin* (2 µl/ml) and *brefeldin A* (2 µl/ml). After staining for surface markers with antibodies against CD4 (PE-Cy7), CD8 (PerCP) and viability (eFluor® 780), cells were fixed in 2% PFA for 20 min at RT in the dark and permeabilized to allow O/N staining with intracellular staining antibodies against IFNγ, IL-4, IL-17, IL-22, FoxP3 and IL-10, as well as anti-GFP, followed by a staining with anti-rabbit IgG (Alexa Fluor® 488) for 1 h at 4°C. *In vitro* differentiated T_{reg} cells were fixed in 2% FA for 20 min at RT and treated with the *permeabilization buffer* from *eBioscience FoxP3/Transcription Factor Staining Buffer Set* as suggested by the manufacturer without previous re-stimulation with *PMA* and *ionomycin*. Following, the cells were washed with *permeabilization buffer* and analyzed by flow cytometry.

3.2.12. Quantitative Real-Time PCR

3.2.12.1. RNA isolation and cDNA synthesis

Samples of small intestine were either snap frozen in liquid nitrogen or transferred in 500 µl *RNAlater™* after removal. RNA was isolated from small intestine using the *RNeasy fibrous tissue mini kit* from *Qiagen* according to manufacturer's guidelines. Approximately 30 mg of tissue was homogenized in cryotubes containing glass beads and the provided buffer supplemented with β-mercaptoethanol using the *Precellys* homogenizer for 30 s at 6800 rpm three times including 30 sec breaks between each cycle. The RNA concentration

was measured using a *NanoDrop* and the RNA samples were stored at -80°C until cDNA synthesis.

For cDNA synthesis 1 µg RNA was transcribed to complementary DNA (cDNA) using the *RevertAid reverse transcriptase* from *Thermo Scientific*. 2 µl Oligo(dt)18 primer (1 µg/ml) and 22,4 µl DEPC water were added and then the RNA was denatured in a thermocycler for 10 min at 70°C to allow primer binding. In Table 4 further components are listed which were added to the samples.

Table 4 – PCR reaction setup for cDNA synthesis.

Reagent	1 PCR reaction
5x RT Reaction buffer	8 µl
dNTP (10 mM)	4 µl
DTT (100 nM)	4 µl
RiboLock RNase Inhibitor	0.8 µl
RevertAid reverse transcriptase	0.8 µl
Total	17.6 µl

The samples were then placed back in the thermocycler for 1 h at 42°C, followed for 5 min at 95°C. To analyze whether the cDNA synthesis was successful, a PCR using the synthesized cDNA was performed to detect the house keeping gene ribosomal protein S6 (RPS6) according to the protocol depicted in Table 5 and the previously mentioned general PCR reaction setup (Table 1). The cDNA samples were stored at -80°C until real-time analysis was performed.

Table 5 – PCR cycle protocol for RPS6 PCR.

Number of cycles	Incubation time	Incubation temperature
1x	5 min	95°C
35x	60 sec	95°C
	60 sec	55°C
	60 sec	72°C
1x	10 min	72°C

3.2.12.2. Quantitative Real-Time PCR

In a quantitative Real-Time PCR (qRT-PCR) the analysis of the amplified product is enabled by the addition of *Absolute qPCR Sybr Green* to the PCR mixture, allowing detection of fluorescence after intercalation, which was measured with a wavelength of 520 nm using the *Real-Time System CFX96*. In the following tables the qRT-PCR mix (Table 6) and the protocol (Table 7) are described.

Table 6 – PCR reaction setup for qRT-PCR.

Reagent	1 reaction
Absolute qPCR Sybr Green ROX Mix	7.5 µl
Primer fwd	0.2 µl
Primer rev	0.2 µl
A. Dest.	2.1 µl
cDNA (diluted 1:10)	5 µl
Total	15 µl

Table 7 – Cycle protocol for qRT-PCR.

Number of cycles	Incubation time	Incubation temperature
1x	15 min	95°C
40x	20 sec	94°C
	1 min	60°C
1x	30 sec	65°C

In order to exclude the possible amplification of unwanted DNA sequences, a melting curve analysis was performed by continuously raising the temperature by 0.5°C at a time from 65°C to 95°C. *Sybr Green* will be released at the temperature (T_m value, from m*elting* t*emperature*) resulting to the denaturation of the amplified fragment from a double strand to single strands, allowing the distinction of unspecific primer dimers and off-target amplificates by comparing the dissociation curves of the different fragments.

The *cycle threshold* (C_T value) describes the number of cycles at which the fluorescence exceeds the threshold, which is determined by means of the background fluorescence in the first cycles (approximately 3-5). The expression of the gene of interest was quantified by calculating the delta C_T value (ΔC_T) by subtracting the C_T value of the gene of interest from the C_T value of the house-keeping gene GAPDH. Subsequently, the difference (termed $\Delta\Delta C_T$) between the ΔC_T values from treated and untreated samples was calculated and displayed as the x-fold induction by calculating the negative power of 2.

3.2.13. *Toxoplasma gondii* infection

3.2.13.1. Parasite passaging

The parasite *Toxoplasma gondii* was passaged in female outbred CD1 mice, which are resistant to the health impairments of the infection. This was achieved by injecting the mice i.p. with 20 lysed *Toxoplasma gondii* ME 49 cysts. After 3 to 4 weeks after infection the parasite has formed cysts in the brain. The infected mouse was sacrificed, the brain was explanted and transferred to a falcon tube containing PBS. The brain was then moved to another falcon containing PBS to flush off blood and then transferred to a 5 cm petri dish, where it was cut into small pieces. Next, 4 ml PBS were added, and the tissue was homogenized using a 10 ml syringe and successively smaller needles (start with G18, then G20, then G22, lastly G23). The suspension was then centrifuged at 800 rpm for 5 min. The supernatant was discarded, the pellet was resuspended in 15 ml PBS and underlaid with 10 ml *Ficoll-Paque™ PLUS (density 1.077 g/ml)* and centrifuged for 25 min at 2500 rpm with moderate acceleration (level 7 from 9) and no brake. Afterwards the supernatant containing tissue debris was carefully discarded; the pellet was washed with 50 ml PBS and centrifuged at 2000 rpm for 15 min. The supernatant was discarded, the pellet was resuspended in 500 µl PBS and the number of cysts was counted. The cysts were diluted in PBS and the desired number of cysts per mouse was administered orally by gavage to the experimental mice, whereas 40 cysts were taken aside, lysed to release bradyzoites in order to reinfect two new CD1 mouse. The lysis was performed by

transferring the cysts to a 24-well plate in a volume of 500 µl PBS and the addition of 150 µl Trypsin-EDTA. The bursting of the cysts was observed under the microscope and stopped by the addition of 500 µl FCS. The suspension was transferred to a 15 ml falcon, the well was washed twice with 2 ml PBS and the suspension was centrifuged at 1800 rpm for 15 min. The pellet was resuspended in 200 µl PBS per 20 lysed cysts and injected i.p. to a CD1 mouse.

3.2.13.2. Experimental procedure for survival analysis

Age-matched female $AhRR^{+/+}$ and $AhRR^{E/E}$ mice were weighed before conducting the experiments. The mice were orally infected with either 200 cysts, 100 cysts, 50 cysts or 25 cysts per mouse diluted in 200 µl PBS. After infection the survival of the mice was monitored twice per day. Furthermore, they were scored and weighed each day. Control mice received a gavage with 200 µl PBS. All experiments were performed in accordance with institutional, state, and federal guidelines and with the permission of the state government of North-Rhine-Westphalia, Germany, (file reference: 84-02.04.2011.A405 for experiments performed in Düsseldorf and 84-02.04.2013.A084 for experiments performed in Bonn).

3.2.13.3. Clinical score

The following clinical assessment (Table 8) was used to assess the clinical score of the mice infected with *Toxoplasma gondii* cysts.

Table 8 – Clinical scoring system used to assess mice that were orally infected with *Toxoplasma gondii* cysts.

Criteria		Points
Appearance	Normal appearance	0
	Slight grooming deficit	1
	Increasing grooming deficit	2
	Distinct grooming deficit	3
Behaviour	Mouse explores the cage	0
	Mouse refrains from exploring, but full body movement is intact	1
	Hunched bearing, impaired sense of balance	2
	No movement observable	3
Faecal consistency	Normal amount of faeces in the cage Defecation during assessment	0
	Normal amount of faeces in the cage Diarrhea	1
	Less amount of faeces in the cage	2
	No faeces in the cage since last assessment	3
Body weight	Less than 1% lower than initial weight	0
	Between 1 to 5% lower than initial weight	1
	Between 5 to 10% lower than initial weight	2
	Between 10 to 20% lower than initial weight	3
	Between 20 to 25% lower than initial weight	4

3.2.13.4. Experimental procedure for *ex vivo* analysis

Age- and weight-matched female $AhRR^{+/+}$ and $AhRR^{E/E}$ mice were orally infected with 50 cysts diluted in 200 µl PBS per mouse. After infection the mice were monitored twice a day, scored and weighed each day. On day 8 after infection, blood was collected for cytokine analysis by ELISA. Next, the mice were sacrificed and the small intestine was harvested and stored on ice cold PBS until further preparation. The small intestine was flushed with ice cold PBS using a 10 ml syringe and a gavage needle. Next, the fat tissue

was removed using forceps. The length of the intestine was determined before samples were taken for the different analytical procedures. Approximately 30 mg ileum, jejunum and duodenum were removed and either snap frozen in liquid nitrogen or stored in *RNAlater™* at -20°C until RNA preparation. For histological analysis, roughly 1 cm ileum, jejunum and duodenum were transferred into a 6-well plate containing 3 ml 4% PFA for at least 4 h until further processing. For organ culture, approximately 30 mg ileum, jejunum and duodenum were transferred into 300 µl RPMI medium in a 48 well plate for 6 h. Alternatively, approximately 30 mg ileum, jejunum and duodenum were homogenized in cryotubes containing glass beads using the *Precellys* homogenizer for 30 s at 6800 rpm three times including 30 sec breaks between each cycle. The supernatants were used to determine cytokine secretion by ELISA.

3.2.14. Colon Ascendens Stent Peritonitis

To induce polymicrobial peritonitis in mice, the CASP model, a highly standardized rodent model was used.

In this model, a small stent is surgically inserted into the ascending colon of mice, creating a continuous link between the intestinal lumen and the peritoneal cavity resulting in a septic peritonitis [152]–[154]. The severity of the infection can be controlled by the diameter of the inserted stent (14G, 16G, 18G or 20G).

Age-matched male and female $AhRR^{+/+}$ and $AhRR^{E/E}$ mice were weighed before conducting the experiments. Prior to the surgery, the plastic tubing of a vein catheter, which serves as the stent, was carved approximately 2 mm from the tip using a scissor. The mouse was anesthetized using *Forene (Isoflurane)* supplemented with oxygen. Thereafter, the abdominal skin was firstly disinfected with 70% EtOH and then incised along the midline. Next, the peritoneum was cut along the *linea alba* to expose the peritoneal cavity. The caecum with the terminal ileum and ascending colon was carefully pulled out of the abdomen using sterile swabs previously moistened with sterile PBS. Approximately 1.5 cm above the ileocecal valve, the ascending colon was fixed using *surgical suture (nylon, DSM 11)* by two surgical knots [154]. Then the vein catheter was

inserted above the suture into the ascending colon up to the carving in the plastic tube. To prevent the pointy iron tube of the catheter to damage the other side of the colon, it was pulled back just enough to be covered by the plastic tube but to still facilitate stability. The free end of the surgical suture from the stitch just underneath the catheter was placed around the plastic tube lined into the furrow and fixed by two knots. Subsequent, the suture was stitched above the plastic tube through the colonic wall, fixed by two surgical knots and cut off. The iron tube was then removed further and the plastic tube was cut off approximately 1 mm from the lined suture. In the next step, the plastic tube was carefully stabilized using forceps, and the stool was slowly pushed from the end of the caecum towards the stent until a small drop of faeces appears in the stent. The caecum, terminal ileum and ascending colon was then carefully placed back into the peritoneal cavity, which was then rehydrated with 0.5 ml sterile PBS administered straight into the peritoneal cavity. Finally the peritoneum and the abdominal skin were closed using *surgical suture (nylon, DSM 13)* with a continuous stitch and fixed by three surgical knots. During the whole surgery the gut and the open cavity were repeatedly rehydrated with sterile PBS. The mouse was then removed from anesthesia, and placed back in its cage, where it was monitored until full recovery from anesthesia. The insertion of the vein catheter was omitted in sham operated mice, all other steps however were conducted in the same manner. All experiments were performed in accordance with institutional, state, and federal guidelines and with the permission of the state government of North-Rhine-Westphalia, Germany, (file reference: 87-51.04.2011.A013).

3.2.14.1. Clinical score

The following clinical assessment (Table 9) was used to score the health status of the mice and the severity of the induced sepsis. The mice were weighed every day, which was correlated to their initial weight prior to the surgery.

Table 9 – Clinical scoring system used to assess mice that underwent a CASP operation.

Criteria		Points
Body weight	Less than 5% lower than initial weight	0
	Less than 15% lower than initial weight	1
	Less than 20% lower than initial weight	2
	More than 20% lower than initial weight	3
Appearance	Normal appearance	0
	Slight grooming deficit	1
	Increasing grooming deficit	2
	Distinct grooming deficit	3
Behaviour	Mouse explores the cage	0
	Mouse detains from exploring, but full body movement is intact	1
	Hunched bearing, impaired sense of balance	2
	No movement observable	3
Provoked behaviour	Mouse tries to escape upon opening the cage Normal muscle tone	0
	Mouse only tries to escape upon approaching hand Slight deficit in muscle tone	1
	Mouse only tries to escape upon touching Increased deficit in muscle tone	2
	Mouse detains from escaping Distinct deficit in muscle tone	3
Abdominal palpation	No tenderness on abdominal palpation Soft abdomen	0
	Slight tenderness on abdominal palpation Soft abdomen	1
	Increased tenderness on abdominal palpation Abdominal resistence	2
	Distinct tenderness on abdominal palpation Firm abdomen	3
Faecal consistency	Normal amount of faeces in the cage Defecation during assessment	0
	Less amount of faeces in the cage	1
	Diarrhea	2
	No faeces in the cage since last assessment	3

3.2.15. Endotoxin tolerance assay

3.2.15.1. Experimental procedure

Age- and weight-matched male $AhR^{+/+}$, $AhR^{-/-}$, $AhRR^{+/+}$ and $AhRR^{E/E}$ mice received either PBS or 4 mg/kg LPS (0111:B4) i.p. on day 1 and were challenged with 15 mg/kg LPS (0111:B4) on the day 4. Control mice received 200 µl PBS on day 1 and day 4. 90 minutes after the challenge on day 4 the mice were sacrificed, blood was collected and the serum was analyzed for TNF production. For survival analysis, mice were primed with 4 mg/kg LPS (0111:B4) on the day 1 and challenged with 20 mg/kg LPS (0111:B4) on day 4. To compare our setup to a model used by Bessede *et al.* [161], the mice were primed with 0.5 mg/kg LPS (055:B5) on the day 1 and challenged with 40 mg/kg LPS (055:B5) on the day 7 [161]. In all cases the survival was monitored over 7 days after the 2^{nd} challenge. All experiments were performed in accordance with institutional, state, and federal guidelines and with the permission of the state government of North-Rhine-Westphalia, Germany, (file reference: 8.87-50.10.37.09.193).

3.2.15.2. Clinical score

The following clinical score (Table 10) was used to assess the health of the mice and the severity of the LPS treatment.

Table 10 – Clinical scoring system used to assess LPS treated mice.

Criteria		Points
Appearance	Normal appearance	0
	Slight grooming deficits	1
	Increasing grooming deficit	2
	Distinct grooming deficit	3
Behaviour	Mouse explores the cage	0
	Mouse fails from exploring, but body movement is intact	1
	Hunched posture, impaired sense of balance	2
	No movement observable	3

3.2.16. Generation of AhRR-dsRed-reporter mice

AhRR-dsRed-reporter mice were generated using a targeting vector, which was constructed by Markus Korkowski (*IUF*, Düsseldorf). In this targeting vector the second exon of the *ahrr* gene was replaced by the reporter gene *dsRed*, a *Discosoma sp.* Red fluorescent protein.

200 µg of this targeting vector was linearized for 4 h at 37°C using the restriction endonuclease *ClaI*. The DNA was then precipitated by the addition of 1/10 of the sample volume 3 M Na-Acetate and 2.5x of the sample volume 100% EtOH and an incubation O/N at -80°C. The following day the sample was centrifuged, the pellet was washed with 70% EtOH, resuspended in PBS and dissolved for 1 h at 37°C. The targeting vector was then transfected into 5 x 10^7 HM-1 mouse embryonic stem (ES) cells suspended in 7 ml *complete ES cells medium* by electroporation using the *Electroporator Gene pulser Xcell™* at 250 V and 250 µF (Figure 11). The transfection was performed in a volume of 800 µl in cuvettes. The transfected ES cells, which were kept in *complete ES cell medium* on culture plates coated with gelatine, underwent a selection process using 200 µg/ml G418 starting 2 days after the transfection. The media supplemented with G418 was changed every other day. Approximately 10 to 14 days later, resistant cell clones were isolated using Trypsin and transferred to a 96 well plate. Without selective pressure, the ES cells were

expanded, tested by southern blot to ensure successful integration of the modified allele and frozen away at -80°C in 80% FCS supplemented with 20% DMSO. Positive ES cell clones were then injected into blastocysts and implanted into pseudo pregnant surrogate mothers, thereby generating chimeric offspring (Figure 11). Blastocysts injection was performed by the *transgenic service* of the *LIMES GRC*.

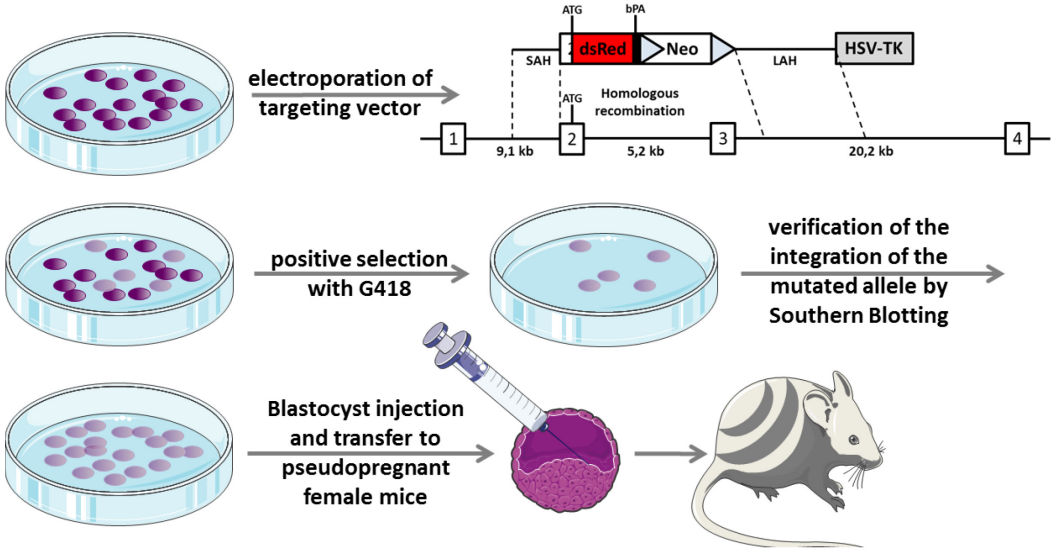

Figure 11 – Schematic of ES cell targeting strategy.

Chimeric offspring was mated with C57BL/6J WT mice, germline transmission was obtained and their progeny was genotyped using PCR. Following, BMDCs were generated from heterozygous progeny, stained and analyzed using flow cytometry. Skin, ear and intestinal samples were taken for histological analysis in order to verify dsRed expression.

3.2.17. Statistical analysis

Statistical analysis was performed using *GraphPad Prism*. Data were in general presented as mean plus Standard Error of the Mean (SEM). Significances were calculated using *(un)paired student t-test* and in the case of survival studies, significances were calculated using *Log-rank (Mantel-Cox) test*. Significant differences were depicted as *$p < 0.05$; **$p < 0.01$; ***$p < 0.001$.

4. Results

4.1. Analysis of AhRR expression in different helper T cell subsets

It has been shown that AhR expression was found, among other cell types, in lymphocytes located in barrier organs such as the gut, the lung and the skin (reviewed in [162]). In the literature, the AhR has been described to regulate helper T cell 17 (T_h17), regulatory T cell (T_{reg}) [90], [91], [94] and helper T cell 22 (T_h22) development [163]. In contrast, AhR expression is nearly undetectable in T_h1 and T_h2 cells (reviewed in [162]). In addition, parallel to this thesis, work on the influence of AhRR deficiency in a DSS-induced colitis model conducted in our group revealed an enhanced frequency of T_h17 cells and a reduced number of T_h1 cells in AhRR-deficient mice in comparison to wild-type mice [76]. Based on these insights and in light of characterizing AhRR expression and analyzing the influence of AhRR deficiency in various T lymphocyte populations, an *in vitro* helper T cell differentiation assay was established in this thesis comparing AhRR-deficient mice, expressing EGFP instead of the AhRR ($AhRR^{E/E}$), with wild-type littermate control mice.

4.1.1. Establishment of an *in vitro* helper T cell differentiation assay

In order to analyze the expression pattern and influences of the AhRR in different helper T cell populations, naïve splenic $CD4^+$ T cells from AhRR-deficient and wild-type mice were isolated, stimulated with plate-bound α-CD3 and soluble α-CD28 and a combination of different cytokines and antibodies, thereby differentiated into T_h1, T_h2, T_h17, T_h22 and T_{reg} populations. After 5 days in culture, cytokines in the supernatants were analyzed by ELISA, and the cells were used for intracellular cytokine staining. They were analyzed for production of key cytokines of each helper T cell population, namely IFNγ for T_h1, IL-4 for T_h2, IL-17 for T_h17 and IL-22 for T_h22 cells. For T_{reg}, TGFβ levels were measured in the

supernatant and the expression of the transcription factor FoxP3 was analyzed in the intracellular staining.

Initially, naïve splenic $CD4^+$ T cells were isolated and purified by magnetic separation using the *$CD4^+$ $CD62L^+$ T cell Isolation Kit II*. However, some difficulties arose, not only in insufficient reproducibility, but also regarding high background cytokine production detected in T_h0 differentiated cells, when measuring key cytokines of each helper T cell population in the supernatants by ELISA (Figure 12). Furthermore, only low numbers in intracellular cytokine positive cells were detected (data not shown).

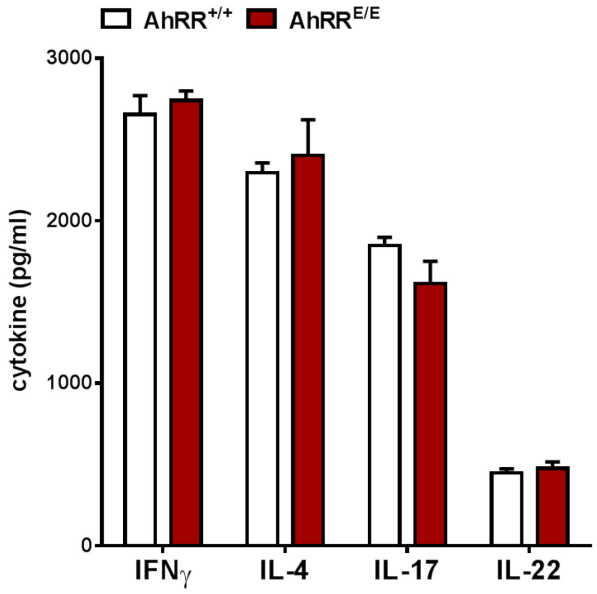

Figure 12 – Background cytokine levels produced by *in vitro* cultured T_h0 cells. Key cytokine levels (IFNγ for T_h1, IL-4 for T_h2, IL-17 for T_h17 and IL-22 for T_h22) measured in the supernatants of AhRR-deficient ($AhRR^{E/E}$, red bars) or wild-type ($AhRR^{+/+}$, white bars) T_h0 cells cultured for 5 days in IMDM medium after the addition of antibodies against IFNγ and IL-4. Naïve splenic $CD4^+$ T cells were purified by magnetic separation. n=3-5, pooled samples from 5 independent experiments. The results are presented as mean plus SEM.

Therefore, the assay was re-performed using Fluorescent Activated Cell Sorting (FACS) to enrich naïve splenic $CD4^+$ T cells, ensuring higher cell purity, after non-T cell and $CD8^+$ T cell were eliminated by magnetic separation. Low purity in naïve $CD4^+$ T cells might have been the reason for the high cytokine background due to the presence of previously activated or matured T cells. Prior to FACS analysis, the cells were stained with fluorescently labeled antibodies specific for CD3, CD4, CD8, CD44, CD62L and CD25

(Figure 13A). The staining for CD4 and CD8 allowed the exclusion of $CD8^+$ T cells; CD44 is a marker for lymphocyte activation; CD62L is an adhesion molecule expressed on naïve lymphocytes, which enter secondary lymphoid tissues via high endothelial venules and is down-regulated on memory or activated T cells; CD25 is the alpha chain of the IL-2 receptor and is found on activated T and B cells and was used to exclude regulatory T cells and activated T cells. The sorted cells were CD3-positive, CD4-positive, CD8-negative, CD44-low, CD62L-high and CD25-negative. The cells were sorted with an efficiency of approximately 99.8%, leading to a purity of 99.6%, which was verified by re-analyzing the sorted cells (Figure 13B).

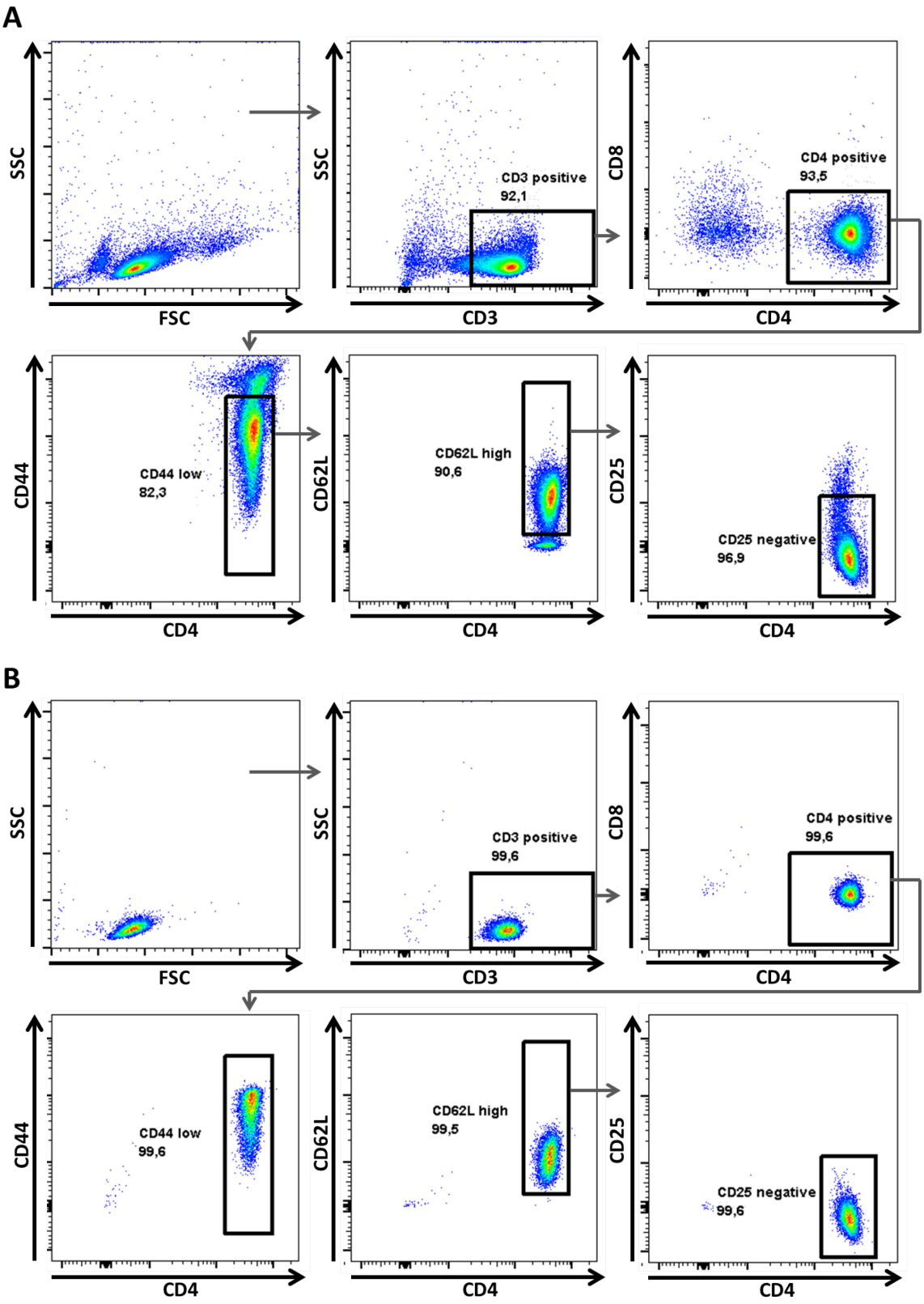

Figure 13 – Staining and gating strategy used in Fluorescent Activated Cell Sort (FACS) analysis and verification of the purity of sorted cells. MACS purified splenic $CD4^+$ T cells were sorted according to the depicted staining strategy (**A**) using fluorescently labeled antibodies against CD3, CD4, CD8, CD44, CD62L and CD25. T cells were gated on CD3-positive, CD4-positive, CD44-low, CD62L-high and CD25-negative. (**B**) The purity of naïve $CD4^+$ T cells was verified after FACS analysis. A representative re-analysis of sorted naïve $CD4^+$ T cells exhibited a purity of 99.6%.

In 2008 Veldhoen *et al.* investigated the effect of different culture media on *in vitro* T_h1 and T_h17 differentiation [91]. The authors were able to show that culturing naïve $CD4^+$ T cells in IMDM medium, instead of using the more commonly used RPMI medium, led to 10% more IFNγ producing T_h1 cells and 30% more IL-17 positive T_h17 cells due to the higher amount of aromatic amino acids, which serve as AhR agonists. Furthermore, the addition of the AhR ligand FICZ during T_h17 differentiation led to an increase of approximately 15% IL-17 producing T_h17 cells. Therefore, these insights were included in the *in vitro* T cell differentiation protocol performed in this project. Moreover, the cytokine cocktail T_h22 differentiation was altered by adding TNF to the differentiation protocol.

After 5 days of culture, intracellular key cytokines and the transcription factor FoxP3 were analyzed in order to identify properly differentiated helper T cells. After removal of the supernatants for ELISA analysis, the cells were stimulated with PMA, ionomycin, brefeldin A and monensin for 4 h, with the exception of T_{reg} cells. After an extracellular staining specific for CD4 and intracellular staining for key cytokines and FoxP3, the cells were analyzed by flow cytometry. The general gating strategy (Figure 14) included gating on viable cells, followed by the gating on $CD4^+$ cells and lastly on cytokine positive cells, which was based on fluorescent minus one (FMO) controls as well as T_h0 control cells.

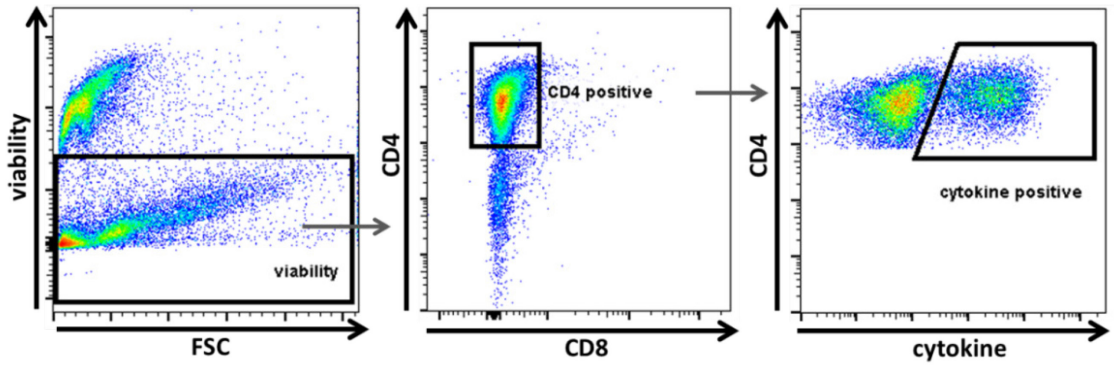

Figure 14 – Gating strategy used for flow cytometry analysis of *in vitro* differentiated helper T cell subsets. Depiction of a representative gating strategy used to evaluate cytokine or FoxP3 expression in *in vitro* differentiated helper T cell subsets. After 5 days of culture, cells were extracellularly stained against CD4 and intracellularly stained against specific key cytokines or FoxP3. Additionally, a viability stain was used.

The adjustments of the protocol described above resulted in well distinguishable cytokine or FoxP3 positive populations in T_h1, T_h17 and T_{reg} cultures as well as in a detectable presence of cytokine positive cells in T_h2 and T_h22 cultures, visible by shifts in differentiated cell populations in contrast to unstimulated or FMO controls (Figure 15).

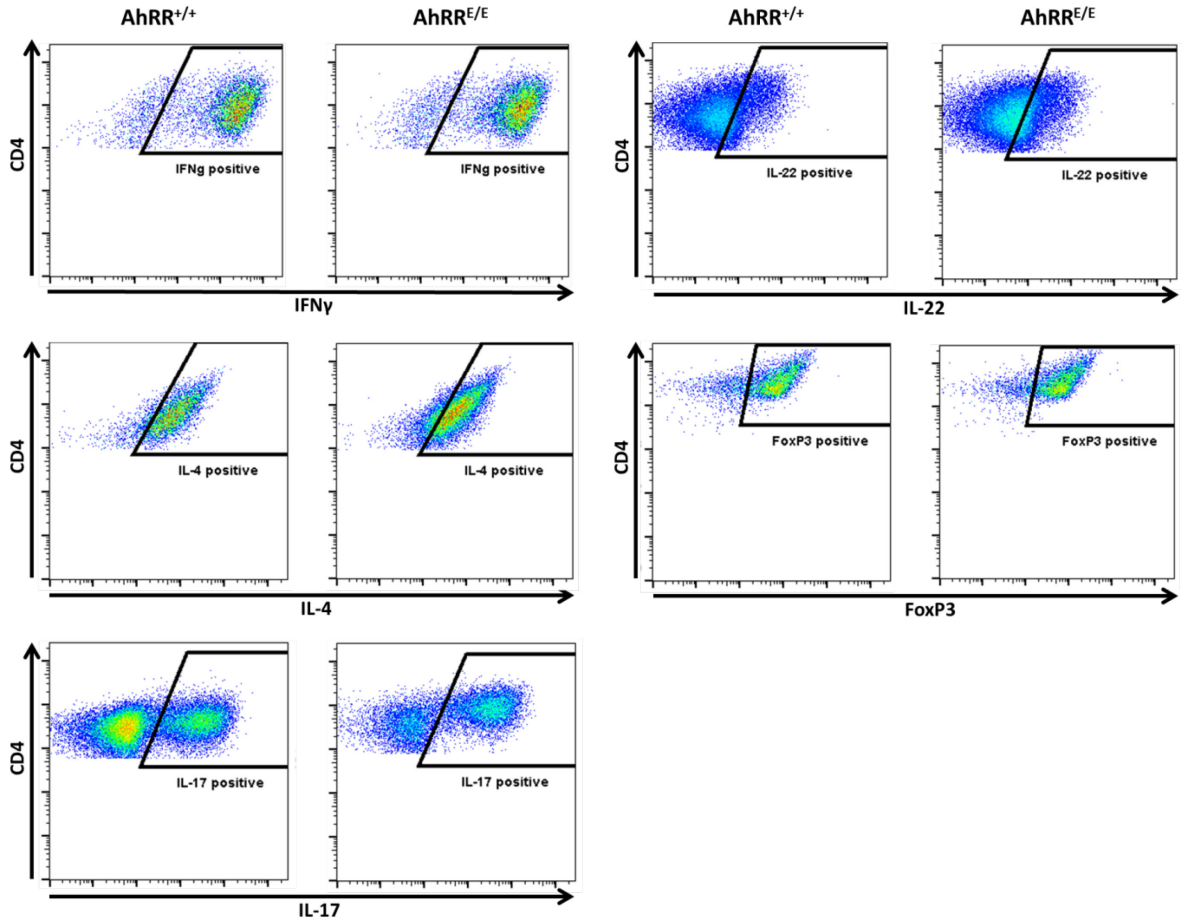

Figure 15 – Representative flow cytometry plots of different *in vitro* differentiated helper T cell subsets. Using intracellular staining the successful differentiation of different helper T cell subsets was assessed according to the production of key cytokines, namely IFNγ for T_h1, IL-4 for T_h2, IL-17 for T_h17 and IL-22 for T_h22 cells. For T_{reg} cells the expression of the transcription factor FoxP3 was analyzed.

4.1.2. Influence of AhRR deficiency on *in vitro* differentiated helper T cell subsets

Using the improved protocol approximately 85% IFNγ expressing T_h1 cells, 50% IL-4 positive T_h2 cells, 30% IL-17 expressing T_h17 cells and 60% FoxP3 expressing T_{reg} cells were detected for wild-type cells. Approximately 8% T_h22 cells that express IL-22 were

measured (Figure 16A). However, no significant differences were observed between AhRR-deficient cells and wild-type cells regarding median fluorescence intensities (MFI) or frequencies of cytokine or FoxP3 positive cells (Figure 16). Only a slight reduction of T_h17 and T_{reg} cells could be observed in AhRR-deficient differentiated cells compared to wild-type cells (Figure 16A). However, the same tendencies were not detected in MFI values (Figure 16B). The MFI of AhRR-deficient T_h17 cells was even slightly higher than that of wild-type cells, but the difference was not significant.

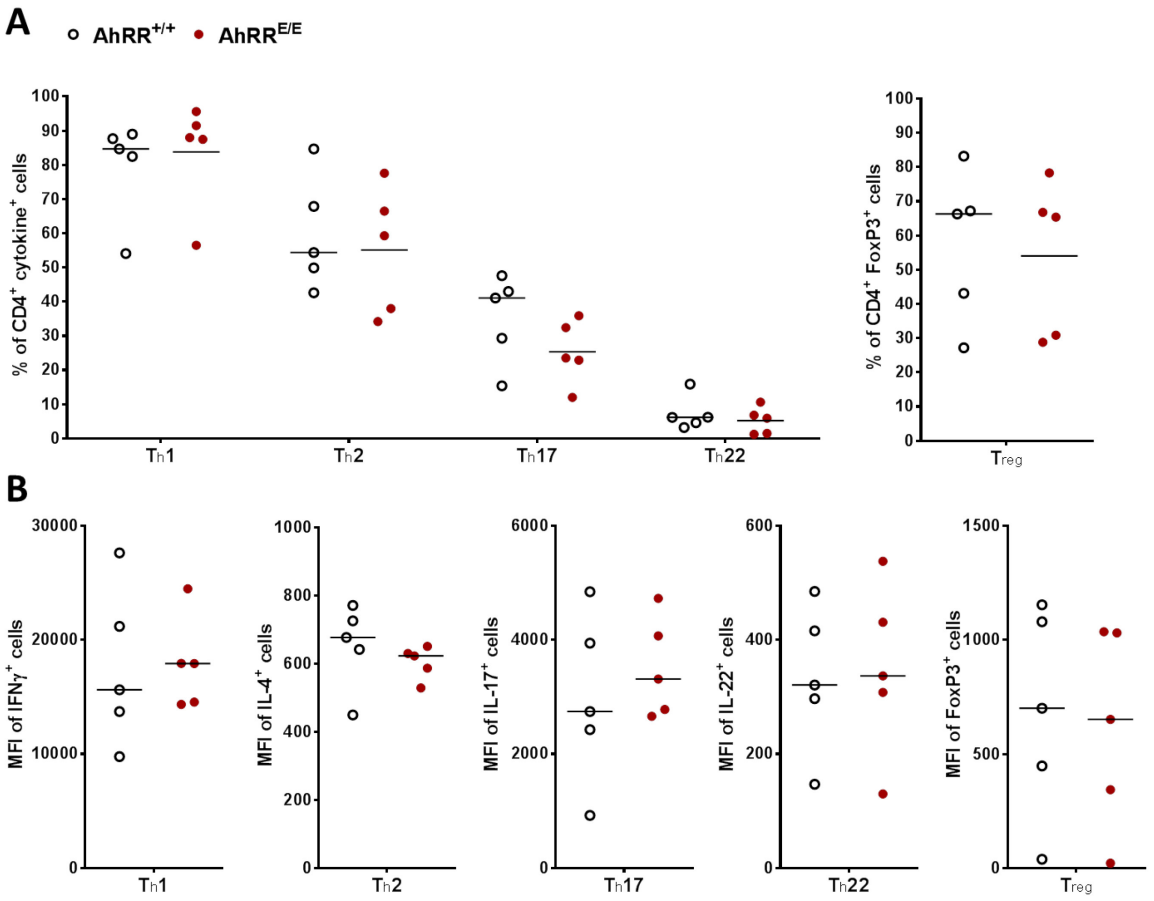

Figure 16 – Frequencies and MFI values of cytokine or FoxP3 positive CD4⁺ T cells of different *in vitro* differentiated helper T cell subsets. Quantification of the frequency (**A**) and median fluorescence intensity (MFI) (**B**) of IFNγ (T_h1), IL-4 (T_h2), IL-17A (T_h17) and IL-22 (T_h22) producing CD4⁺ T cells, and the frequency (**A**) and MFI (**B**) of FoxP3⁺ CD4⁺ T cells (T_{reg}) from cultures of AhRR-deficient ($AhRR^{E/E}$, red filled circles) and wild-type ($AhRR^{+/+}$, open circles) T cells. Different helper T cell populations were stained intracellularly for a specific key cytokine after a 5 day culture in IMDM medium with the addition of helper T cell specific cytokine and antibody cocktails. n=5, pooled samples from 5 independent experiments. The black line represents the median.

All key cytokines for each T cell subset were also measured in the supernatants of the 5 day cultures by ELISA. Because of the changes in the *in vitro* differentiation protocol mentioned above, background cytokine levels measured in the supernatants of T_h0 cells were strongly reduced (data not shown). Yet, no significant differences between AhRR-deficient and wild-type cells were detectable (Figure 17).

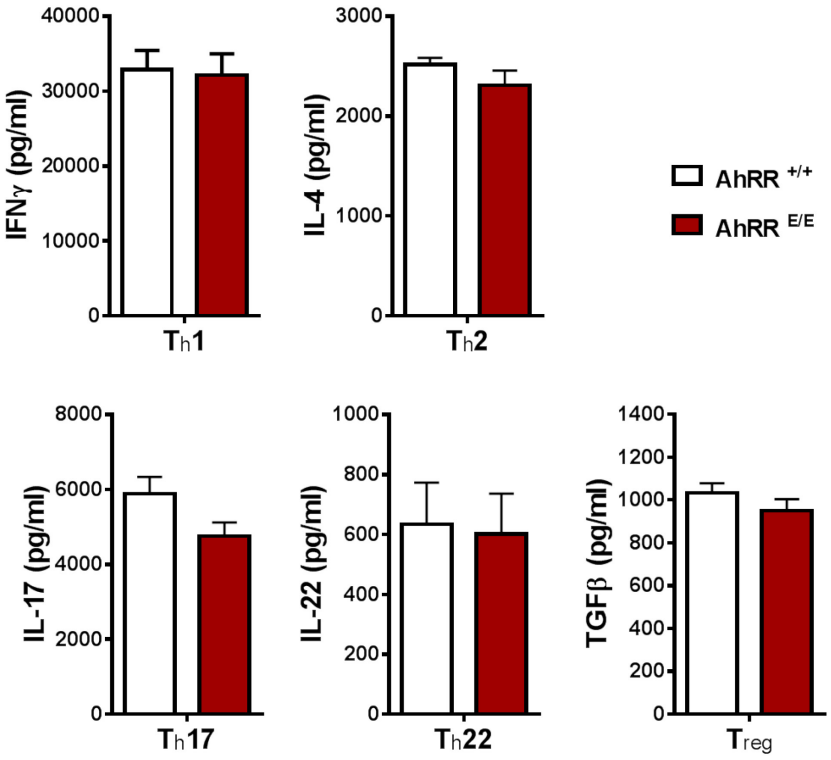

Figure 17 – Cytokine levels of *in vitro* differentiated helper T cell subsets. Cytokine levels measured in the supernatants of AhRR-deficient ($AhRR^{E/E}$, red bars) or wild-type ($AhRR^{+/+}$, white bars) T_h1, T_h2, T_h17, T_h22 and regulatory T (T_{reg}) cells after a 5 day culture in IMDM medium with the addition of helper T cell specific cytokine and antibody cocktails. n=5, pooled samples from 5 independent experiments. The results are presented as mean plus SEM.

These results suggest that AhRR deficiency has no significant effect on the differentiation of helper T cell populations *in vitro.* There was also no difference in the expression of key cytokines measured either by flow cytometry or by ELISA. Furthermore, these experiments revealed that the increased differentiation of T_h17 cells and decreased frequency of T_h1 cells observed in DSS-treated AhRR-deficient mice [76] cannot be explained by a T cells intrinsic change in differentiation.

4.1.3. AhRR expression in different *in vitro* differentiated helper T cell subsets

Moreover, the AhRR/EGFP expression was analyzed in key cytokine/transcription factor positive cells of the various helper T cell subsets. It could clearly be demonstrated that the AhRR/EGFP reporter is highly expressed in T_h17, T_h22 and T_{reg} cells (Figure 18A).

T_h17 cells exhibit the highest AhRR/EGFP expression with approximately 85% AhRR-expressing IL-17 positive T_h17 cells (Figure 18A), which is visible as a distinct EGFP positive population compared to wild-type cells (Figure 18B). In contrast, T_h22 and T_{reg} cells also show AhRR/EGFP expression, but only with approximately 20% and 18% positive EGFP positive cells, respectively. T_h1 and T_h2 cells do not display notable frequencies of AhRR/EGFP positive cells (Figure 18).

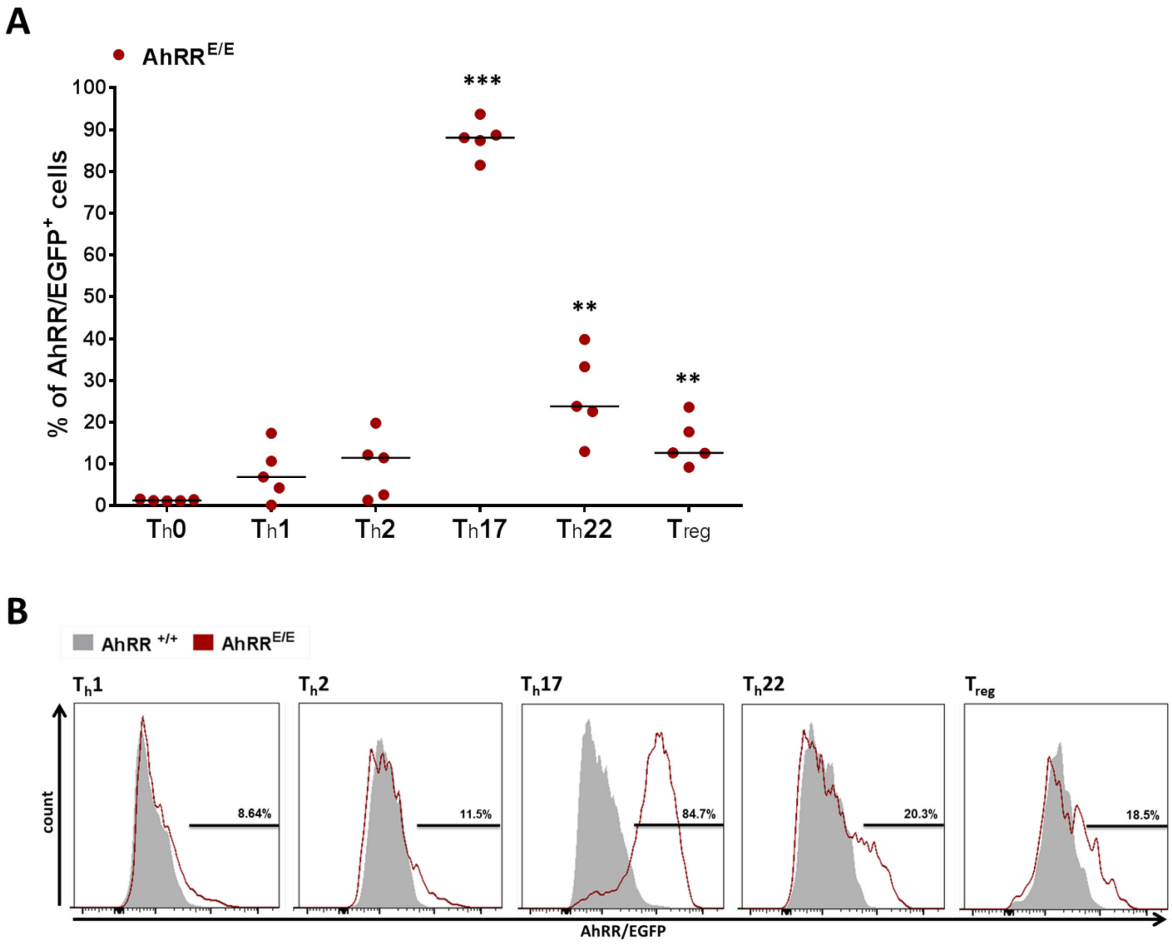

Figure 18 – AhRR/EGFP expression in specific key cytokine/FoxP3 positive cells from *in vitro* differentiated helper T cell subsets. (**A**) Quantification of the frequency of AhRR/EGFP expressing T_h1, T_h2, T_h17, T_h22 and T_{reg} cells. n=5, pooled samples from 5 independent experiments. The black line represents the median. Significant differences are depicted as **p<0.01 and ***p<0.001 (compared to T_h0). Significance was calculated using unpaired students t-test. (**B**) Representative histograms depicting the AhRR/EGFP expression compared between wild-type ($AhRR^{+/+}$, grey filled) and AhRR-deficient ($AhRR^{E/E}$, red line) helper T cell subsets. AhRR/EGFP expression was analyzed in $CD4^+$ cytokine or $FoxP3^+$ cells only.

These results are in line with studies describing the AhR to regulate T_h17 and T_{reg} development [90], [91], [94], considering that the AhRR is a target gene of the AhR and therefore may share the same expression pattern regarding helper T cell subsets. Furthermore, these data reveal that AhRR is also possibly playing a role in T_h22 cells, next to T_h17 and T_{reg} cell, indicated by AhRR/EGFP expression in *in vitro* differentiated IL-22 producing T cells. This too, would be in agreement with the role of the AhR in maintaining T_h22 development [163].

4.1.4. Influence of AhRR deficiency and hypoxia on *in vitro* differentiated helper T cell subsets

In the literature it has been described that the transcription factor hypoxia-inducible factor 1 (HIF-1) regulates the differentiation of T_h17 cells [164]. HIF-1 is a basic helix-loop-helix-PAS domain transcription factor consisting of an oxygen-sensitive HIF-1α subunit and constitutively expressed HIF-1β subunit (reviewed in [165]). HIF-1α directly interacts with RORγt, recruiting it to the IL-17 promotor, resulting in the regulation of T_h17 signature genes and T_h17 cell development [164]. Hypoxia can lead to the expression of HIF-1α during helper T cell differentiation. Therefore, the *in vitro* differentiation of T_h17 cells was repeated under hypoxic conditions. Moreover, T_h17 differentiation under these new circumstances, which may resemble the physiological situation in the intestines more closely, might still provide new insights to the increased T_h17 numbers observed in AhRR-deficient mice in a DSS-induced colitis model described by Brandstätter *et al.* [76].

In addition, T_{reg} cells were differentiated under hypoxia since this subset was also described to be regulated by hypoxia [164]. More precisely, HIF-1α can bind to the transcription factor FoxP3, thereby targeting it for proteasomal degradation, leading to a decrease of T_{reg} development [164]. Additionally, type 1 regulatory T cells (T_r1) were differentiated. These cells are characterized by their production of IL-10 and the absence of the transcription factor FoxP3 (reviewed in [97], [166]). Their differentiation is initiated and regulated by IL-27 and the AhR [95]. Mascanfroni *et al.* were able to demonstrate that the expression of HIF-1α leads to a suppression of T_r1 development [97].

Similar to the *in vitro* differentiation protocol under normoxic conditions, naïve splenic $CD4^+$ T cells from AhRR-deficient and wild-type mice were isolated by magnetic separation, purified by FACS and differentiated into T_h17, T_{reg} and T_r1 populations with the help of a combination of different cytokines and antibodies. 24 h after the naïve $CD4^+$ T cells were taken into culture, the cells were transferred to hypoxic conditions (1% O_2). After 5 days, cytokines in the supernatants were analyzed by ELISA and cells were used for intracellular cytokine staining. The cells were analyzed for production of key cytokines,

namely IL-17 for T_h17 and IL-10 for T_r1 cells, according to the gating strategy depicted in Figure 14. For T_{reg} cells, TGFβ levels were measured in the supernatant and the expression of the transcription factor FoxP3 was analyzed by intracellular staining.

Comparable to the experiments described above (Figure 16A), similar frequencies of IL-17 producing T_h17 cells and FoxP3 expressing T_{reg} cells were detected for wild-type cells cultured under normoxic conditions. Approximately 25% IL-17 expressing T_h17 differentiated cells (Figure 19A) and 65% FoxP3 expressing T_{reg} differentiated cells (Figure 19C) were detected. Approximately 35% differentiated T_r1 cells that express IL-10 were measured under normoxic conditions (Figure 19B). No significant differences were observed comparing AhRR-deficient cells and wild-type cells regarding frequencies or MFI values of cytokine or FoxP3 positive cells.

T_h17 have been described to exhibit increased differentiation of IL-17 producing cells when cultured in hypoxia [164]. Dang *et al.* were able to show that IL-17 producing cells exhibited an increase of approximately 22% [164]. Conversely, in the experiments performed in this thesis, no increase in the frequency of IL-17 producing cells under hypoxic conditions was identified (Figure 19A). However, an increase in MFI values for both AhRR-deficient cells and wild-type cells was observed, yet this increase was not significant.

T_r1 cells exhibited only marginal decreases in frequencies under hypoxic conditions compared to cells cultured under nomoxia (Figure 19B). Interestingly, IL-10 expressing T_r1 cells displayed higher MFI values under hypoxic culture conditions. However, the MFI median value was only calculated on the basis of 3 samples, which exhibited a large deviation between each other (Figure 19B).

In contrast, significantly lower frequencies of $FoxP3^+$ cells were measured in T_{reg} cultures for AhRR-deficient cells and wild-type cells under hypoxia with approximately 25% FoxP3 expressing T_{reg} cells (Figure 19C), exhibiting a decrease by 40% compared to normoxic cells. MFI values were also reduced. These results are in line with the literature, describing the attenuation of T_{reg} development by the expression of HIF-1α under hypoxia, leading to the degradation of FoxP3 and thereby regulating differentiation [164].

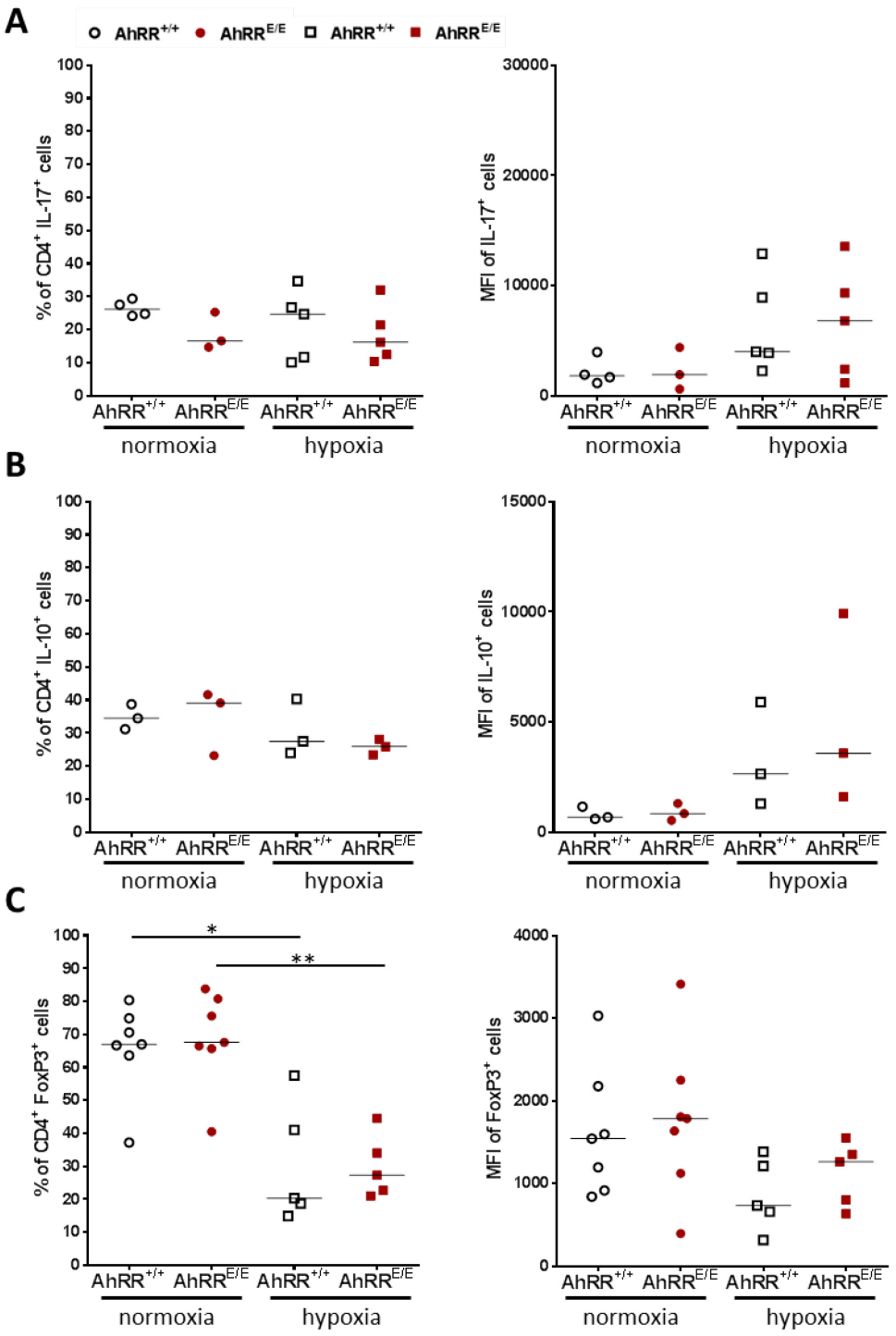

Figure 19 – Frequencies and MFI values of cytokine/FoxP3 positive CD4⁺ T cells of different *in vitro* differentiated helper T cell subsets cultured under normoxia or hypoxia. Quantification of the frequency and median fluorescence intensity (MFI) of IL-17A (T_h17) (**A**) and IL-10 (T_r1) (**B**) producing cells, and the frequency and MFI of FoxP3⁺ cells (T_{reg}) (**C**) from cultures of AhRR-deficient ($AhRR^{E/E}$, red) and wild-type ($AhRR^{+/+}$, open) CD4⁺ T cells differentiated under normoxia (circles) or hypoxia (squares). Different helper T cell populations were stained intracellularly for specific key cytokines after a 5 day culture in IMDM medium with the addition of helper T cell specific cytokine and antibody cocktails. n=3-7, pooled samples from 7 independent experiments. The black line represents the median. Significant differences are depicted as *p<0.05 and **p<0.01. Significance was calculated using unpaired students t-test.

Additionally, all key cytokines for each T cell subset were measured by ELISA. However, no significant differences between AhRR-deficient and wild-type cells were detected in the different helper T cell subsets differentiated under normoxia as wells as under hypoxia (Figure 20). Nevertheless, the same tendencies observed in the frequencies and MFI values, were also visible in the cytokine production. T_h17 cells, which exhibited slightly higher MFI values under hypoxic conditions (Figure 19A) also displayed a marginally higher IL-17 production under hypoxia compared to normoxia (Figure 20A). A reduced FoxP3 expression was detected in hypoxic T_{reg} cultures (Figure 19B), translating into significant reduction in TGFβ levels in both AhRR-deficient and wild-type cells (Figure 20B). Also, IL-10 levels were slightly lower in hypoxic T_r1 cells (Figure 20C).

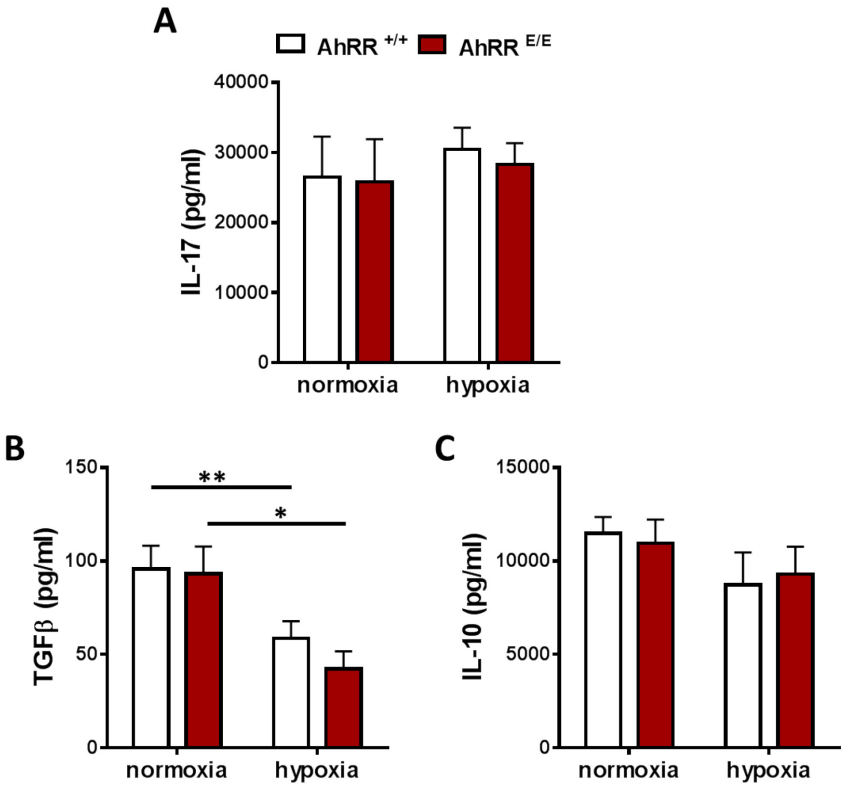

Figure 20 – Cytokine levels of *in vitro* differentiated helper T cell subsets under normoxia or hypoxia. Cytokine levels measured in the supernatants of AhRR-deficient ($AhRR^{E/E}$, red bars) or wild-type ($AhRR^{+/+}$, white bars) T_h17 cells (**A**), regulatory T cells (T_{reg}) (**B**) and T_r1 cells (**C**) after a 5 day culture in IMDM medium under normoxia or hypoxia with the addition of helper T cell specific cytokine and antibody cocktails. n=3-7, pooled samples from 7 independent experiments. The results are presented as mean plus SEM. Significant differences are depicted as *p<0.05 and **p<0.01. Significance was calculated using unpaired students t-test.

These results suggest that AhRR deficiency also does not exert a significant effect on *in vitro* differentiation of helper T cell subsets, such as T_h17, T_r1 and T_{reg} cells, when cultured under hypoxic conditions.

4.1.5. AhRR expression in different *in vitro* differentiated helper T cell subsets under hypoxic conditions

The AhRR/EGFP expression was analyzed in key cytokine/FoxP3 positive cells of the various helper T cell subsets directly comparing cells differentiated under normoxia with cells cultured under hypoxia (Figure 21). It could clearly be shown that AhRR/EGFP is significantly higher expressed in T_h17 and T_{reg} cells cultured under normoxic conditions as already seen in the results shown above (Figure 18 and 21). Furthermore, under hypoxia T_h17 and T_{reg} cells also show AhRR/EGFP expression, however, to a slightly lower extent (Figure 21). T_r1 cells express AhRR/EGFP under normoxia as well as under hypoxia, even to a higher extent than T_{reg} cells (Figure 21A).

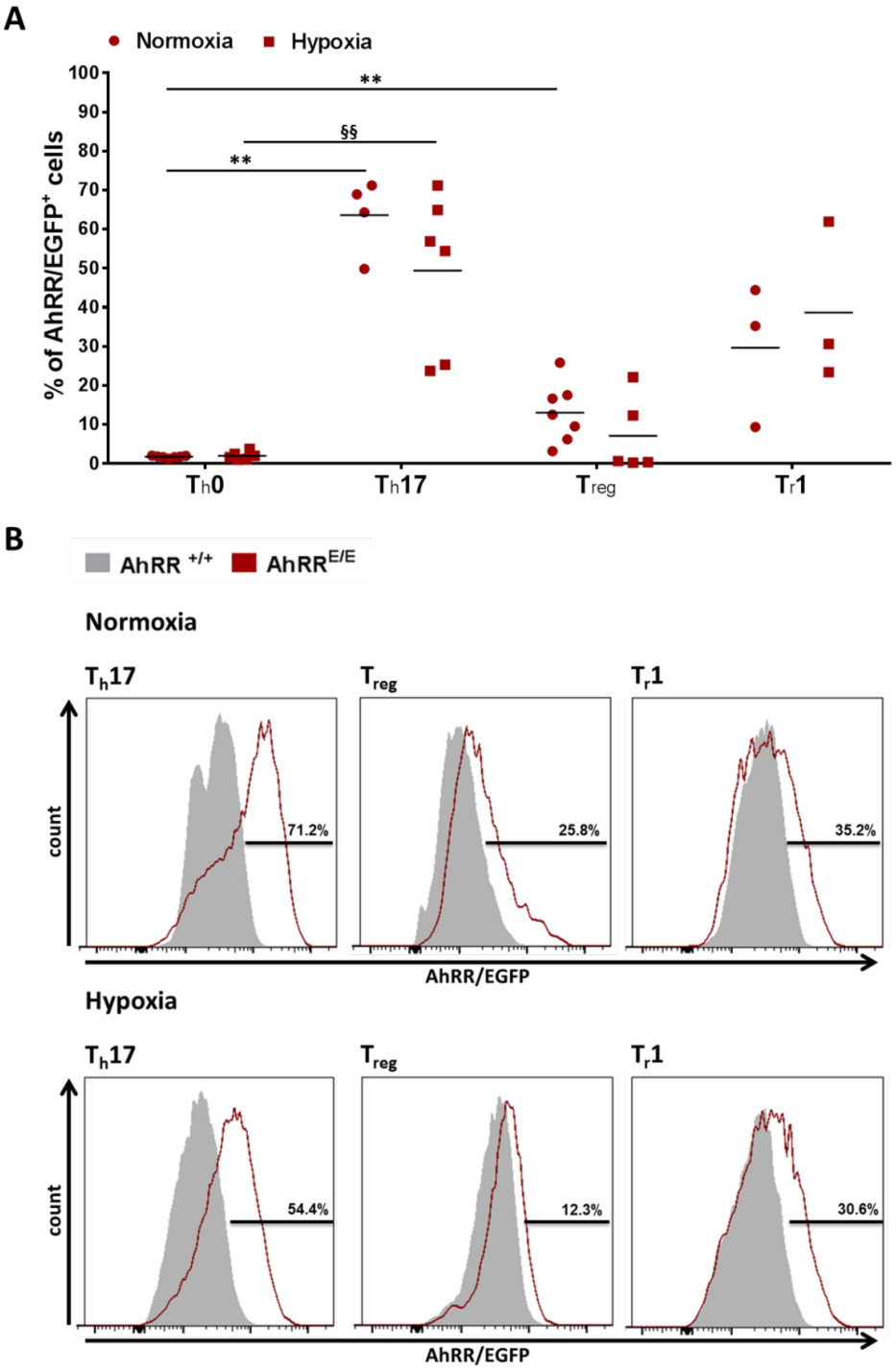

Figure 21 – AhRR/EGFP expression in specific key cytokine/FoxP3 positive cells from *in vitro* differentiated helper T cell subsets cultured under normoxia or hypoxia. (**A**) Quantification of the frequencies of AhRR/EGFP expressing T_h17, T_{reg} and T_r1 cells. n=3-7, pooled samples from 7 independent experiments. The black line represents the median. Significant differences are depicted as **p<0.01 (between data obtained from cultures under normoxia) and §§p<0.01 (between data obtained from cultures under hypoxia). Significance was calculated using unpaired students t-test. (**B**) Representative histograms depicting the AhRR/EGFP expression compared between wild-type ($AhRR^{+/+}$, grey filled) and AhRR-deficient ($AhRR^{E/E}$, red line) helper T cell subsets. AhRR/EGFP expression was analyzed in $CD4^+$ cytokine or $FoxP3^+$ cells only.

4.2. Role of the AhRR in parasitic infection with *Toxoplasma gondii*

As the AhRR is more prominently expressed in the small intestine in comparison to the large intestine [76], the role of the AhRR in an infection model causing an inflammation of the small intestine was analyzed. Oral infection of mice with the parasite *Toxoplasma gondii* results in an ileitis, which resembles the pathology of Morbus Crohn in humans [129].

AhR-deficient mice were shown to be highly susceptible to *Toxoplasma gondii* infections, as indicated by increased weight loss [84]. Furthermore, an enhanced susceptibility in both AhR and AhRR knock out mice was observed in DSS-induced colitis [76], [101]. Considering these findings, investigating the role of the AhRR in *Toxoplasma gondii* infections might provide additional information on the interplay between AhR and its repressor.

The *Toxoplasma gondii* infection model was established with the help of Daniel Degrandi and Klaus Pfeffer (Institute of Medical Microbiology, Heinrich Heine University Düsseldorf). CD-1 mice are resistant to *Toxoplasma gondii* induced pathology and were therefore used to propagate the parasite. The parasites were isolated from the brain and were then orally administered to female AhRR-deficient and wild-type littermate control mice.

4.2.1. Survival analysis of *Toxoplasma gondii* infections in AhRR-deficient mice and wild-type littermate control mice

First survival experiments were performed by oral administration of 200 cysts per mouse (Figure 22). The mice were weighed regularly and it was attempted to harvest stool samples to examine possible occult blood as a sign of inflammation of the small intestine. This, however, turned out to be impossible. Instead of having diarrhea as a result of the inflammation, the infected mice seemed to stop feeding, and hence excreted almost no

feces. Coherently, a severe weight loss was observed in addition to grooming deficits and impaired behavior indicated by a high clinical score (Figure 22B). Thus, the application of 200 cysts per mouse appeared to induce a very severe infection, which led to a 100% death rate 9 days post infection in both AhRR-deficient and wild-type mice (Figure 22A). Control mice received PBS and as expected did not show any weight loss, grooming deficits or behavioral changes.

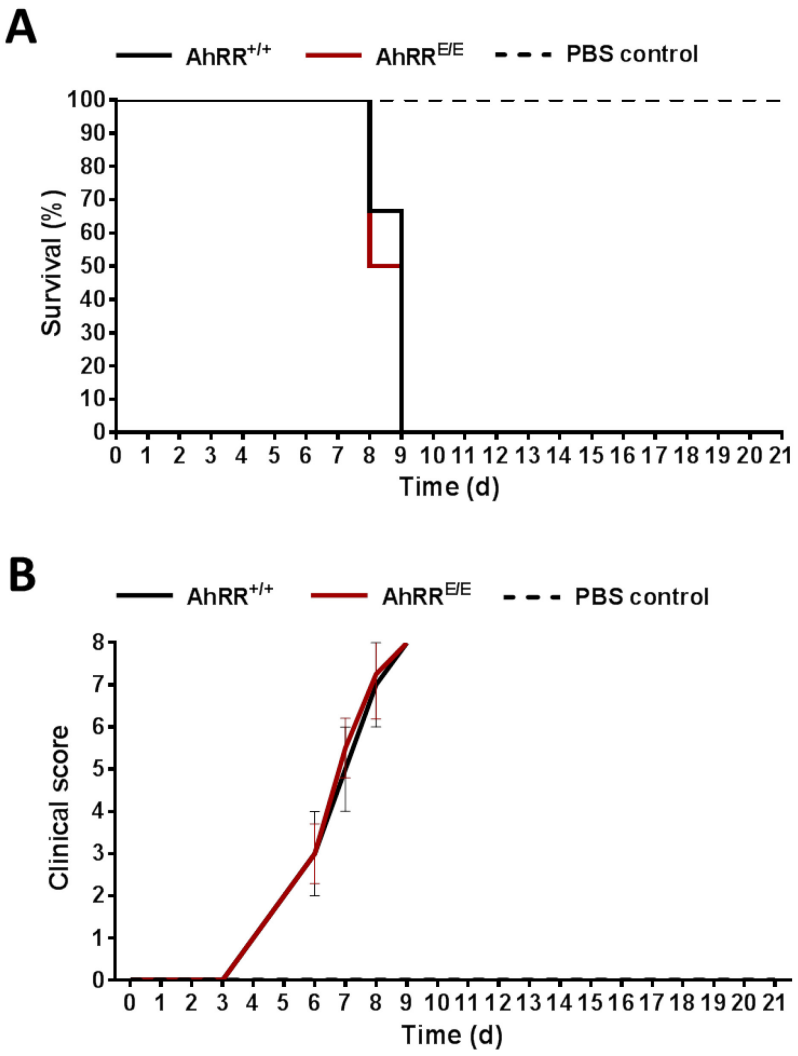

Figure 22 – *Toxoplasma gondii*-induced ileitis using 200 cysts leads to 100% lethality and severe weight loss. Survival curves (**A**) and clinical scores (**B**) of AhRR-deficient ($AhRR^{E/E}$, red line) and wild-type ($AhRR^{+/+}$, black line) female mice after *Toxoplasma gondii* infection with 200 cysts were analyzed. Control mice (dotted black line) of each genotype received PBS. n=3-4 ($AhRR^{E/E}$ n=4, with all mice sacrificed after obtaining a clinical score of 8, $AhRR^{+/+}$ n=3, with all mice sacrificed after obtaining a clinical score of 8)

Consequently, the next survival experiments were performed with only 100 orally administered cysts per mouse (Figure 23). In this setup, AhRR-deficient mice displayed a

higher susceptibility to this parasite induced ileitis with a 100% death rate by day 12 post infection compared to wild-type controls, which showed an 88% death rate (Figure 23A). During the progression of the infection the mice suffered from drastic weight loss and grooming deficits as seen in the raised clinical score (Figure 23B).

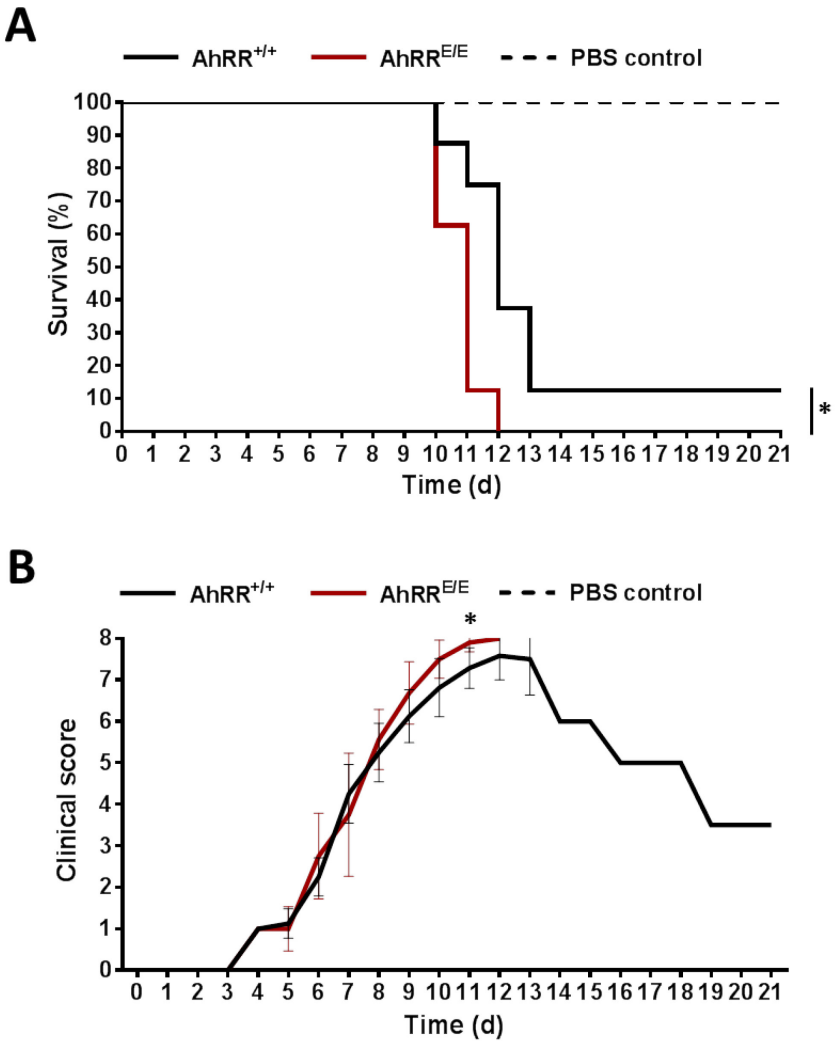

Figure 23 – AhRR deficiency leads to 100% lethality and drastic weight loss after administration of 100 *Toxoplasma gondii* cysts. Survival curves (**A**) and clinical scores (**B**) of AhRR-deficient ($AhRR^{E/E}$, red line) and wild-type ($AhRR^{+/+}$, black line) female mice after *Toxoplasma gondii* infection with 100 cysts were analyzed. Control mice (dotted black line) of each genotype received PBS. n=8, data pooled from 2 independent experiments ($AhRR^{E/E}$ n=8, with all mice sacrificed after obtaining a clinical score of 8, $AhRR^{+/+}$ n=8, with 7 mice sacrificed after obtaining a clinical score of 8). Significant differences are depicted as *$p<0.05$. Significance was calculated using Log-rank (Mantel-cox) test.

As the infection with 100 cysts was still rather severe, the next experiments were performed with 50 orally administered cysts per mouse (Figure 24). In this setting, AhRR-deficient mice were clearly more susceptible to *Toxoplasma gondii* induced ileitis with

18% survival rate compared to wild-type controls with 50% survival rate (Figure 24A). Using this lower number of cysts, the clinical score also displayed a visible difference between AhRR-deficient mice and wild-type mice (Figure 24B).

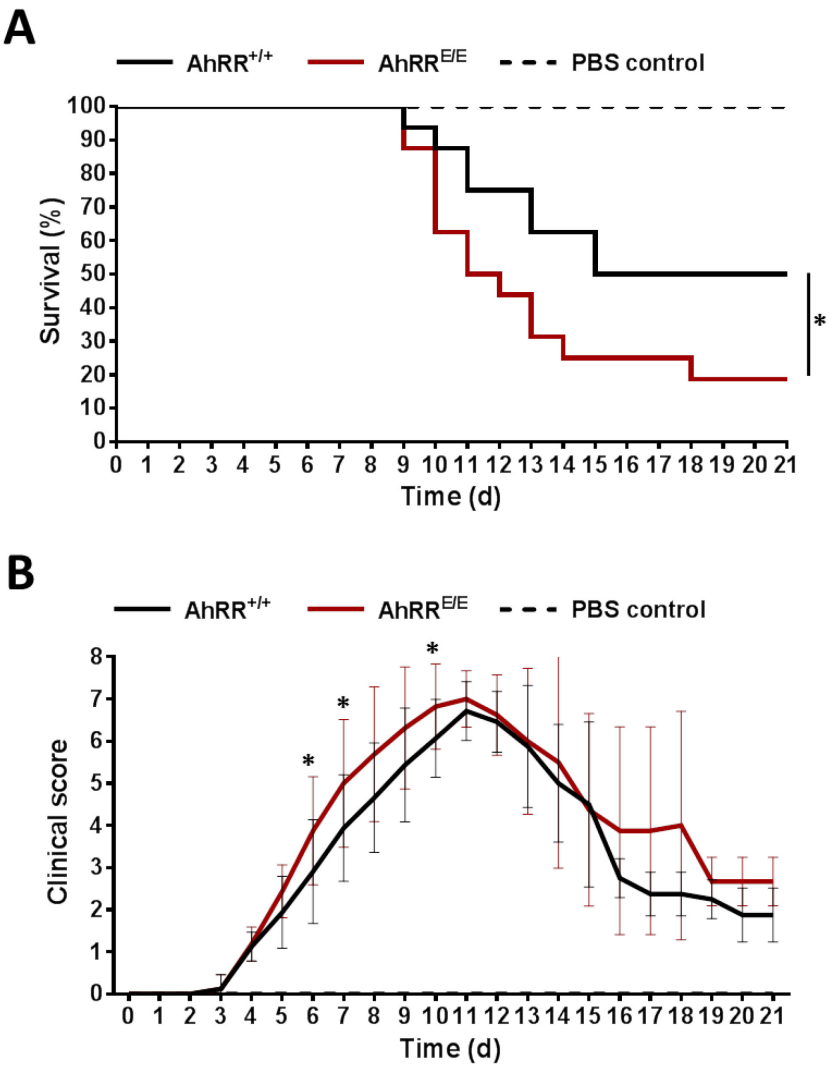

Figure 24 – *Toxoplasma gondii*-induced ileitis with 50 cysts leads to significantly enhanced susceptibility in AhRR-deficient mice compared to wild-type mice. Survival curves (**A**) and clinical scores (**B**) of AhRR-deficient ($AhRR^{E/E}$, red line) and wild-type ($AhRR^{+/+}$, black line) female mice after *Toxoplasma gondii* infection with 50 cysts were analyzed. Control mice (dotted black line) of each genotype received PBS. n=16, data pooled from 3 independent experiments ($AhRR^{E/E}$ n=16, with 13 mice sacrificed after obtaining a clinical score of 8, $AhRR^{+/+}$ n=16, with 8 mice sacrificed after obtaining a clinical score of 8). Significant differences are depicted as *p<0.05. Significances were calculated using (**A**) Log-rank (Mantel-cox) test and (**B**) unpaired students t-test.

Survival experiments with only 25 orally administered cysts per mouse (Figure 25) demonstrated even more prominently that AhRR-deficient mice are significantly more sensitive compared to wild-type littermate controls, exhibiting a 20% survival rate in

contrast to a 71% survival rate, respectively (Figure 25A). This differences in survival between AhRR-deficient mice and wild-type mice were also reflected in the clinical scores (Figure 25B). Over the course of infection AhRR-deficient mice weighed less than wild-type mice, exhibited more grooming deficits and behavioral changes, as indicated by significant differences in the clinical score (Figure 25B).

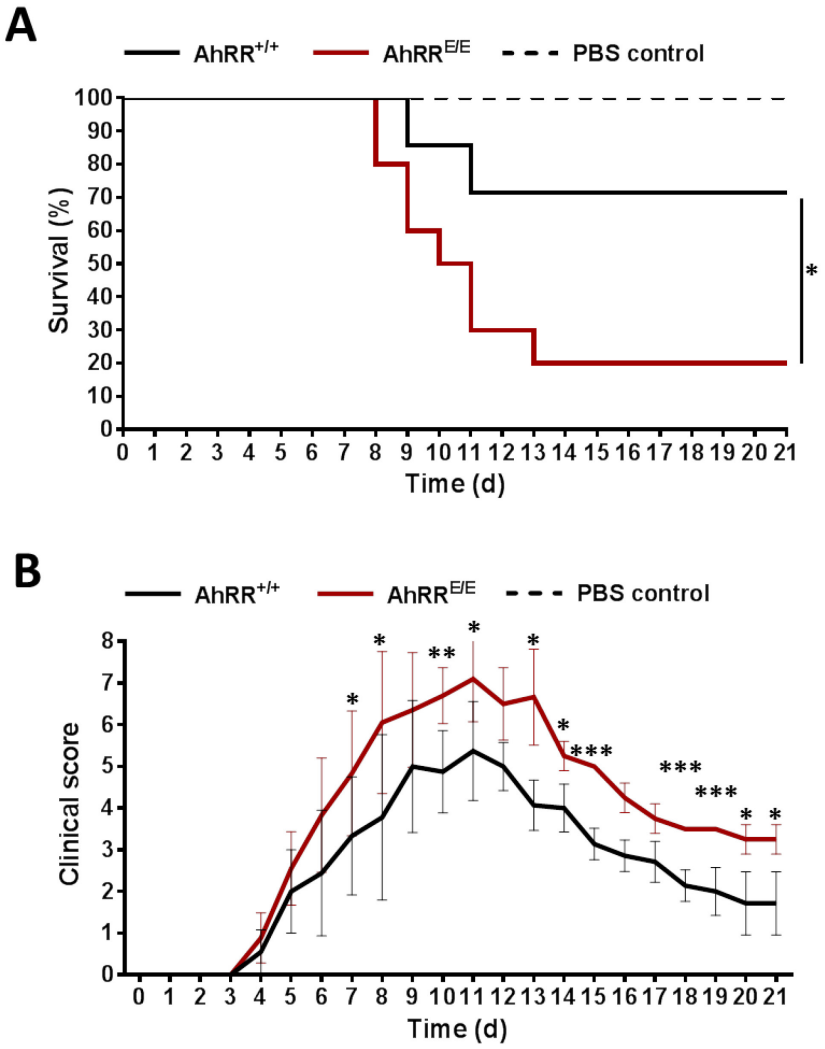

Figure 25 – AhRR-deficient mice are significantly more sensitive to *Toxoplasma gondii*-induced ileitis with 25 cysts compared to wild-type littermate control mice. Survival curves (**A**) and clinical scores (**B**) of AhRR-deficient ($AhRR^{E/E}$, red line) and wild-type ($AhRR^{+/+}$, black line) female mice after *Toxoplasma gondii* infection with 25 cysts were analyzed. Control mice (dotted black line) of each genotype received PBS. n=7-10 ($AhRR^{E/E}$ n=10, with 8 mice sacrificed after obtaining a clinical score of 8, $AhRR^{+/+}$ n=7, with 2 mice sacrificed after obtaining a clinical score of 8). Significant differences are depicted as *p<0.05, **p<0.01 and ***p<0.001. Significances were calculated using (**A**) Log-rank (Mantel-cox) test and (**B**) unpaired students t-test.

These results demonstrate that AhRR-deficient mice are significantly more susceptible to *Toxoplasma gondii* induced ileitis than wild-type littermate control mice. Furthermore, the difference in survival was more apparent using lower numbers of administered cysts and could be mirrored in the clinical scores.

In summary, these data demonstrate that AhRR deficiency results in enhanced susceptibility in *Toxoplasma gondii* induced ileitis similar to AhR deficiency [84]. This finding is in line with previous studies, showing that both AhR- and AhRR-deficient mice are susceptible to DSS-induced colitis [76], [101], [102] and indicating that the extent of AhR activation in the intestine needs to be tightly balanced for prevention of intestinal immunopathology.

4.2.2. *Ex vivo* analysis of *Toxoplasma gondii* infected AhRR-deficient and wild-type littermate control mice

In order to understand why AhRR deficiency causes enhanced susceptibility in *Toxoplasma gondii* induced ileitis, infected tissues were analyzed *ex vivo*. *Ex vivo* analysis was performed at day 8 post infection, as in all survival experiments, irrespective of the number of administered cysts, the infected mice succumbed earliest 8 days post infection. These observations are in line with published data, showing that C57BL/6 mice infected with *Toxoplasma gondii* develop an acute phase of inflammation between day 6 and day 8 post infection [167]. The mice used for the *ex vivo* analysis were orally infected with 50 *Toxoplasma gondii* cysts.

Several parameters were used to evaluate the severity of the infection, such as the intestinal length, the parasite burden present in the small intestine, histological analysis of the structural changes, and *Toxoplasma gondii* distribution along the ileum as well as the production of pro-inflammatory cytokines.

The shortening of the small intestine can be used as a parameter for the establishment of the infection and is commonly used in the assessment of infection in colitis models. In the ileitis model used in this thesis, infected mice also exhibited reduced small intestinal length in comparison to naïve control mice (Figure 26). For both AhRR-deficient mice and

wild-type littermate control mice there was a significant difference between uninfected, naïve mice and *Toxoplasma gondii* infected mice. As initial values of intestinal length determined for naïve mice differed between AhRR-deficient and wild-type mice, it was difficult to define whether there are differences between the infection-related intestinal shortening of AhRR-deficient and wild-type mice. Therefore, the relative intestinal shortening was calculated according to Heimesaat *et al.* [167], revealing that infected wild-type mice displayed a relative intestinal shortening of 14,17% and infected AhRR-deficient mice exhibited 14,73% relative intestinal shortening. Consequently, it can be concluded that there are no differences in the intestinal shortening between AhRR-deficient and wild-type mice after *Toxoplasma gondii* infection.

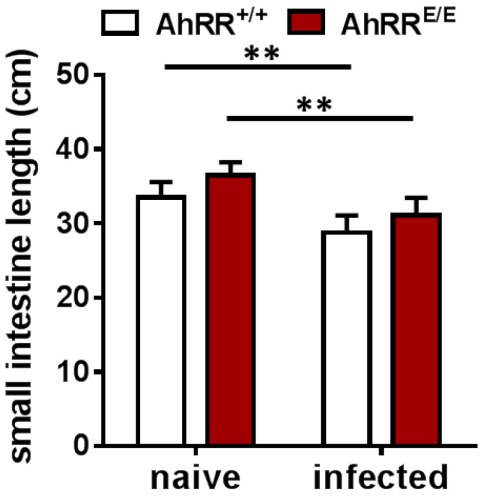

Figure 26 – AhRR-deficient mice exhibit no differences in intestinal shortening compared to wild-type mice 8 days post *Toxoplasma gondii* infection with 50 cysts. Intestinal shortening of naïve AhRR-deficient ($AhRR^{E/E}$, red bar) and wild-type ($AhRR^{+/+}$, white bar) female mice and infected mice 8 days after *Toxoplasma gondii* infection with 50 cysts. n=4-12, pooled from 4 independent experiments. The results are presented as mean plus SEM. Significant differences are depicted as **p<0.01. Significance was calculated using unpaired students t-test.

Next, the parasite load in the small intestine was analyzed by qRT-PCR. Both infected AhRR-deficient mice and infected wild-type mice displayed approximately 2 to 3 fold higher parasite burden than naïve AhRR-deficient mice and wild-type mice, respectively, when normalized to naïve wild-type mice (Figure 27). Despite of a tendency that infected

AhRR-deficient mice exhibited a lower parasite burden compared to infected wild-type mice (Figure 27) no statistical significant level could be reached.

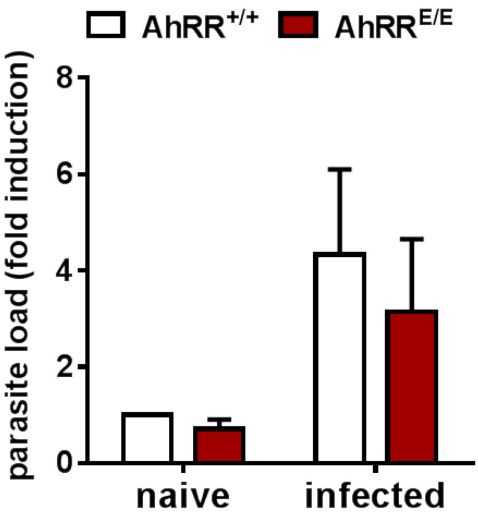

Figure 27 – AhRR-deficient mice exhibit slightly reduced parasite burden compared to wild-type mice 8 days post *Toxoplasma gondii* infection with 50 cysts. Parasite burden of naïve AhRR-deficient ($AhRR^{E/E}$, red bar) and wild-type ($AhRR^{+/+}$, white bar) female mice and infected mice 8 days after *Toxoplasma gondii* infection with 50 cysts. n=4-12, pooled from 4 independent experiments. The results are presented as mean plus SEM.

In summary, these results were not anticipated, as AhRR deficiency led to higher susceptibility analyzed in survival experiments. Therefore, it was expected that AhRR-deficient mice would exhibit greater intestinal shortening as well as an equal or higher parasite burden. After oral *Toxoplasma gondii* infection, however, the survival rate not only depends on the parasite load, but also on the immunopathology induced by the parasite.

For this reason, intestinal histopathology was analyzed 8 days post infection with *Toxoplasma gondii* using H&E stained paraffin sections. The representative microscopic images shown in Figure 28A clearly depict that ileum samples from infected AhRR-deficient mice exhibit more tissue damage compared to ileum samples from infected wild-type mice. This observation is supported by a significant difference in the histological score (Figure 28B). The histological scores were calculated by classifying epithelial changes in the mucosa and submucosa, such as erosions, ulcerations or necrosis, and changes in the mucosal architecture, such as the distortion of villous structure [160]. Ileal

mucosa samples of infected AhRR-deficient mice were visibly necrotic and fibrotic, and exhibited distorted villi, whereas ileum samples of infected wild-type mice mostly displayed diffuse cell infiltrates in the mucosa or submucosa, marginal villous blunting and only rarely distortions of the villi (Figure 28A).

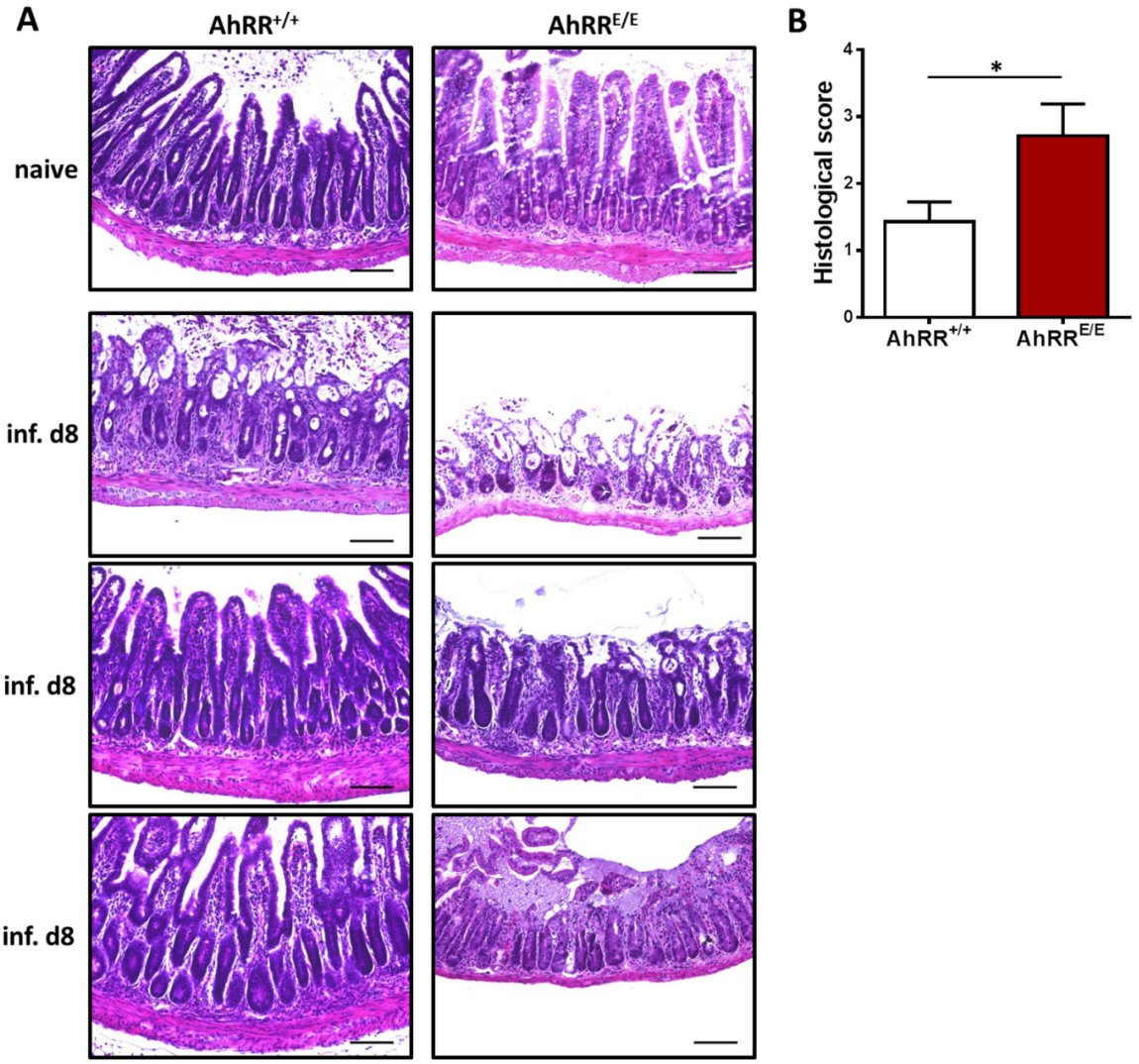

Figure 28 – AhRR-deficient mice displayed significantly stronger ileal tissue damage than wild-type mice 8 days post *Toxoplasma gondii* infection with 50 cysts. Representative H&E staining (**A**) of naïve AhRR-deficient ($AhRR^{E/E}$) and wild-type ($AhRR^{+/+}$) female mice, and infected mice 8 days after *Toxoplasma gondii* infection. Scale bar: 100 µm. Histological scores (**B**) of H&E stained paraffin ileal sections from AhRR-deficient ($AhRR^{E/E}$, red bar) and wild-type ($AhRR^{+/+}$, white bar) female mice 8 days after *Toxoplasma gondii* infection. n=7, pooled from 3 independent experiments. The results are presented as mean plus SEM. Significant differences are depicted as *$p<0.05$. Significance was calculated using unpaired students t-test.

To sum up, histopathology of AhRR-deficient mice was more severe than that of wild-type mice and in line with the results obtained in survival experiments. AhRR deficiency caused

significantly more damage to the intestinal structure, which may have caused the higher lethality in *Toxoplasma gondii*-induced ileitis.

Next, colonization of ileal tissue with *Toxoplasma gondii* was assessed. Using *Toxoplasma gondii* specific rabbit serum, which was kindly provided by Ingrid Reiter-Owona (University Hospital Bonn), murine intestinal samples from infected AhRR-deficient mice and wild-type mice were stained. Strikingly, the *Toxoplasma gondii* staining pattern revealed a patchy distribution as seen in the four representative microscopic pictures of infected ileal samples of both AhRR-deficient mice and wild-type mice depicted in Figure 29. As described in the literature, *Toxoplasma gondii* infects epithelial cells, proliferates and then spreads to neighboring cells, possibly accounting for the patchy appearance of the staining [121], [122]. Spreading of the parasite from one cell to the next cell, leaves the infected cells damaged, leading to the loss of EGFP as it leaks out of the injured cell (Figure 29).

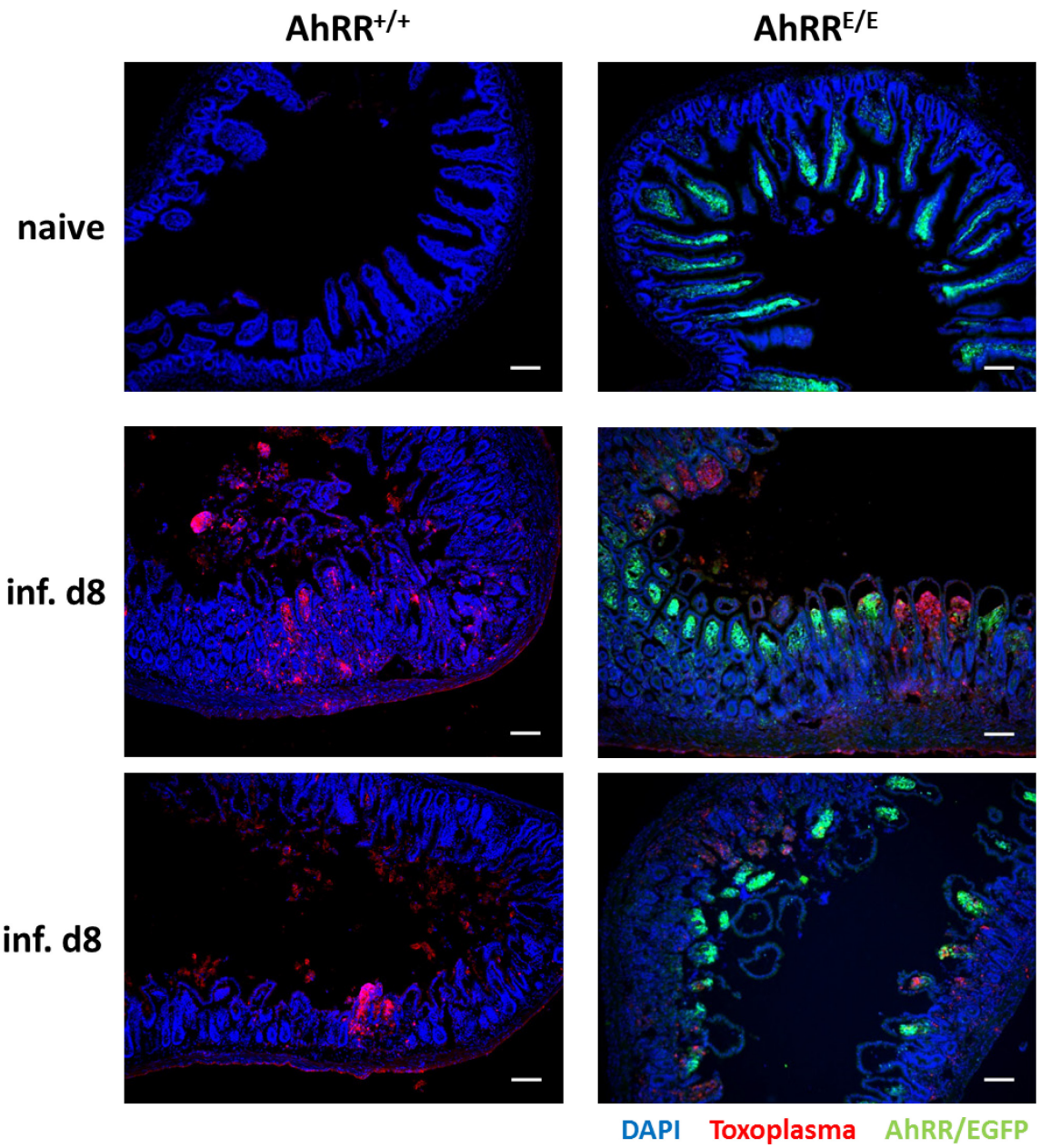

Figure 29 – Immunofluorescent staining of *Toxoplasma gondii* infected ilea from AhRR-deficient and wild-type mice 8 days post *Toxoplasma gondii* infection with 50 cysts. Representative immunofluorescent stainings of naïve AhRR-deficient ($AhRR^{E/E}$) and wild-type ($AhRR^{+/+}$) female mice, and infected mice 8 days after *Toxoplasma gondii* infection. Sections were stained with rabbit serum against *Toxoplasma gondii* ME49/α-rabbit-eFluor594 (red) and counterstained with DAPI (blue). Scale bar: 100 µm.

The analysis of the *Toxoplasma gondii* infection pattern, however, did not reveal any differences between infected AhRR-deficient and wild-type mice. Furthermore, no obvious difference in the quantity of *Toxoplasma gondii* infected tissue was observed.

Moreover, it was attempted to measure the production of different pro-inflammatory cytokines in the the duodenum, jejunum and ileum of the small intestine. In addition, two different methods for the extraction and measurement of cytokines were tested. On the one hand, cytokines were measured in the supernatants of organ cultures, in which the three different intestinal parts were incubated in complete RPMI medium for 6 h (Figure 30), and the cytokine concentration was normalized to the weight of the tissue sample. On the other hand, the samples of the different intestinal regions were homogenized, cellular debris was removed by centrifugation and the cytokines were measured in the supernatant (Figure 31). Again, the cytokine concentration was calculated based on the weight of the tissue sample. *Toxoplasma gondii* induced ileitis has been characterized by an overproduction of pro-inflammatory cytokines, such IFNγ and TNF, in a helper T cell-dependent manner [168], [169]. Furthermore, elevation in IL-12 levels indicate the activation of the helper T cells by DCs, which are critical for the pathology of the small intestine [170]. In addition to that, IL-23 has been described to play a role in the inflammation of the small intestine during *Toxoplasma gondii* infection [169]. Most interestingly, IL-17 expression was elevated in the intestinal mucosa of IBD patients (reviewed in [171]). Therefore, the panel of cytokines measured included IFNγ, TNF, IL-1β, IL-12p70, IL-23 and IL-17.

All cytokine levels measured in jejunal and ileal samples showed the same tendencies using both methods. Regarding the duodenal samples however, homogenized samples displayed very low cytokine levels compared to jejunal und ileal samples (Figure 31), whereas cytokines measured in the supernatants of duodenum cultures exhibited rather high levels in comparison to jejunal and ileal samples (Figure 30).

Toxoplasma gondii infection has been described to mainly affect the ileum, possibly spreading to the jejunum [129]. Since the cytokine levels measured in the duodenal samples differ between the different methods and therefore might be unreliable, only the data obtained from the jejunal and ileal samples were considered for further discussion.

Of particular note is the significant decrease in IFNγ levels in AhRR-deficient ileal samples measured in the supernatants of ileum cultures (Figure 30A). A similar tendency was observable in jejunum cultures. This might be an explanation for the impaired survival, as IFNγ is a key player in the defense against *Toxoplasma gondii* infection [116], [129]. Apart

from IFNγ, all other cytokine levels measured in ileum cultures revealed no significant differences between infected AhRR-deficient and wild-type mice, whereas the pro-inflammatory cytokines TNF (Figure 30B), IL-1β (Figure 30C), IL-12 (Figure 30) and IL-23 (Figure 30E) appeared elevated in jejunum cultures of AhRR-deficient mice.

In addition, IL-17 levels were elevated in jejunum cultures from AhRR-deficient mice (Figure 30F), indicating a possible role for T_h17/T_c17 cells in the defense against *Toxoplasma gondii* infection as well as suggesting influences of pathogenic T_h17 cells.

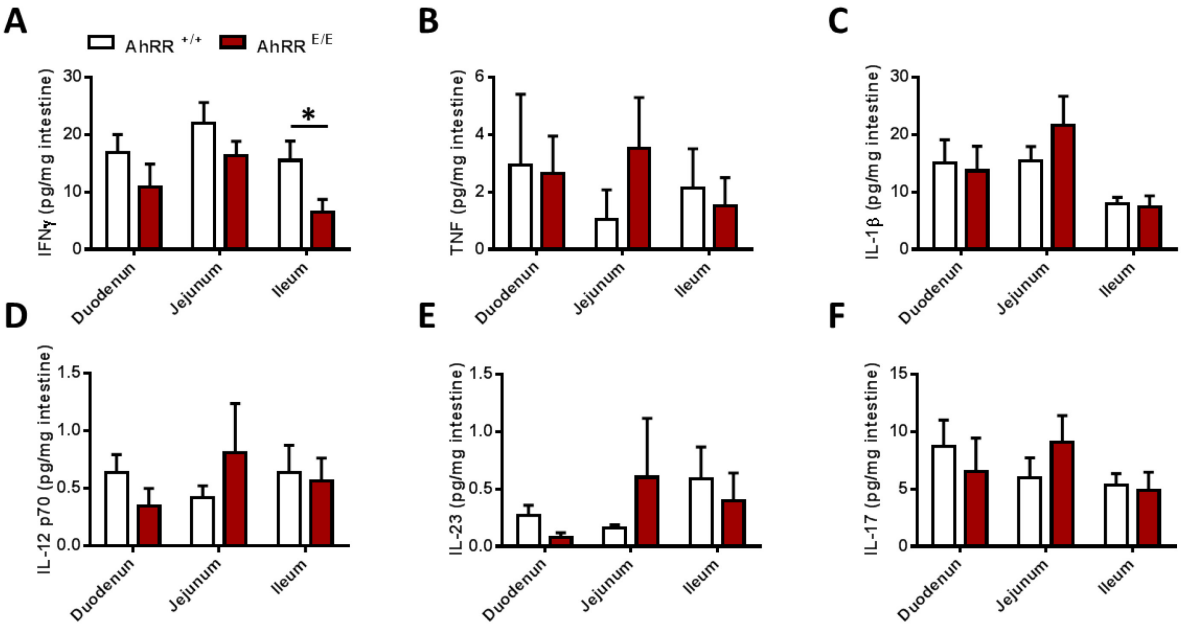

Figure 30 – Cytokine levels of intestinal cultures of AhRR-deficient and wild-type mice 8 days post *Toxoplasma gondii* infection with 50 cysts. Intestinal cultures of naïve AhRR-deficient ($AhRR^{E/E}$, red bar) and wild-type ($AhRR^{+/+}$, white bar) female mice, and infected mice 8 days after *Toxoplasma gondii* infection with 50 cysts were analyzed for IFNγ (**A**), TNF (**B**), IL-1β (**C**), IL-12p70 (**D**), IL-23 (**E**) and IL-17 (**F**). n=9, pooled samples from 3 independent experiments. The results are presented as mean plus SEM. Significant differences are depicted as *p<0.05. Significance was calculated using unpaired students t-test.

In contrast to cytokines measured in the supernatants of organ cultures, the method of homogenizing intestinal samples led to higher cytokine levels. But the same tendencies were also detected with this method. As mentioned before, IFNγ levels were decreased in AhRR-deficient homogenized jejunal samples in comparison to wild-type samples (Figure 31A). In contrast, pro-inflammatory cytokines, such as TNF (Figure 31B), IL-1β (Figure 31C), IL-12p70 (Figure 31D), IL-23 (Figure 31E) and IL-17 (Figure 31F) were elevated in

jejunal samples from infected AhRR-deficient mice similar to the effects observed in jejunum organ cultures (Figure 30). Ileal samples also showed no distinct differences for all cytokines measured, except for slightly increased IL-1β levels in AhRR-deficient ileal samples (Figure 31C).

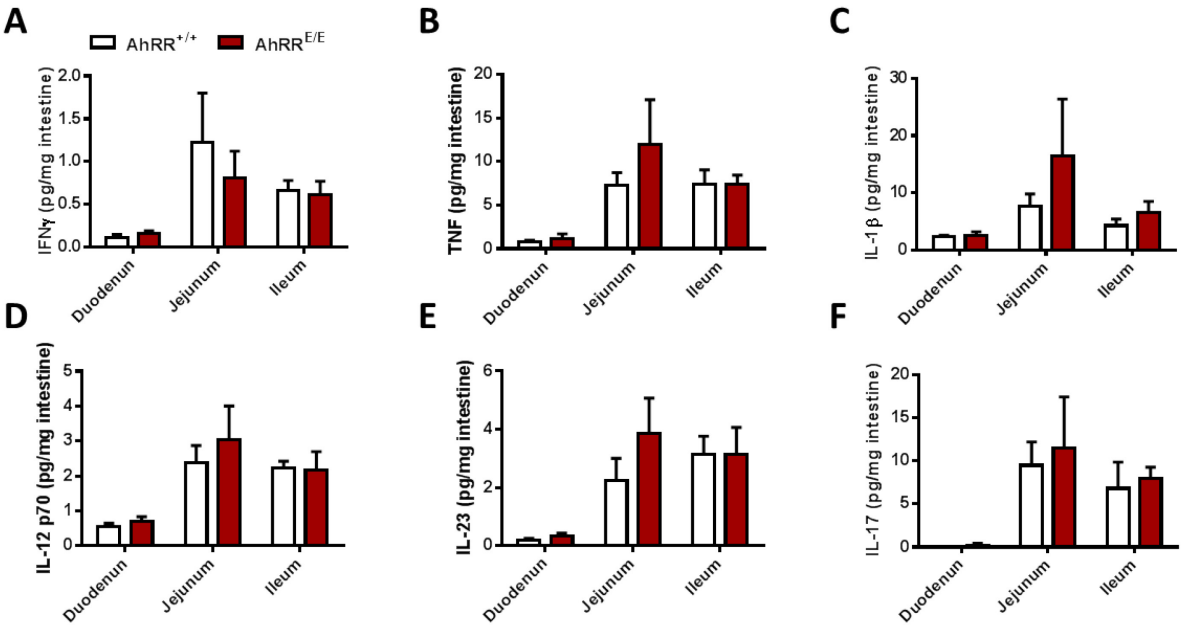

Figure 31 – Cytokine levels of homogenized intestinal tissue of AhRR-deficient and wild-type mice 8 days post *Toxoplasma gondii* infection with 50 cysts. Homogenized intestinal tissue of naïve AhRR-deficient ($AhRR^{E/E}$, red bar) and wild-type ($AhRR^{+/+}$, white bar) female mice, and infected mice 8 days after *Toxoplasma gondii* infection with 50 cysts were analyzed for IFNγ (**A**), TNF (**B**), IL-1β (**C**), IL-12p70 (**D**), IL-23 (**E**) and IL-17 (**F**). n=4. The results are presented as mean plus SEM.

In summary, measurement of cytokine levels after *Toxoplasma gondii* infection revealed a slight increase in several pro-inflammatory cytokines in the jejunum of AhRR-deficient mice compared to wild-type mice. In contrast, IFNγ levels were clearly reduced in intestinal samples of AhRR-deficient mice.

4.3. Influence of the AhRR in polymicrobial sepsis induced by the colon ascendens stent peritonitis model

To induce a polymicrobial peritonitis in mice, the CASP model, a standardized rodent model for sepsis was used [152]. In this model, a small stent is surgically inserted into the ascending colon of mice, creating a continuous link between the intestinal lumen and the peritoneal cavity resulting in a septic peritonitis. The severity of the infection can be controlled by the diameter of the inserted stent (14G, 16G, 18G or 20G). At first, an experiment with female wild-type mice was carried out, comparing 14G and 16G stents (Figure 32A). As expected, mice, which received a 14G stent had a lower survival rate of 33%, whereas 66% mice, which received the smaller stent (16G), survived. Additionally, the mice with the surgically inserted 14G stent on average developed lethal septic shock syndrome 19 hours earlier than the mice with the 16G stent (Figure 32A).

As a result, survival experiments were performed with 16G stents, since the sepsis induced with 14G stents might have been too severe to be able to properly detect differences in susceptibility to sepsis comparing AhRR-deficient mice to heterozygous AhRR-EGFP-reporter and wild-type littermate control female mice. A slightly higher survival rate of 20% in AhRR-deficient female mice compared to wild-type littermate controls after induction of polymicrobial sepsis by CASP using 16G stents was detectable (Figure 32B). Heterozygous AhRR-EGFP-reporter mice also displayed a higher survival rate than wild-type mice. However, they did not show the same protection as observed in AhRR-deficient mice (Figure 32B).

Additionally, the survival experiments were performed with male mice, in order to compare possible gender differences in response to the septic infection (Figure 32C). Here, similar tendencies as seen in female mice were also observed in male mice, however, less pronounced. Male AhRR-deficient mice showed a 10% higher survival rate compared to wild-type control mice (Figure 32C). Heterozygous AhRR-EGFP-reporter mice again exhibited a survival rate between AhRR-deficient and wild-type mice (Figure 32C). These findings are in line with the observed protection of AhRR-deficient mice against

LPS-induced septic shock [76], allowing the conclusion that the AhR/AhRR-system plays a role in the defense against pathogens.

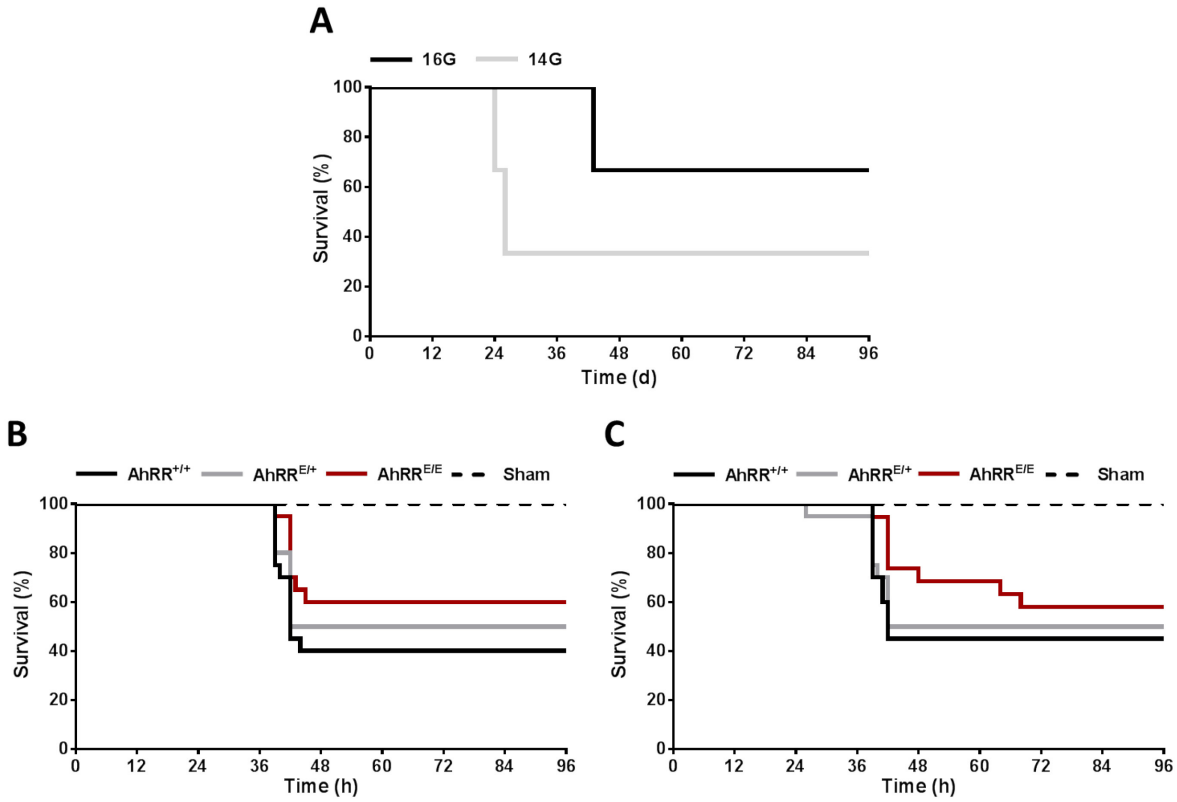

Figure 32 – Survival analysis of AhRR-deficient and wild-type mice after the induction of polymicrobial sepsis using the Colon Ascendens Stent Peritonitis (CASP) model. (**A**) Survival rate of wild-type female mice after CASP surgery using 14G stents (grey) and 16G stents (black) was assessed. n=3. Survival curve of AhRR-deficient ($AhRR^{E/E}$, red), AhRR-EGFP-reporter ($AhRR^{E/+}$, grey) and wild-type ($AhRR^{+/+}$, black) female mice (**B**) and male mice (**C**) after CASP surgery using a 16G sized stent was analyzed. n=20, pooled from 8 independent experiments. ($AhRR^{E/E}$ n=20, with 8 female and 8 male mice sacrificed, $AhRR^{E/+}$ n=20, with 10 female and 10 male mice sacrificed, $AhRR^{+/+}$ n=20, with 8 female and 11 male mice sacrificed after obtaining to severe clinical scores)

4.4. Role of the AhR and AhRR in endotoxin tolerance

Our group could show that the AhRR is upregulated by TLR stimulation in DCs and macrophages *in vitro* and *in vivo*. Furthermore, it has been shown that AhRR-deficient mice are less susceptible to LPS-induced septic shock compared to wild-type control mice [76]. As repeated stimulation with LPS leads to endotoxin tolerance [140]–[143], it was interesting to assess whether the AhR/AhRR system also plays a role in the induction of

endotoxin tolerance. In fact, requirement of AhR signaling for development of endotoxin tolerance was recently described in the literature [161].

4.4.1. *In vitro* endotoxin tolerance analysis of AhR-deficient, AhRR-deficient and wild-type BMMϕ

To induce endotoxin tolerance *in vitro,* bone marrow derived macrophages (BMMϕ) from AhR-deficient (Figure 33A), AhRR-deficient mice (Figure 33B) or wild-type littermate controls were stimulated with three different low dose LPS treatments (1, 10 and 20 ng/ml) for 20 hours. Subsequently, the cells were challenged once with the same LPS doses for 6 hours. The supernatants were analyzed for TNF production by ELISA. However, no differences in endotoxin tolerance induction between BMMϕ from the different genotypes were observed (Figure 33A and B). These results indicate that AhR or AhRR deficiency plays no obvious role in the induction of endotoxin tolerance *in vitro*. BMMϕ which were only challenged with LPS once exhibited high TNF levels, independently of AhR or AhRR deficiency (Figure 33A and B).

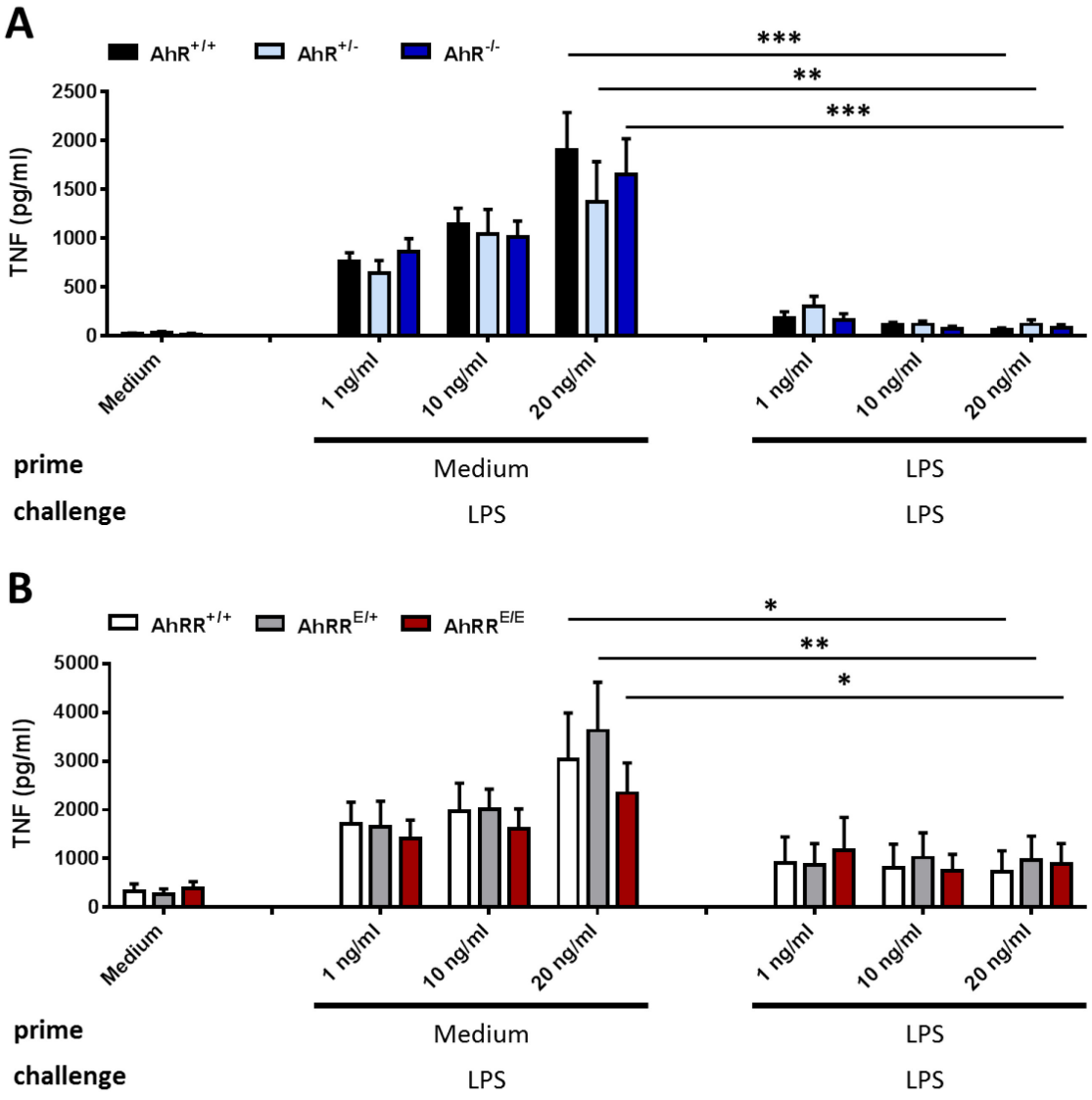

Figure 33 – *In vitro* endotoxin tolerance induction in bone marrow-derived macrophages of AhR, AhRR and wild-type mice. TNF levels in the supernatants measured by ELISA in BMMϕ cultures of AhR-deficient ($AhR^{-/-}$, blue bars), AhR-heterozygous ($AhR^{+/-}$, light blue bars) and wild-type ($AhR^{+/+}$, black bars) mice (**A**) and in BMMϕ cultures of AhRR-deficient ($AhRR^{E/E}$, red bars), AhRR-EGFP-reporter ($AhRR^{E/+}$, grey bars) and wild-type ($AHRR^{+/+}$, white bars) mice (**B**) after 1st LPS stimulation for 20 hours followed by 2nd LPS stimulation for 6 hours (depicted on the right), as well as after only 2nd LPS stimulation (depicted in the middle) and medium control (neg. control, depicted on the left)). (**A**) n=4-5, pooled samples from 4 independent experiments; (**B**) n=4, pooled samples from 4 independent experiments. The results are presented as mean plus SEM. Significant differences are depicted as *p<0.05, **p<0.01 and ***p<0.001. Significance was calculated using unpaired students t-test.

4.4.2. *In vivo* endotoxin tolerance analysis of AhR-deficient, AhRR-deficient and wild-type mice

Since the analysis *in vitro* might not necessarily reflect the situation *in vivo*, an *in vivo* endotoxin tolerance assay was also established. AhR-deficient, AhRR-deficient and wild-type mice were primed i.p. with a low dose of LPS (4 mg/kg). Four days later, the mice were challenged i.p. with a higher dose of LPS (15 mg/kg). 90 minutes thereafter the mice were sacrificed and the serum was collected and analyzed for TNF levels by ELISA. However, also *in vivo* no differences between LPS primed and challenged wild-type and AhR-deficient mice could be observed (Figure 34A). Also, analysis of AhRR-deficient and wild-type mice revealed that both were able to establish endotoxin tolerance (Figure 34B). Notably, AhRR-deficient mice that received only the 2nd LPS challenge leading to LPS-induced septic shock in wild-type mice, displayed significantly reduced TNF levels compared to wild-type mice, in accordance with the protective effect facilitated by AhRR deficiency (Figure 34B) [76]. In contrast, AhR-deficient mice exhibited TNF levels comparable to wild-type mice after a single challenge with high dose LPS (Figure 34A).

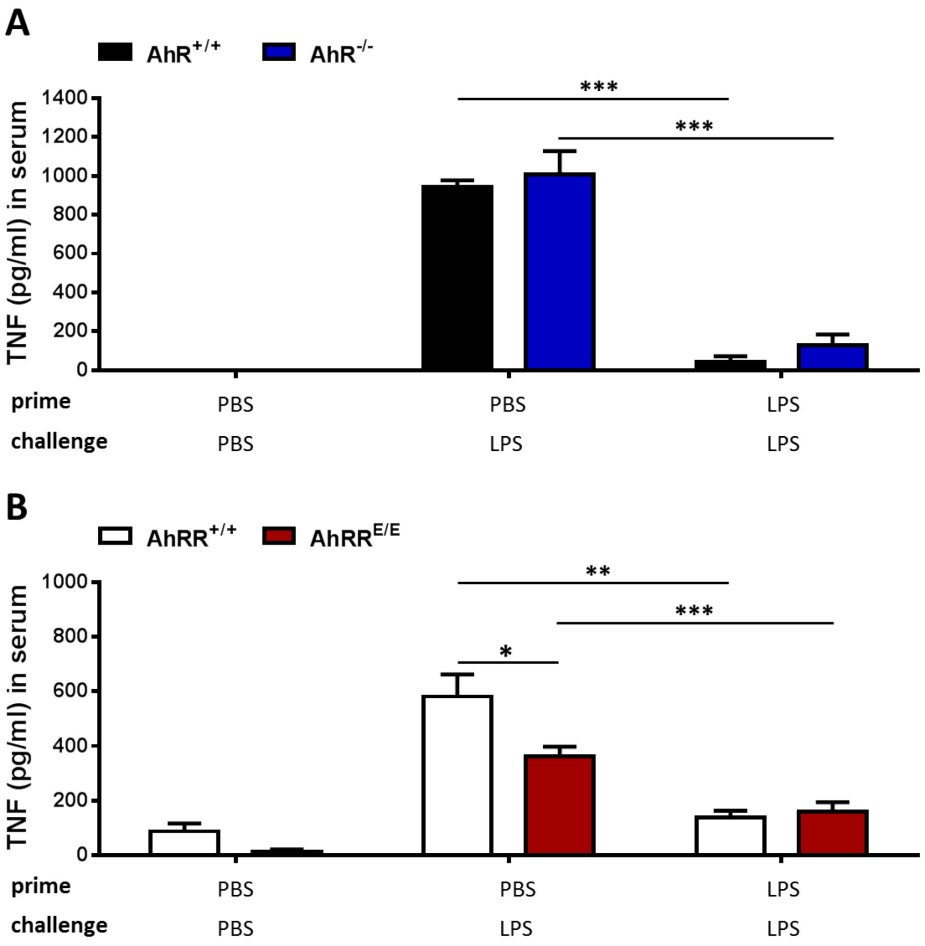

Figure 34 – Endotoxin tolerance induction in AhR-deficient, AhRR-deficient and wild-type mice *in vivo*. AhR-deficient ($AhR^{-/-}$, blue bars) and wild-type ($AhR^{+/+}$, black bars) mice (**A**) as well as AhRR-deficient ($AhRR^{E/E}$, red bars) and wild-type ($AhRR^{+/+}$, white bars) mice (**B**) were treated on day 1 with either 200 µl PBS (depicted on the left and in the middle) or primed with 4 mg/kg LPS, followed on day 4 by a second treatment with 200 µl PBS (neg. control, depicted on the left) or challenged with 15 mg/kg LPS (depicted in the middle and on the right). TNF levels were measured in serum, which was collected from mice 90 minutes after the second PBS treatment or LPS challenge. n=5-9, pooled samples from 3 independent experiments. The results are presented as mean plus SEM. Significant differences are depicted as *p<0.05, **p<0.01 and ***p<0.001. Significance was calculated using unpaired students t-test.

4.4.3. Survival analysis of AhR-deficient and wild-type mice during establishment of endotoxin tolerance

In a recent publication from Bessede *et al.* in *Nature* 2014, the authors showed that AhR-deficient mice are not able to induce endotoxin tolerance *in vivo* [161]. Their protocol differed from the protocol used in this thesis. Using our *in vivo* protocol, however, it could be shown that in contrast to the results of Bessede *et al.*, LPS primed AhR-deficient mice

(Figure 35B), like the LPS primed wild-type mice (Figure 35A), have a 100% survival rate. Furthermore, the previously described high susceptibility of AhR-deficient mice to LPS-induced septic shock was also shown (Figure 35) [100]. These results are in line with the *in vivo* data, where no differences in TNF production in serum of LPS primed AhR-deficient and wild-type mice were demonstrated (Figure 34A).

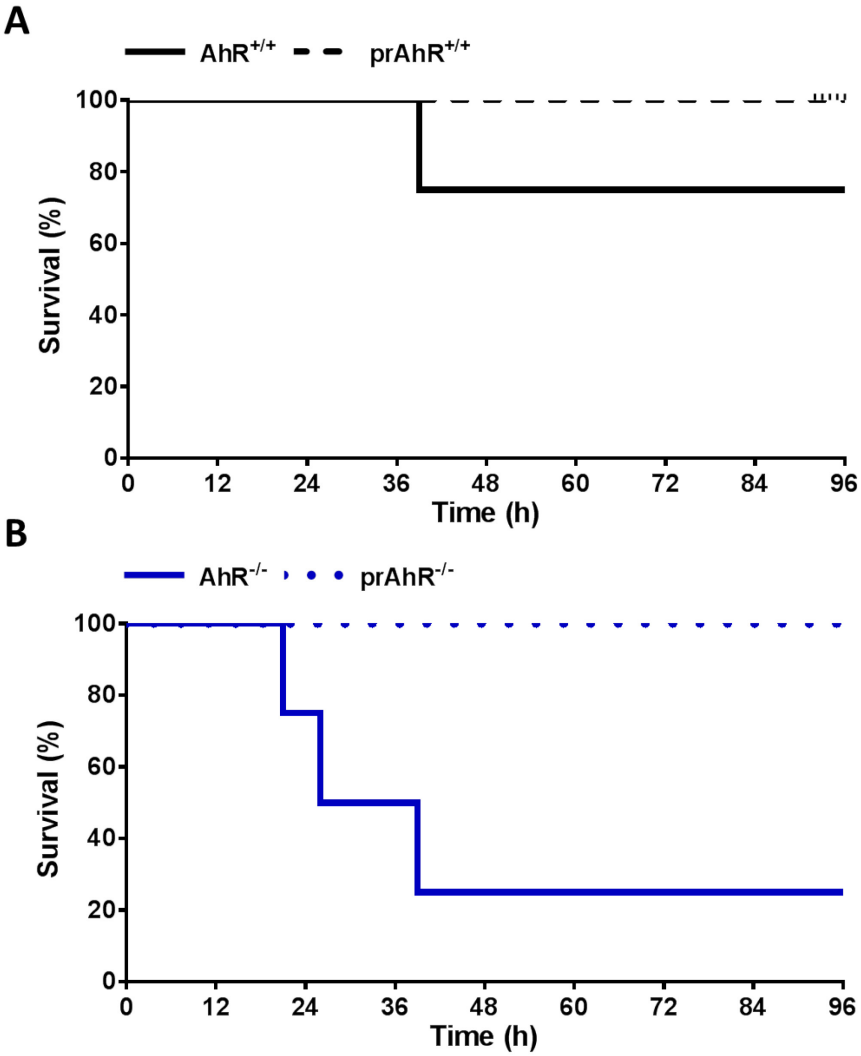

Figure 35 – AhR-deficient mice are able to establish an endotoxin tolerance *in vivo*. Survival curves of wild-type ($AhR^{+/+}$, black line) (**A**) and AhR-deficient ($AhR^{-/-}$, blue line) (**B**) mice and LPS-primed wild-type ($prAhR^{+/+}$, dashed black line) (**A**) and AhR-deficient ($prAhr^{-/-}$, dotted blue line) (**B**) mice after a second challenge with LPS. Mice were primed with 4 mg/kg LPS and challenge on day 4 with 20 mg/kg LPS. LPS originated from *E.coli* strain 0111:B4. n=4-5.

In order to get a better comparison of these results to the published data, the survival experiments were repeated with precisely the same protocol used by Bessede *et al.* [161]. This includes the application of a lower LPS dose for priming (0,5 mg/kg instead of

4 mg/kg), a higher dose of LPS for the second challenge (40 mg/kg instead of 20 mg/kg), which was performed on day 7 instead of day 4, as well as the use of a different type of LPS from the same *E. coli* strain. In agreement with the first survival experiments and in contrast to the results published by Bessede *et al.,* it was shown that also using the new protocol AhR-deficient mice can establish endotoxin tolerance indicated by a 100% survival rate in LPS primed and re-challenged mice (Figure 36B). LPS-induced septic shock led to a significantly higher susceptibility in AhR-deficient mice compared to wild-type control mice as described previously by Sekine *et al.* (Figure 35 and 36) [100].

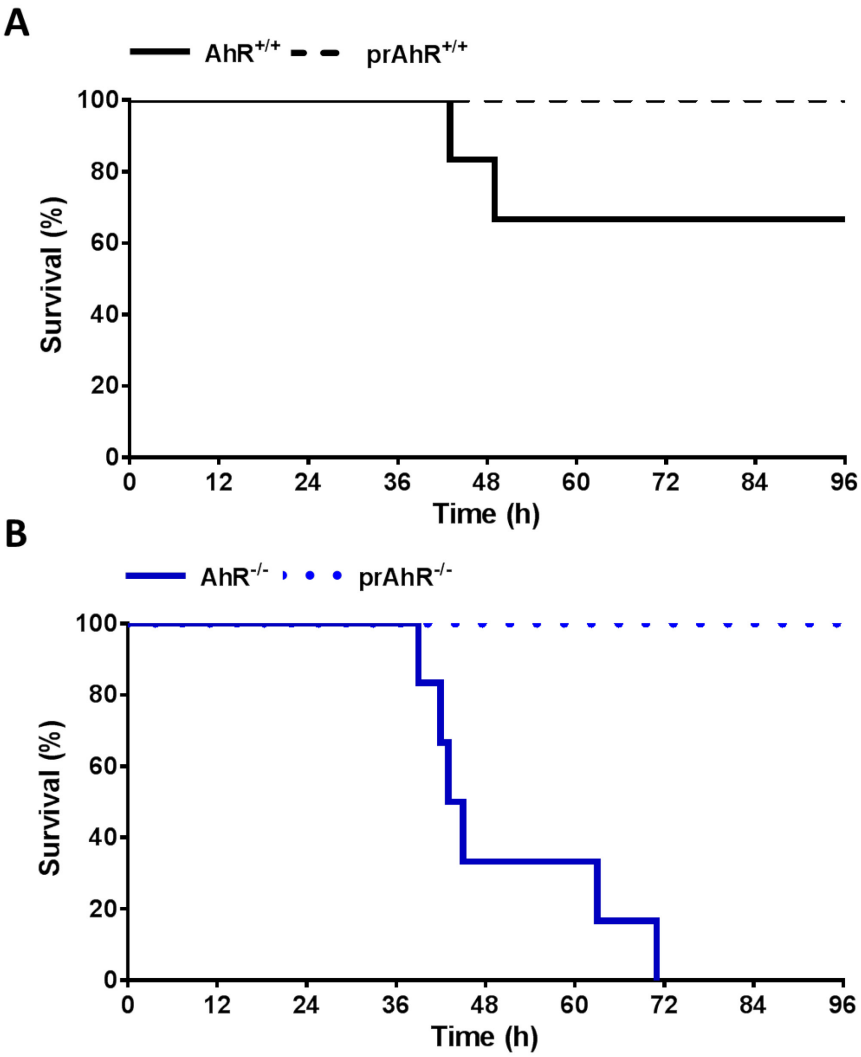

Figure 36 – AhR-deficient mice are able to establish an endotoxin tolerance *in vivo*. Survival curves of wild-type ($AhR^{+/+}$, black line) (**A**) and AhR-deficient ($AhR^{-/-}$, blue line) (**B**) mice and LPS-primed wild-type ($prAhR^{+/+}$, dashed black line) (**A**) and AhR-deficient ($prAhr^{-/-}$, dotted blue line) (**B**) mice after a second challenge with LPS. Mice were primed with 0,5 mg/kg LPS and challenge on day 7 with 40 mg/kg LPS. LPS originated from *E.coli* strain 055:B5 according to [161]. n=6.

In summary, neither AhR nor AhRR is required for development of endotoxin tolerance. Furthermore, the findings by Bessede *et al.* could not be confirmed in this thesis.

4.5. Generation of AhRR-dsRed-reporter mice

In many cases intercrosses of the AhRR-EGFP-reporter mouse line with other reporter mouse lines are hampered as most other reporter systems also utilize GFP. In order to be able to precisely compare the cell-type specific expression of the AhRR with the expression of other molecules of interest, a new AhRR-reporter mouse line was generated using dsRed instead of EGFP.

The AhRR-dsRed-reporter mice were generated using a targeting vector, which was constructed by Markus Korkowski (IUF, Düsseldorf). In this targeting vector the reporter gene *dsRed*, a *Discosoma sp.* red fluorescent protein was inserted into the second exon of the *ahrr* gene (Figure 37). The third exon was completely deleted to avoid the generation of a truncated protein due to alternative splicing.

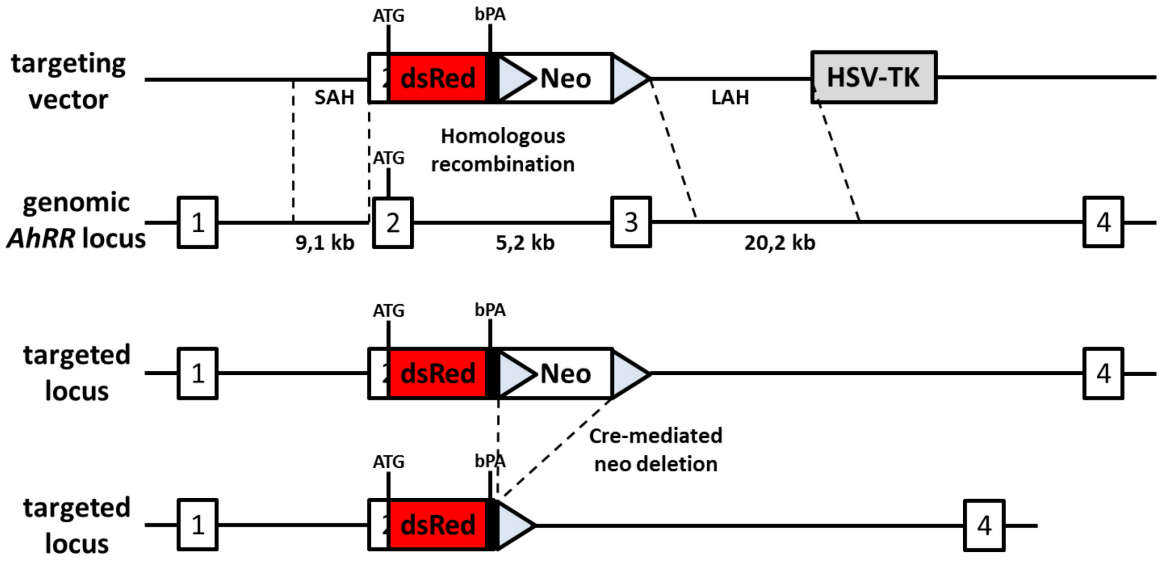

Figure 37 – Targeting-strategy used for the generation of AhRR-dsRed-reporter mice. The *dsRed* gene was inserted into the second exon of the *AhRR* gene. The third exon was deleted. A loxP-flanked neomycin resistance cassette was inserted to allow selection during ES cell targeting.

This vector was transfected into cultured HM-1 mouse embryonic stem (ES) cells by electroporation. The transfected cells underwent a selection process using G418. Only ES cell clones, in which homologous recombination between the targeting vector and the genomic DNA occurred successfully, survive the selection process due to positive selection for the integration of the neomycin resistance cassette and negative selection against integration of the HSV-TK cassette (Figure 37). Genomic DNA was isolated from G418 and ganciclovir resistant clones and tested by PCR with primers specific for the targeting vector. Genomic DNA of PCR positive as well as negative clones (data not show) were restricted using the endonuclease *DraI* and then tested by southern blot to ensure a successful integration of the modified allele at the correct location (Figure 38).

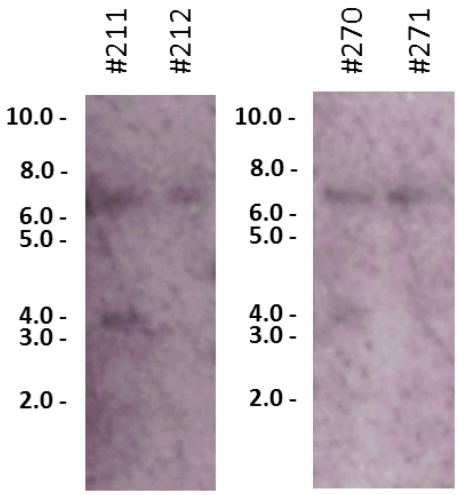

Figure 38 – Southern blot analysis of PCR positive clones. Two PCR positive clones (#211 and #270) and neighboring negative clones (#212 and #271) were hybridized with a 5' probe after digestion with the restriction enzyme *DraI*. The wild-type allele displays a fragment of 6.7 kb and the mutated allele displays a fragment of 3.7 kb. The positives clones #211 and #270 display both fragments.

PCR and Southern blot positive ES cell clones were injected into blastocysts, four chimeric mice were born and germline transmission was obtained.

AhRR-dsRed targeted mice were analyzed immunohistologically in sections of colon, small intestine and skin (Figure 39), as it was already described in our group that AhRR-EGFP-reporter mice expressed AhRR/EGFP at these sites [76]. Indeed, the expression pattern of AhRR-dsRed-reporter mice was comparable to the EGFP expression of AhRR-EGFP-reporter mice, exhibiting dsRed expression in the colon, in the LP of the small intestine and in the skin (Figure 39).

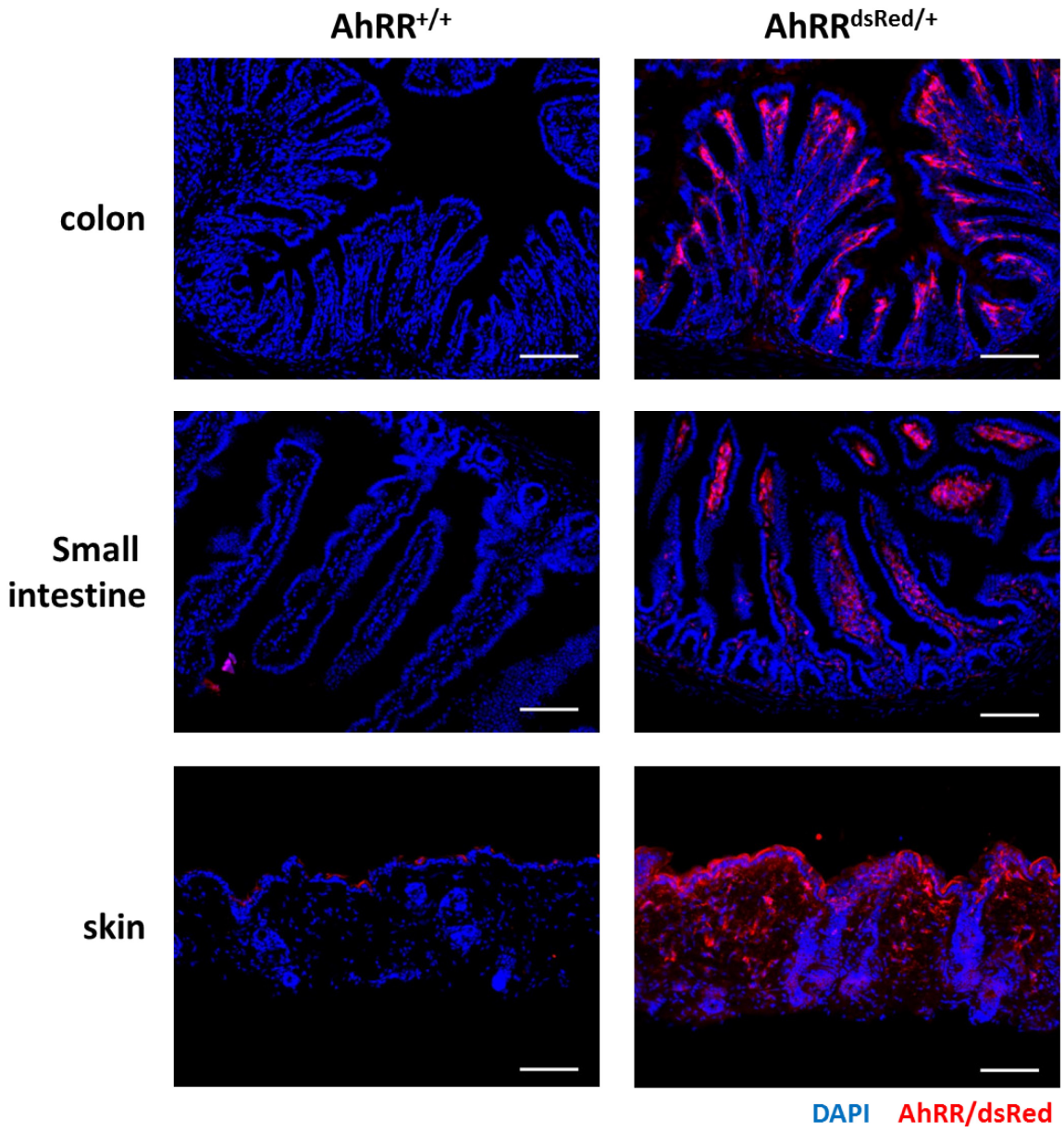

Figure 39 - Immunofluorescence AhRR/dsRed staining of frozen sections of colon, small intestine and skin from AhRR-dsRed-reporter mice and wild-type mice. Representative immunofluorescent stainings of heterozygous AhRR-dsRed-reporter ($AhRR^{dsRed/+}$) and wild-type ($AhRR^{+/+}$) mice. Sections were stained against dsRed (red) and counterstained with DAPI (blue). Scale bar: 100 µm.

Furthermore, it was shown in our group that AhRR-EGFP was expressed in 16% of cells in activated BMDCs, defined as $CD11c^{+}$ and $MHCII^{high}$. This frequency was boosted to approximately 50% positive AhRR-EGFP cells in BMDC cultures after LPS stimulation.

AhRR-dsRed-reporter BMDCs exhibited similar frequencies of AhRR/dsRed positive $CD11^{+}MHCII^{high}$ cells. Approximately 20% AhRR-dsRed positive cells were found in unstimulated AhRR-dsRed BMDC cultures (Figure 40). LPS stimulation led to a 2-fold increase of AhRR-dsRed expression.

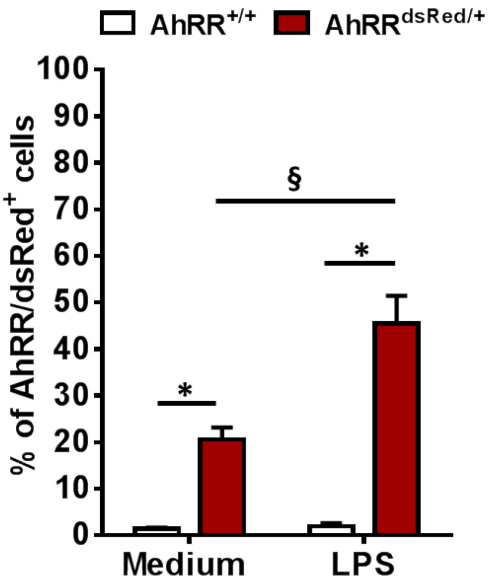

Figure 40 – Expression of AhRR/dsRed in BMDC generated from AhRR-dsRed-reporter mice and wild-type mice. $CD11c^{+}$ $MHCII^{high}$ *in vitro* generated BMDC were left untreated or stimulated with LPS and analyzed for AhRR/dsRed expression. n=3, pooled samples from 2 independent experiments. The results are presented as mean plus SEM. Significant differences are depicted as *p<0.05 (between $AhRR^{+/+}$ and $AhRR^{dsRed/+}$ BMDCs) and §p<0.05 (between untreated $AhRR^{dsRed/+}$ and LPS stimulated $AhRR^{dsRed/+}$ BMDCs). Significance was calculated using unpaired students t-test.

Next, the expression of the dsRed protein was analyzed in BMDC protein lysates obtained from wild-type and AhRR-dsRed-reporter mice (Figure 41). The dsRed protein has a size of 28 kDa [172]. In the Western blot shown in Figure 41, it is clearly visible that dsRed protein expression can only be found in BMDC protein lysates from AhRR-dsRed-reporter mice, whereas BMDC protein lysates from wild-type mice displayed no dsRed protein expression. GAPDH protein expression was used as a loading control and was detected in AhRR-dsRed-reporter as well as wild-type protein lysates (Figure 41).

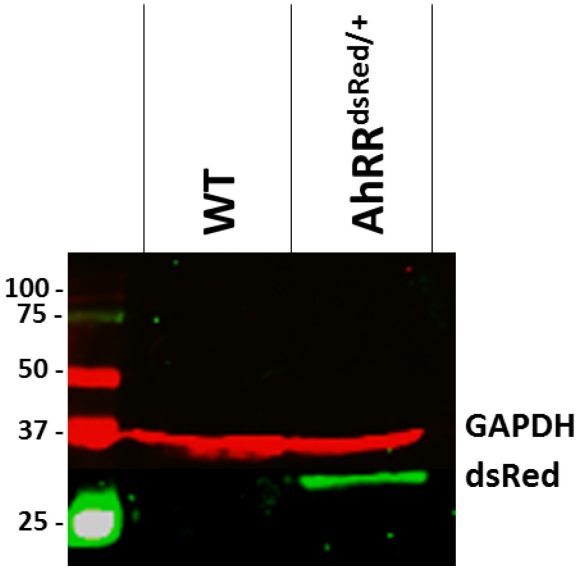

Figure 41 – Expression analysis of dsRed protein in BMDCs using Western blot. DsRed protein (28 kDa) expression was analyzed in BMDCs from wild-type (WT) and heterozygous AhRR-dsRed-reporter mice ($AhRR^{dsRed/+}$). Analysis of GAPDH protein (37 kDa) expression was used as a loading control.

Thus, AhRR-dsRed-reporter mice were successfully generated and can be used to create double reporter mouse lines, allowing the analysis of the expression pattern of the AhRR by means of dsRed expression as well as the expression pattern of the molecule of interest on the basis of GFP expression, which is the most commonly used fluorescent reporter protein.

5. Discussion

The AhR is a well conserved ancient transcription factor with orthologues among various species [173]. Much of todays' understanding of the AhR function has been revealed originally in toxicological and pharmacological studies. Hence, the AhR is best known for mediating toxicity as response to the binding of dioxin (2,3,7,8-tetrachloro-dibenzo-*p*-dioxin (TCDD)). Activated through dioxin or other xenobiotics, the AhR leads to the expression of xenobiotic metabolizing enzymes, thus promoting detoxification of those environmental toxins.

However, the understanding of the AhR refined, when it was identified that the AhR not only binds to environmental toxins, but also endogenous ligands and dietary ligands (reviewed in [60]). Moreover, it has been described that the AhR plays a role in growth, differentiation, liver development and physiology, and fertility [52]–[55]. Furthermore, it has been shown that the AhR is important for the development of immune cells. In addition, the AhR influences immune responses to infections, nutrition and microbiota (reviewed in [39]).

The activity of the AhR can be regulated by negative feedback inhibition through the AhRR, which is one of the AhR target genes [73]. In contrast to the AhR, less is known about the AhRR. Our group generated AhRR-EGFP-reporter mice, which express EGFP under the control of the *ahrr* promotor, allowing the analysis of the expression pattern, but also permit the investigation of AhRR deficiency and its effects [76]. Using this mouse strain, it was demonstrated that the AhRR is expressed in immune cells mainly located in barrier organs, such as the skin and the intestine. Interestingly, AhRR expression does not strictly correlate with AhR expression and is not entirely dependent on AhR activation. In addition, it was revealed that in the absence of AhRR, mice are protected from LPS-induced septic shock [76] in contrast to high sensitivity in AhR knock out mice [100]. Conversely, AhRR-deficient mice are more sensitive to DSS-induced colitis similar to AhR-deficient mice [76], [101]. In this thesis, the function and influence of the AhRR was further analyzed in systemic infections on the one hand and intestinal inflammation on

the other hand, in order to shed more light into the selective expression pattern of the AhR/AhRR system and its balance in systemic and intestinal homeostasis.

5.1. Tissue and cell specific expression of the AhRR

Analysis of *ahrr* expression by qRT-PCR performed in our group revealed that skin, small intestine, Peyer's patches (PP) and mesenteric lymph nodes (mLNs) show *ahrr* expression, while liver, spleen and lung displayed no *ahrr* expression. These findings were strengthened by the detection of *ahrr* expression in single cell suspensions of the lamina propria (LP) of the small intestine, PPs and mLNs [174]. Most interestingly, it demonstrated that AhR and AhRR expression are not entirely overlapping, evident by the absence of AhRR expression in lung and liver, in which high expression of the AhR has been described [51]. Using flow cytometry, it was confirmed that the AhRR is strongly expressed in the gut, especially in the LP of the small intestine, in the dome region of PPs and in the LP of the colon. In contrast to the absence of AhRR expression in splenic T cells, high AhRR expression was found in 20-40% of $CD4^+$ and $CD8^+$ T cells in the small intestinal LP, while in PPs only 20% of $CD8^+$ T cells express the AhRR. Additionally, all intestinal DC subsets express the AhRR, as well as ILC3 and IEL [76]. Several groups could show that the AhR is involved in T_h17, T_h22, T_r1 and T_{reg} cell development [90], [91], [97], [163]. However, there have been some inconsistent reports regarding T_h17 cells in AhR knock out mice. Veldhoen *et al.* demonstrated that AhR deficiency has no influence on T_h17 frequencies but leads to the impairment of IL-22 production, while Kimura *et al.* could not differentiate T_h17 cells from AhR-deficient naïve $CD4^+$ T cells [90], [91]. The latter group speculated that the reason for these opposing findings is the marker profile of the naïve $CD4^+$ T cells. Veldhoen *et al.* did not differentiate between CD62L positive and negative cells, thereby including both cell fractions and only purifying CD4 positive and CD25 negative T cells isolated from lymph nodes [91]. Kimura *et al.* on the other hand were able to show that $CD4^+CD25^-CD62L^-$ T cells spontaneously express IL-17 without IL-6 or TGFβ stimulation and therefore excluded these cells and used $CD4^+CD25^-CD62L^+$ T cells in their differentiation assays [90]. Furthermore, there have also been some inconsistent reports about the AhR expression in T_{reg} cells (reviewed in [162]). Some groups described

clear AhR expression in T_{reg} cells [90], [94], whereas another group reported only marginal AhR expression in T_{reg} cells [91].

5.2. AhRR expression in T_h17, T_h22, T_r1 and T_{reg} *in vitro* differentiated T cells

In this thesis, the analysis of different *in vitro* differentiated helper T cell subsets clearly shows AhRR expression in T_h17, T_h22, T_r1 and T_{reg} cells, whereas AhRR expression in T_h1 and T_h2 cells was less prominent. T_h17 cells express the highest amount of AhRR. Furthermore, AhRR expression was found in T_{reg} cells, but at lower levels than in T_h17 cells. AhRR expression was clearly measurable in *in vitro* differentiated IL-22 producing T_h22 cells, which is in line with reports of AhR expression in T_h22 cells, as well as the importance and influence of the AhR on IL-22 production[175]. Lastly, AhRR expression was found in T_r1 cells. T_r1 cells are characterized by the production of IL-10 and a lack of FoxP3 expression. In 2015, it was described that TGFβ and AhR activation can promote the conversion of T_h17 cells into T_r1 cells *in vivo* during an immune response [176], highlighting the plasticity of T_h17 cells and giving a plausible explanation for the AhR and AhRR expression in both helper T cell subsets. In summary, these results are additional examples of overlapping AhR and AhRR expression patterns, in line with the AhRR being a target gene of the AhR.

Apart from gaining more insights in the AhRR expression pattern, the use of homozygous AhRR-EGFP-reporter mice allows the analysis of the influence of AhRR deficiency on helper T cell differentiation as well as on cytokine production. It was clearly shown that AhRR deficiency had no influence on either differentiation or cytokine production capacities in any helper T cell subsets. Parallel to this thesis, work on the influence of AhRR deficiency in DSS-induced colitis revealed that AhRR-deficient mice exhibited increased numbers in T_h17 cells in the LP of the small intestine [76]. In contrast, *in vitro* differentiation of T_h17 cells showed marginal decreases of T_h17 cell frequencies in AhRR-deficient mice compared to wild-type control mice. These results were not anticipated. In order to further compare the *in vivo* data obtained from DSS-treated mice with the *in vitro* data, a more physiological situation during *in vitro* helper T cell differentiation was

investigated. This was achieved by differentiating helper T cells under hypoxic conditions. In the gut of naïve mice hypoxia was observed in epithelial cells adjacent to the intestinal lumen, creating a gradient from the tips of the villi to the base of the villi with increasing oxygen levels (reviewed in [177]). In colitis, however, it was shown that oxygen levels decrease throughout the mucosa, causing increased expression of hypoxia-inducible factors (HIF), such as HIF-1, which is important for maintaining oxygen homeostasis (reviewed in [165]). The subunit HIF-1α directly interacts with RORγt, thereby regulating T_h17 cell differentiation [164]. Literature reports that when T_h17 cells were cultured under hypoxic conditions, T_h17 frequencies were doubled [164]. Interestingly, a general increase in T_h17 frequencies cultured under hypoxia was not detected in my own experiments. In addition, when differentiating T_h17 cells in this setup, there were also no significant differences in T_h17 cell frequencies and IL-17 production between AhRR-deficient mice and wild-type mice. In opposition to the experimental setup described by Dang *et al.*, T_h17 cells were differentiated in this thesis using double the concentration of TGFβ and even 5 times the concentration of IL-6. More importantly, I also added the AhR ligand FICZ to the cultures. FICZ has been described to have a boosting effect on T_h17 differentiation [93]. Perhaps these differences in the differentiation cocktail resulted in the maximal frequencies of T_h17 cells that can be obtained during an *in vitro* differentiation culture and therefore no further increase could be detected under hypoxia. In contrast to T_h17 cells, I also detected decreased T_{reg} frequencies in hypoxic cultures. These observations are in agreement with the literature, demonstrating reduced T_{reg} numbers when culturing T_{reg} cells under hypoxia and reports describing that HIF-1 was shown to lead to proteasomal degradation of FoxP3 resulting in attenuated T_{reg} development [164]. Marginal decreases in T_r1 frequencies as well as decreases in IL-10 production were also detected. These findings are in line with literature describing suppressive regulatory effects of HIF-1 on T_r1 development [97]. Of note, AhRR expression was not altered in T cells cultured under hypoxia. Taken together, especially regarding T_h17 frequencies in AhRR-deficient T cells cultured under normoxia or hypoxia, these results are not in line with the increased T_h17 cell numbers in the LP of DSS-induced colitis mice. However, another aspect that has to be taken into account is that the naïve $CD4^+$ T cells used in these differentiation assays were isolated from the spleen and might therefore not be comparable to the T cells analyzed in the LP of the small intestine.

Nevertheless, the results of this thesis support the conclusion that the AhRR does not act directly on helper T cells and that changes in T_h17 frequencies are not due to T cell intrinsic AhRR effects. It can be speculated that the AhRR acts indirectly, possibly through myeloid cells interacting with T cells.

5.3. Increased susceptibility of AhRR-deficient mice during intestinal inflammation

Our group was able to show that AhRR expression was stronger in the small intestine compared to the colon. Therefore, the influence of the AhRR in the small intestinal immune system was addressed. An oral infection with the parasite *Toxoplasma gondii* was performed in AhRR-deficient mice and wild-type mice. Oral infection with this parasite leads to an inflammatory pathology resembling Crohn's disease [129]. Immune cells and inflammatory cytokines associated with Crohn's disease have been widely characterized, revealing that the pathology is dominated by a T_h1 response. Next to a strong IFNγ production by T_h1 cells as well as NK cells, activated macrophages, DCs and neutrophils produce large amounts of IL-12, TNF and IL-1β [178].

Initially, the number of administered cysts was titrated to determine the optimal amount of cysts for oral infection. Evidently, the administration of 200 cysts led to very severe intestinal inflammation resulting in 100% lethality of wild-type as well as AhRR-deficient mice by day 9 post infection. Reducing the number of cysts to 100 prolonged the duration of the lifespan of wild-type mice and allowed a small, but significant distinction to the survival rate of AhRR-deficient mice. This significant difference in survival between wild-type and AhRR knock out mice was further enhanced when orally infecting mice with 50 cysts, permitting *ex vivo* analysis to further investigate intestinal pathology, parasite load and infection pattern, intestinal shortening and cytokine production. Infecting mice with 25 cysts resulted in an even more striking difference between the survival rate of wild-type and AhRR-deficient mice. In summary, the survival experiments clearly revealed that the AhRR has a role in the defense against *Toxoplasma gondii* induced ileitis, indicated by the increased susceptibility of infected AhRR-deficient mice in comparison to infected wild-type mice. These results are in line with the effect of AhRR deficiency in DSS-induced

colitis [76]. Of note, AhR-deficient mice also exhibit a high susceptibility in *Toxoplasma gondii* induced ileitis and DSS-induced colitis [84], [101]. All these findings demonstrate and highlight the importance, but also the complexity of the AhR/AhRR system in maintaining immune homeostasis in the intestine.

Both wild-type and AhRR-deficient mice exhibited a similar small intestinal shortening in comparison to naïve wild-type and AhRR-deficient mice. However, this parameter only served as an indicator for the establishment of the infection and does not necessarily reflect the severity of the infection.

The examination of morphological changes in the ileum caused by the parasitic infection showed a stronger pathology in AhRR-deficient mice, displayed by a fibrotic and necrotic mucosa as well as blunted and distorted villi evaluated according to the literature [160]. The high susceptibility of AhRR-deficient mice detected during the survival analysis was in accordance with the significantly more damaged morphology of the intestinal structure. These results are comparable with the necrosis of the LP observed in *Toxoplasma gondii* infected AhR-deficient mice [84].

In contrast to the distinct differences between wild-type and AhRR-deficient mice regarding the morphological changes after infection, there were no visible differences in the infection pattern and distribution of the parasite in the ileum. Wild-type and AhRR-deficient ileal sections were stained with an antiserum against *Toxoplasma gondii*, revealing that parasite infection occurs in a patchy manner, infecting single villi. In addition, no overlap of the AhRR-EGFP signal and the parasite staining was detected. *Toxoplasma gondii* has the ability to invade a wide variety of cells [119]. The parasite attaches to the host cell membrane with the help of adhesins, which recognize host cell receptors. By a process termed gliding motility the parasite enters the host cell in approximately 15 to 30 sec in an actin-myosin dependent manner, followed by the formation of a parasitophorous vacuole (PV) protecting the parasite. Within the PV, the parasitic tachyzoites divide in a 6 to 9 h cycle. After reaching approximately 64 to 128 parasites within a PV, the tachyzoites exit the PV, leading to the disruption of the host cell, followed by the infection of the neighboring cells [119]. This could explain the patchy infection pattern observed in infected wild-type and AhRR-deficient mice. Thus, the parasite clearly causes damage to the infected cells resulting in apoptosis and the loss of

EGFP signal, providing an explanation for the lack of overlap between EGFP-AhRR signal and the parasite.

QRT-PCR analysis of the parasite load revealed that infected AhRR-deficient mice tend to exhibit a lower parasite burden in comparison to infected wild-type mice. These differences in parasite burden could be a result of efficient parasite clearing. Another possibility might be that the tachyzoites have already passed the intestinal tissue and have entered the bloodstream of AhRR-deficient mice and therefore cannot be detected in the intestinal tissue anymore. However, these hypotheses cannot be confirmed by the immunostaining of the ileal samples of AhRR-deficient mice, because EGFP-AhRR signal was detected in all villi that did not show parasite staining, thereby implying that the cells were intact and have remained uninfected. Furthermore, no apparent differences in the quantity of the parasites between AhRR-deficient mice and wild-type mice were detected in histological sections stained for *Toxoplasma gondii*. Even though it cannot be clarified how this difference in parasite burden was brought about, it reinforces the notion that AhRR deficiency plays a role in parasite-induced ileitis.

The analysis of pro-inflammatory cytokines production revealed on the one hand that the production varies along the different regions of the small intestine in both wild-type and AhRR-deficient mice. Highest cytokine levels were generally measured in the jejunum. On the other hand, even though similar tendencies were detected using two different methods to extract and measure the cytokines, it was also clear that the two methods yielded different cytokine concentrations. Large differences were especially apparent in cytokine levels measured in the duodenum. While the analysis of homogenized duodenal samples revealed almost no detectable cytokine levels in comparison to jejunal and ileal samples, relatively high cytokine levels were measured in the supernatants of duodenum cultures. In summary, the method of sample acquisition needs further improvement. Particularly with regard to the patchy infection pattern observed in the immunohistological analysis, it might also be necessary to collect either larger samples of each region or to take several size-matching small samples using punch biopsies, in order to make sure that sufficient equally infected tissue is analyzed.

Interestingly, the most striking differences between wild-type and AhRR-deficient mice were observed in cultured as well as homogenized jejunal samples. Pro-inflammatory

cytokines, such as TNF, IL-1β, IL-12p70 and IL-23 were increased in AhRR-deficient mice compared to wild-type mice. In contrast, IFNγ levels were decreased in AhRR-deficient mice. This decrease was also clearly detected in IFNγ levels measured in ileum cultures. IFNγ is very critical for parasite growth control and therefore crucial for survival during *Toxoplasma gondii* infection [179] (reviewed in [180]). But parasite burden was not obviously increased in AhRR-deficient mice, which is discrepant with the lower IFNγ levels. Nevertheless, considering the reduced frequencies of T_h1 cells observed in AhRR-deficient mice after DSS-induced colitis [76], an analysis of T_h1 cell populations in the LP of *Toxoplasma gondii* infected AhRR-deficient mice might give further insight into the differences in IFNγ production. Moreover, in AhR-deficient mice an increased T-bet expression in $CD4^+$ T cells after the induction of *Toxoplasma gondii* ileitis was described, indicating enhanced differentiation of T_h1 cells. Additionally, PMA/ionomycin stimulation resulted in an increased IFNγ production, leading to the proposal that AhR-deficient mice develop a hyperactivated T_h1 cell response [84]. In comparison to IFNγ, IL-1β levels were increased in jejunal samples of AhRR-deficient mice. *Toxoplasma gondii* can lead to activation of the inflammasome, which induces pyroptotic cell death and the processing of IL-1β and IL-18 (reviewed in [119]). In addition, IL-12 production was also visibly increased in jejunum samples of AhRR-deficient mice. It was proposed that IL-12 production is mainly initiated by $CD8\alpha^+$ DCs [181], leading to the activation of NK cells, which also produce large amounts of IFNγ (reviewed in [130]). Interestingly, it has been described that the absence of IFNγ has no influence on IL-12 production [182]. Therefore, the assumption can be made that AhRR-deficient DCs are not impaired in their IL-12 production. IL-23 was analyzed based on reports of its essential role in the development of *Toxoplasma gondii* induced immunopathology and because of its close relation to IL-12 [169]. Both cytokines are heterodimeric cytokines and are made up of the same subunit p40. Similar to IL-12, IL-23 levels were also enhanced in jejunal samples of AhRR-deficient mice. Interestingly, IL-23 has also been described to induce the development of pathogenic T_h17 cells [183]. T_h17 have been reported to become pathogenic during the induction of inflammatory bowel diseases [184]. In agreement with these reports, IL-17 cytokine levels were also slightly increased in AhRR-deficient mice. It has also been shown that *Toxoplasma gondii* infection leads to an increased IL-17 production and that neutralization of IL-17 results in partial protection against *Toxoplasma gondii* induced

inflammation [185]. Furthermore, as mentioned above, it is well described that the AhR regulates T_h17 development [90], [91], [94]. Several mechanisms have been suggested on how the AhR supports T_h17 differentiation (reviewed in [162]). The AhR may directly bind to the IL-17 gene locus inducing transcription [186]. Another study described that the AhR inhibits Stat1 phosphorylation, thereby preventing T_h1 differentiation and promoting T_h17 development [90]. It is tempting to speculate that AhRR deficiency leaves AhR expression unregulated, resulting in increased AhR activity promoting T_h17 development. Furthermore, it has been described that $CD8^+$ T cells and their secretion of IL-17 are also associated with the defense against *Toxoplasma gondii* [187]. To sum up, it would be interesting to isolate $CD4^+$ and $CD8^+$ T cells, specifically T_h17/T_c17 and T_h1/T_c1 cells, from naïve and orally *Toxoplasma gondii* infected wild-type and AhRR-deficient mice and analyze their frequencies and cytokine expression.

The high susceptibility for *Toxoplasma gondii* induced ileitis in AhR-deficient mice has been attributed to reduced frequencies of group 3 ILCs [84]. ILC3 share several similarities with T_h17 cells, such as the cytokine production profile and expression of AhR (reviewed in [162]) and AhRR [76]. Frequencies of ILC3 were not yet analyzed in *Toxoplasma gondii* infected wild-type and AhRR-deficient mice. However, Brandstätter *et al.* were able to show that naïve AhRR-deficient mice and wild-type mice exhibit equal frequencies of $NKp46^+RORγt^+$ ILC3 as well as $NKp46^-RORγt^+$ ILC3 in LP of the small intestine [76]. Furthermore, ILC3 play a vital role in the protection against *Citrobacter rodentium* infections, as they are one of the main sources of IL-22 in the gut (reviewed in [25]). IL-22 is known to boost epithelial cell proliferation and repair, thus maintaining homeostasis at gut mucosal barriers in addition to providing protection against bacterial and fungal infections [188]. It has also been shown to regulate the colonic lymphoid structure in *Citrobacter rodentium* infections [189]. AhR-deficient mice have been described to be highly sensitive to *Citrobacter rodentium* infections [76], [81], whereas AhRR-deficient mice were shown to be as resistant as wild-type mice [76]. Resistance of AhRR-deficient mice against *Citrobacter rodentium* infections therefore indicated that the AhRR deficiency does not influence the functionality of ILC3 cells. Similarly, it is unlikely that the observed susceptibility of AhRR-deficient mice for *Toxoplasma gondii* induced ileitis is due to an impairment of ILC3 functionality. Group 1 ILCs also have been associated with chronic inflammatory diseases, specifically with Crohn's disease. It has been described

that IFNγ producing ILC1 frequencies increase in the gut of patients with Crohn's disease [190]. In addition, it was reported that ILC1 protect wild-type mice against *Toxoplasma gondii* infections by producing high levels of IFNγ and TNF [191]. Therefore, it would be interesting to analyze ILC1 frequencies in naïve and *Toxoplasma gondii* infected AhRR-deficient mice.

In addition, as described above, it is well reported that NK cell activity is vital in the defense against *Toxoplasma gondii*. Interestingly, it has been described that AhR ligands promote NK cell cytotoxicity as well as IFNγ production and that AhR expression is necessary to induce IL-10 production during *Toxoplasma gondii* infection [192]. Another cell type that has been described to produce IFNγ is neutrophils. Analysis of these cells might also provide an explanation for the decreases in IFNγ levels in AhRR-deficient *Toxoplasma gondii* infected mice.

Another aspect that has not yet been addressed in this thesis is the immunoregulation during *Toxoplasma gondii* infection mediated by IL-10 and TGFβ. T_h1 mediated immune responses control parasite growth, but immunosuppressive cytokines are important for counter-regulation, in order to prevent immune-mediated pathology. Therefore, analysis of T_{reg} cells might provide more information. Interestingly, no differences in T_{reg} frequencies could be detected between DSS-treated wild-type and AhRR-deficient mice.

Furthermore, it might be beneficial to analyze the impact of AhRR deficiency on AhR activity. This could be realized by generating an AhR-reporter mouse strain, similar to the AhRR-EGFP-reporter mice or the AhRR-dsRed-reporter mice generated in this thesis. Intercrosses between AhR- and AhRR-reporter mice will allow the investigation of the balance between both molecules in specific cell types in the small intestine during *Toxoplasma gondii* induced ileitis.

5.4. The role of AhRR deficiency in systemic infections

AhR deficiency has been described to lead to an increased susceptibility to LPS-induced septic shock. Increased pro-inflammatory cytokines, such as TNF and IL-6, were detected in hypersensitive AhR-deficient mice after LPS challenge [100]. In contrast, AhRR

deficiency establishes protection against high dose LPS injection, supported by reduced production of TNF, IFNγ, IL-12p70 and IL-1β in AhRR-deficient mice compared to wild-type mice [76]. In order to examine the influence of the AhRR in a more physiological experimental sepsis model, AhRR-deficient mice were analyzed in the colon ascendens stent peritonitis (CASP) model, resulting in a polymicrobial sepsis [152].

As observed for LPS-induced septic shock, AhRR-deficient mice exhibited a reduced susceptibility to septic shock after CASP induction compared to wild-type mice. Heterozygous AhRR-EGFP-reporter mice were also slightly more protected against polymicrobial sepsis compared to wild-type mice, but still displayed a lower survival rate than AhRR-deficient mice. This might be explained by a gene dosage effect, as the AhRR is encoded only on one allele, while the other allele encodes EGFP. Of note, the CASP analysis was performed in female as well as male mice, in order to exclude possible gender differences in response to polymicrobial sepsis. Studies on sepsis with female and male mice reported that females are able to cope better immunologically with the challenges of sepsis, probably due to the lack of male sex steroids [193]. In addition, patient studies also described higher incidences of bacteremic infections, as well as development of infections after surgery in male patients [194], [195]. In this study, however, no obvious differences in response to CASP between male and female mice were detected. Even though a better protection against polymicrobial sepsis was observed in both female and male AhRR-deficient mice compared to wild-type mice, the strength of protection was not nearly as high as seen in LPS-induced septic shock. Whereas AhRR-deficient mice showed approximately a 60% higher survival rate in comparison to wild-type mice in LPS-induced septic shock, AhRR-deficient mice only exhibited about 15 to 20% higher survival rates compared to wild-type mice in the CASP model. Further investigations regarding cytokine production or the analysis of neutrophil infiltration still have to be performed. The analysis of the cytokine profile of AhRR-deficient mice after induction of polymicrobial sepsis might give an explanation for the protective effect observed and potentially also might reveal further differences to the LPS-induced septic shock model. Moreover, it might be interesting to analyze the bacterial burden and composition after CASP surgery. Another experiment, which might round up and give further insights into the influence of the AhR/AhRR system in systemic infections, is the analysis of AhR-deficient mice in the CASP model.

Despite CASP being a more physiological model of sepsis than LPS-induced septic shock, all animal models of sepsis own a few drawbacks when comparing them with human sepsis. One example is the timing of disease progression in the animal models, which is not comparable to the development of sepsis in humans. In humans, sepsis and subsequent multiple organ failure progress over days to weeks, whereas the development of sepsis in animal models occurs in hours to days (reviewed in [135]). The use of LPS-induced septic shock in animal studies is a simple and easily reproducible assay. In contrast to humans, however, it is well described that mice are fairly resistant to LPS. Therefore relatively high LPS doses need to be used in order to induce septic shock. CASP on the other hand, resembles a bacterial postoperative peritonitis many patients suffer from after abdominal surgery. But also this model possesses differences to sepsis progression in humans. While in human patients sepsis is characterized by two phases, namely systemic inflammatory response (SIRS) followed by compensatory anti-inflammatory response (CARS), CASP induction in mice leads to the induction of SIRS and CARS simultaneously (reviewed in [135]).

Since it was already shown that the AhR/AhRR system plays a role in systemic infections and based on the different effects of AhR and AhRR deficiency in LPS-induced septic shock, I also analyzed in this thesis whether AhR or AhRR deficiency has an influence on the establishment of endotoxin tolerance. Endotoxin tolerance describes the reduced immune response to a LPS challenge following pretreatment with LPS. *In vitro* experiments using BMMϕ from AhR-deficient, AhRR-deficient and wild-type littermate control mice showed that repeated stimulation with LPS led to reduced TNF levels in the supernatants of wild-type and both AhR- and AhRR-deficient BMMϕ. These results clearly revealed that AhR-deficient as well as AhRR-deficient cells are able to establish endotoxin tolerance *in vitro*. To reinforce these new insights, an *in vivo* analysis was performed, demonstrating that AhR and AhRR deficiency also had no influence on the induction of endotoxin tolerance *in vivo*. Parallel to the work conducted in this thesis, published data demonstrated that AhR-deficient mice could not establish LPS tolerance using a survival analysis [161]. Bessede *et al.* used LPS derived from a different *E.coli* strain, as well as a longer period between priming and challenge of LPS and different doses for priming and challenge compared to the standard protocol used in our laboratory. However, survival analysis using our parameters as well as the experimental setup used in the publication

demonstrated that AhR-deficient mice are able to establish endotoxin tolerance indicated by 100% survival rate in both experimental setups. Certainly, some differences remain, such as different genetic backgrounds, housing conditions of the mice leading to potentially different commensal colonization, as well as sex and age. Though, both studies were conducted using 8 to 10 weeks old male mice for endotoxin tolerance assays. Furthermore, it has been described that the survival rate in LPS-induced septic shock models is also dependent on the time of day when the mice were treated with LPS. This indicates that the results obtained from LPS treatment can be influenced by the circadian clock [196], which may also be a possible explanation for the discrepant results obtained by Bessede *et al.*[161].

5.5. Clinical relevance and conclusion

A systematic review published in 2012 reported an increasing incidence of IBDs. Thus, IBD is emerging as a global disease, possibly caused by western lifestyle and diet [103]. Another disease that represents a serious, life-threatening condition is sepsis, which is caused by an overwhelming immune response to a systemic bacterial infection. Understanding mechanisms and potential molecular players involved in these diseases can represent an opportunity to identify therapeutic targets and develop treatments.

The findings in this thesis and the work performed in our group identified the AhR/AhRR signaling pathway to play a role in intestinal and systemic infections. On the one hand, the classical view that the AhRR acts as a repressor of AhR activity was supported by the opposing effects of AhR and AhRR deficiency in LPS-induced septic shock and CASP-induced polymicrobial sepsis. On the other hand, AhR and AhRR deficiency provoked comparable increases in intestinal inflammation assessed in DSS-induced colitis and *Toxoplasma gondii* induced ileitis. These insights seem contradicting, however, it can be assumed that these different influences of the AhR/AhRR system might be depending on the restricted expression of the AhRR in immune cells located in barrier organs, whereas AhR expression can be found more ubiquitously, leading to local regulation of AhR activity by the AhRR in specific cells and tissues relevant in immunity. Further analysis of AhR and

AhRR interaction in different cell-types and organs upon diverse ligand stimulation elicited by nutrients, commensals, pathogens and environmental toxins might provide sufficient knowledge to develop promising therapeutic strategies for intestinal and systemic diseases.

6. References

[1] L. T. Nguyen, E. F. Haney, and H. J. Vogel, “The expanding scope of antimicrobial peptide structures and their modes of action,” *Trends Biotechnol.*, vol. 29, no. 9, pp. 464–472, Sep. 2011.

[2] J. K. Chan, J. Roth, J. J. Oppenheim, K. J. Tracey, T. Vogl, M. Feldmann, N. Horwood, and J. Nanchahal, “Alarmins: awaiting a clinical response,” *J. Clin. Invest.*, vol. 122, no. 8, pp. 2711–2719, Aug. 2012.

[3] C. A. Janeway, “Approaching the Asymptote? Evolution and Revolution in Immunology,” *Cold Spring Harb. Symp. Quant. Biol.*, vol. 54, pp. 1–13, Jan. 1989.

[4] S. Akira, S. Uematsu, and O. Takeuchi, “Pathogen Recognition and Innate Immunity,” *Cell*, vol. 124, no. 4, pp. 783–801, Feb. 2006.

[5] T. H. Mogensen, “Pathogen Recognition and Inflammatory Signaling in Innate Immune Defenses,” *Clin. Microbiol. Rev.*, vol. 22, no. 2, pp. 240–273, Apr. 2009.

[6] A. Iwasaki and R. Medzhitov, “Toll-like receptor control of the adaptive immune responses,” *Nat. Immunol.*, vol. 5, no. 10, pp. 987–995, Oct. 2004.

[7] N. Nomura, N. Miyajima, T. Sazuka, A. Tanaka, Y. Kawarabayasi, S. Sato, T. Nagase, N. Seki, K. Ishikawa, and S. Tabata, “Prediction of the coding sequences of unidentified human genes. I. The coding sequences of 40 new genes (KIAA0001-KIAA0040) deduced by analysis of randomly sampled cDNA clones from human immature myeloid cell line KG-1.,” *DNA Res.*, vol. 1, no. 1, pp. 27–35, 1994.

[8] R. Medzhitov, P. Preston-Hurlburt, and C.A. Janeway, “A human homologue of the Drosophila Toll protein signals activation of adaptive immunity,” *Nature*, vol. 388, no. 6640, pp. 394–397, 1997.

[9] F. Hayashi, K. D. Smith, A. Ozinsky, T. R. Hawn, E. C. Yi, D. R. Goodlett, J. K. Eng, S. Akira, D. M. Underhill, and A. Aderem, “The innate immune response to bacterial flagellin is mediated by Toll-like receptor 5.,” *Nature*, vol. 410, no. 6832, pp. 1099–

103, Apr. 2001.

[10] M. Yoneyama, M. Kikuchi, T. Natsukawa, N. Shinobu, T. Imaizumi, M. Miyagishi, K. Taira, S. Akira, and T. Fujita, “The RNA helicase RIG-I has an essential function in double-stranded RNA-induced innate antiviral responses.,” *Nat. Immunol.*, vol. 5, no. 7, pp. 730–7, Jul. 2004.

[11] T.-D. Kanneganti, M. Lamkanfi, and G. Núñez, “Intracellular NOD-like receptors in host defense and disease.,” *Immunity*, vol. 27, no. 4, pp. 549–59, Oct. 2007.

[12] S. Huang, W. Hendriks, A. Althage, S. Hemmi, H. Bluethmann, R. Kamijo, J. Vilcek, R. M. Zinkernagel, and M. Aguet, “Immune response in mice that lack the interferon-gamma receptor.,” *Science*, vol. 259, no. 5102, pp. 1742–5, Mar. 1993.

[13] C. Basset, J. Holton, R. O’Mahony, and I. Roitt, “Innate immunity and pathogen-host interaction.,” *Vaccine*, vol. 21 Suppl 2, pp. S12-23, Jun. 2003.

[14] D. Artis and H. Spits, “The biology of innate lymphoid cells,” *Nature*, vol. 517, no. 7534, pp. 293–301, Jan. 2015.

[15] W. Holtmeier and D. Kabelitz, “gammadelta T cells link innate and adaptive immune responses.,” *Chem. Immunol. Allergy*, vol. 86, pp. 151–83, 2005.

[16] D. Bryder, D. J. Rossi, and I. L. Weissman, “Hematopoietic Stem Cells,” *Am. J. Pathol.*, vol. 169, no. 2, pp. 338–346, Aug. 2006.

[17] T. R. Mosmann and R. L. Coffman, “TH1 and TH2 Cells: Different Patterns of Lymphokine Secretion Lead to Different Functional Properties,” *Annu. Rev. Immunol.*, vol. 7, no. 1, pp. 145–173, Apr. 1989.

[18] W. E. Paul and R. A. Seder, “Lymphocyte responses and cytokines,” *Cell*, vol. 76, no. 2, pp. 241–251, Jan. 1994.

[19] J. Zhu and W. E. Paul, “CD4 T cells: fates, functions, and faults,” *Blood*, vol. 112, no. 5, pp. 1557–1569, Sep. 2008.

[20] H. Park, Z. Li, X. O. Yang, S. H. Chang, R. Nurieva, Y.-H. Wang, Y. Wang, L. Hood, Z. Zhu, Q. Tian, and C. Dong, “A distinct lineage of CD4 T cells regulates tissue inflammation by producing interleukin 17,” *Nat. Immunol.*, vol. 6, no. 11, pp. 1133–

1141, Nov. 2005.

[21] L. E. Harrington, R. D. Hatton, P. R. Mangan, H. Turner, T. L. Murphy, K. M. Murphy, and C. T. Weaver, “Interleukin 17–producing CD4+ effector T cells develop via a lineage distinct from the T helper type 1 and 2 lineages,” *Nat. Immunol.*, vol. 6, no. 11, pp. 1123–1132, Nov. 2005.

[22] I. I. Ivanov, B. S. McKenzie, L. Zhou, C. E. Tadokoro, A. Lepelley, J. J. Lafaille, D. J. Cua, and D. R. Littman, “The Orphan Nuclear Receptor RORγt Directs the Differentiation Program of Proinflammatory IL-17+ T Helper Cells,” *Cell*, vol. 126, no. 6, pp. 1121–1133, Sep. 2006.

[23] G. F. Sonnenberg, L. A. Fouser, and D. Artis, “Border patrol: regulation of immunity, inflammation and tissue homeostasis at barrier surfaces by IL-22,” *Nat. Immunol.*, vol. 12, no. 5, pp. 383–390, May 2011.

[24] A. De Luca, T. Zelante, C. D’Angelo, S. Zagarella, F. Fallarino, A. Spreca, R. G. Iannitti, P. Bonifazi, J.-C. Renauld, F. Bistoni, P. Puccetti, and L. Romani, “IL-22 defines a novel immune pathway of antifungal resistance,” *Mucosal Immunol.*, vol. 3, no. 4, pp. 361–373, Jul. 2010.

[25] O. B. Parks, D. A. Pociask, Z. Hodzic, J. K. Kolls, and M. Good, “Interleukin-22 Signaling in the Regulation of Intestinal Health and Disease,” *Front. Cell Dev. Biol.*, vol. 3, Jan. 2016.

[26] M. C. Fantini, S. Dominitzki, A. Rizzo, M. F. Neurath, and C. Becker, “In vitro generation of CD4+CD25+ regulatory cells from murine naive T cells,” *Nat. Protoc.*, vol. 2, no. 7, pp. 1789–1794, Jul. 2007.

[27] O. J. Harrison and F. M. Powrie, “Regulatory T Cells and Immune Tolerance in the Intestine,” *Cold Spring Harb. Perspect. Biol.*, vol. 5, no. 7, pp. a018341–a018341, Jul. 2013.

[28] R. H. DeKruyff, L. V. Rizzo, and D. T. Umetsu, “Induction of immunoglobulin synthesis by CD4+ T cell clones,” *Semin. Immunol.*, vol. 5, no. 6, pp. 421–430, Dec. 1993.

[29] M. L. Forchielli and W. A. Walker, “The role of gut-associated lymphoid tissues and

mucosal defence," *Br. J. Nutr.*, vol. 93, no. S1, p. S41, Apr. 2005.

[30] C. Jung, J.-P. Hugot, and F. Barreau, "Peyer's Patches: The Immune Sensors of the Intestine," *Int. J. Inflam.*, vol. 2010, pp. 1–12, 2010.

[31] Y. Kanamori, K. Ishimaru, M. Nanno, K. Maki, K. Ikuta, H. Nariuchi, and H. Ishikawa, "Identification of novel lymphoid tissues in murine intestinal mucosa where clusters of c-kit+ IL-7R+ Thy1+ lympho-hemopoietic progenitors develop.," *J. Exp. Med.*, vol. 184, no. 4, pp. 1449–59, Oct. 1996.

[32] R. T. Taylor, A. Lugering, K. A. Newell, and I. R. Williams, "Intestinal Cryptopatch Formation in Mice Requires Lymphotoxin and the Lymphotoxin Receptor," *J. Immunol.*, vol. 173, no. 12, pp. 7183–7189, Dec. 2004.

[33] M. R. Neutra, A. Frey, and J. P. Kraehenbuhl, "Epithelial M cells: Gateways for mucosal infection and immunization," *Cell*, vol. 86, no. 3, pp. 345–348, 1996.

[34] M. R. Neutra, E. Pringault, and J.-P. Kraehenbuhl, "ANTIGEN SAMPLING ACROSS EPITHELIAL BARRIERS AND INDUCTION OF MUCOSAL IMMUNE RESPONSES," *Annu. Rev. Immunol.*, vol. 14, no. 1, pp. 275–300, Apr. 1996.

[35] H. Hamada, T. Hiroi, Y. Nishiyama, H. Takahashi, Y. Masunaga, S. Hachimura, S. Kaminogawa, H. Takahashi-Iwanaga, T. Iwanaga, H. Kiyono, H. Yamamoto, and H. Ishikawa, "Identification of Multiple Isolated Lymphoid Follicles on the Antimesenteric Wall of the Mouse Small Intestine," *J. Immunol.*, vol. 168, no. 1, pp. 57–64, Jan. 2002.

[36] M. Buettner and U. Bode, "Lymph node dissection - understanding the immunological function of lymph nodes," *Clin. Exp. Immunol.*, vol. 169, no. 3, pp. 205–212, Sep. 2012.

[37] A. M. Mowat, "Anatomical basis of tolerance and immunity to intestinal antigens," *Nat. Rev. Immunol.*, vol. 3, no. 4, pp. 331–341, Apr. 2003.

[38] D. Schrenk, "Impact of dioxin-type induction of drug-metabolizing enzymes on the metabolism of endo- and xenobiotics," *Biochem. Pharmacol.*, vol. 55, no. 8, pp. 1155–1162, 1998.

[39] B. Stockinger, P. Di Meglio, M. Gialitakis, and J. H. Duarte, “The Aryl Hydrocarbon Receptor: Multitasking in the Immune System,” *Annu. Rev. Immunol.*, vol. 32, no. 1, pp. 403–432, Mar. 2014.

[40] A. P. Poland, E. Glover, J. R. Robinson, and D. W. Nebert, “Genetic expression of aryl hydrocarbon hydroxylase activity. Induction of monooxygenase activities and cytochrome P1-450 formation by 2,3,7,8-tetrachlorodibenzo-p-dioxin in mice genetically ‘nonresponsive’ to other aromatic hydrocarbons.,” *J. Biol. Chem.*, vol. 249, no. 17, pp. 5599–606, Sep. 1974.

[41] S. A. Skene, I. C. Dewhurst, and M. Greenberg, “Polychlorinated dibenzo-p-dioxins and polychlorinated dibenzofurans: the risks to human health. A review.,” *Hum. Toxicol.*, vol. 8, no. 3, pp. 173–203, May 1989.

[42] O. Sorg, “AhR signalling and dioxin toxicity,” *Toxicol. Lett.*, vol. 230, no. 2, pp. 225–233, Oct. 2014.

[43] A. Poland and E. Glover, “Comparison of 2,3,7,8-tetrachlorodibenzo-p-dioxin, a potent inducer of aryl hydrocarbon hydroxylase, with 3-methylcholanthrene.,” *Mol. Pharmacol.*, vol. 10, no. 2, pp. 349–59, Mar. 1974.

[44] K. M. Burbach, a Poland, and C. a Bradfield, “Cloning of the Ah-receptor cDNA reveals a distinctive ligand-activated transcription factor.,” *Proc. Natl. Acad. Sci. U. S. A.*, vol. 89, no. 17, pp. 8185–8189, 1992.

[45] Y.-Z. Gu, J. B. Hogenesch, and C. A. Bradfield, “The PAS Superfamily: Sensors of Environmental and Developmental Signals,” *Annu. Rev. Pharmacol. Toxicol.*, vol. 40, no. 1, pp. 519–561, Apr. 2000.

[46] P. Reddy, A. C. Jacquier, N. Abovich, G. Petersen, and M. Rosbash, “The period clock locus of D. melanogaster codes for a proteoglycan.,” *Cell*, vol. 46, no. 1, pp. 53–61, Jul. 1986.

[47] J. R. Nambu, J. O. Lewis, K. A. Wharton, and S. T. Crews, “The Drosophila single-minded gene encodes a helix-loop-helix protein that acts as a master regulator of CNS midline development.,” *Cell*, vol. 67, no. 6, pp. 1157–67, Dec. 1991.

[48] E. C. Hoffman, H. Reyes, F. F. Chu, F. Sander, L. H. Conley, B. A. Brooks, and O.

Hankinson, “Cloning of a factor required for activity of the Ah (dioxin) receptor.,” *Science*, vol. 252, no. 5008, pp. 954–8, May 1991.

[49] C. Murre, G. Bain, M. A. van Dijk, I. Engel, B. A. Furnari, M. E. Massari, J. R. Matthews, M. W. Quong, R. R. Rivera, and M. H. Stuiver, “Structure and function of helix-loop-helix proteins.,” *Biochim. Biophys. Acta*, vol. 1218, no. 2, pp. 129–35, Jun. 1994.

[50] M. B. Kumar, “The Q-rich Subdomain of the Human Ah Receptor Transactivation Domain Is Required for Dioxin-mediated Transcriptional Activity,” *J. Biol. Chem.*, vol. 276, no. 45, pp. 42302–42310, Nov. 2001.

[51] W. Li, S. Donat, O. Dohr, K. Unfried, and J. Abel, “Ah Receptor in Different Tissues of C57BL/6J and DBA/2J Mice: Use of Competitive Polymerase Chain Reaction to Measure Ah-Receptor mRNA Expression,” *Arch. Biochem. Biophys.*, vol. 315, no. 2, pp. 279–284, Dec. 1994.

[52] P. Fernandez-Salguero, T. Pineau, D. M. Hilbert, T. McPhail, S. S. Lee, S. Kimura, D. W. Nebert, S. Rudikoff, J. M. Ward, and F. J. Gonzalez, “Immune system impairment and hepatic fibrosis in mice lacking the dioxin-binding Ah receptor.,” *Science*, vol. 268, no. 5211, pp. 722–6, May 1995.

[53] J. V Schmidt, G. H. Su, J. K. Reddy, M. C. Simon, and C. A. Bradfield, “Characterization of a murine Ahr null allele: involvement of the Ah receptor in hepatic growth and development.,” *Proc. Natl. Acad. Sci. U. S. A.*, vol. 93, no. 13, pp. 6731–6, Jun. 1996.

[54] J. Mimura, K. Yamashita, K. Nakamura, M. Morita, T. N. Takagi, K. Nakao, M. Ema, K. Sogawa, M. Yasuda, M. Katsuki, and Y. Fujii-Kuriyama, “Loss of teratogenic response to 2,3,7,8-tetrachlorodibenzo-p-dioxin (TCDD) in mice lacking the Ah (dioxin) receptor,” *Genes to Cells*, vol. 2, no. 10, pp. 645–654, Nov. 1997.

[55] L. P. Nguyen and C. A. Bradfield, “The Search for Endogenous Activators of the Aryl Hydrocarbon Receptor,” *Chem. Res. Toxicol.*, vol. 21, no. 1, pp. 102–116, Jan. 2008.

[56] G. P. Lahvis, S. L. Lindell, R. S. Thomas, R. S. McCuskey, C. Murphy, E. Glover, M. Bentz, J. Southard, and C. A. Bradfield, “Portosystemic shunting and persistent fetal

vascular structures in aryl hydrocarbon receptor-deficient mice," *Proc. Natl. Acad. Sci.*, vol. 97, no. 19, pp. 10442–10447, Sep. 2000.

[57] P. M. Fernandez-Salguero, J. M. Ward, J. P. Sundberg, and F. J. Gonzalez, "Lesions of aryl-hydrocarbon receptor-deficient mice.," *Vet. Pathol.*, vol. 34, no. 6, pp. 605–14, Nov. 1997.

[58] T. Baba, J. Mimura, N. Nakamura, N. Harada, M. Yamamoto, K. -i. Morohashi, and Y. Fujii-Kuriyama, "Intrinsic Function of the Aryl Hydrocarbon (Dioxin) Receptor as a Key Factor in Female Reproduction," *Mol. Cell. Biol.*, vol. 25, no. 22, pp. 10040–10051, Nov. 2005.

[59] N. T. Nguyen, H. Hanieh, T. Nakahama, and T. Kishimoto, "The roles of aryl hydrocarbon receptor in immune responses," *Int. Immunol.*, vol. 25, no. 6, pp. 335–343, 2013.

[60] S. Zhang, C. Qin, and S. H. Safe, "Flavonoids as aryl hydrocarbon receptor agonists/antagonists: effects of structure and cell context.," *Environ. Health Perspect.*, vol. 111, no. 16, pp. 1877–82, Dec. 2003.

[61] C. J. Sinal and J. R. Bend, "Aryl hydrocarbon receptor-dependent induction of cyp1a1 by bilirubin in mouse hepatoma hepa 1c1c7 cells.," *Mol. Pharmacol.*, vol. 52, no. 4, pp. 590–9, Oct. 1997.

[62] D. L. Kroetz and D. C. Zeldin, "Cytochrome P450 pathways of arachidonic acid metabolism.," *Curr. Opin. Lipidol.*, vol. 13, no. 3, pp. 273–83, Jun. 2002.

[63] A. Rannug, U. Rannug, H. S. Rosenkranz, L. Winqvist, R. Westerholm, E. Agurell, and A. K. Grafström, "Certain photooxidized derivatives of tryptophan bind with very high affinity to the Ah receptor and are likely to be endogenous signal substances.," *J. Biol. Chem.*, vol. 262, no. 32, pp. 15422–7, Nov. 1987.

[64] G. H. Perdew, "Association of the Ah receptor with the 90-kDa heat shock protein," *J. Biol. Chem.*, vol. 263, no. 27, pp. 13802–13805, 1988.

[65] A. Kazlauskas, L. Poellinger, and I. Pongratz, "Evidence that the co-chaperone p23 regulates ligand responsiveness of the dioxin (aryl hydrocarbon) receptor," *J. Biol. Chem.*, vol. 274, no. 19, pp. 13519–13524, 1999.

[66] Q. Ma and J. P. Whitlock, “Cell Biology and Metabolism : A Novel Cytoplasmic Protein That Interacts with the Ah Receptor , Contains Tetratricopeptide Repeat Motifs , and Augments the Transcriptional Response to A Novel Cytoplasmic Protein That Interacts with the Ah Receptor , Conta,” vol. 272, no. 14, pp. 1–8, 1997.

[67] S. Tomita, H.-B. Jiang, T. Ueno, S. Takagi, K. Tohi, S. Maekawa, A. Miyatake, A. Furukawa, F. J. Gonzalez, J. Takeda, Y. Ichikawa, and Y. Takahama, “T cell-specific disruption of arylhydrocarbon receptor nuclear translocator (Arnt) gene causes resistance to 2,3,7,8-tetrachlorodibenzo-p-dioxin-induced thymic involution.,” *J. Immunol.*, vol. 171, no. 8, pp. 4113–20, Oct. 2003.

[68] Y. Fujii-Kuriyama, M. Ema, J. Mimura, and K. Sogawa, “Ah receptor: a novel ligand-activated transcription factor.,” *Exp. Clin. Immunogenet.*, vol. 11, no. 2–3, pp. 65–74, 1994.

[69] C. Weiß, S. K. Kolluri, F. Kiefer, and M. Göttlicher, “Complementation of Ah Receptor Deficiency in Hepatoma Cells: Negative Feedback Regulation and Cell Cycle Control by the Ah Receptor,” *Exp. Cell Res.*, vol. 226, no. 1, pp. 154–163, Jul. 1996.

[70] C. W. Barker, J. B. Fagan, and D. S. Pasco, “Interleukin-1 beta suppresses the induction of P4501A1 and P4501A2 mRNAs in isolated hepatocytes.,” *J. Biol. Chem.*, vol. 267, no. 12, pp. 8050–5, Apr. 1992.

[71] Y. Tian, S. Ke, M. S. Denison, A. B. Rabson, and M. A. Gallo, “Ah receptor and NF-kappaB interactions, a potential mechanism for dioxin toxicity.,” *J. Biol. Chem.*, vol. 274, no. 1, pp. 510–5, Jan. 1999.

[72] C. F. A. Vogel, E. Sciullo, W. Li, P. Wong, G. Lazennec, and F. Matsumura, “RelB, a New Partner of Aryl Hydrocarbon Receptor-Mediated Transcription,” *Mol. Endocrinol.*, vol. 21, no. 12, pp. 2941–2955, Dec. 2007.

[73] J. Mimura, M. Ema, K. Sogawa, and Y. Fujii-Kuriyama, “Identification of a novel mechanism of regulation of Ah (dioxin) receptor function.,” *Genes Dev.*, vol. 13, no. 1, pp. 20–5, 1999.

[74] T. Baba, J. Mimura, K. Gradin, A. Kuroiwa, T. Watanabe, Y. Matsuda, J. Inazawa, K. Sogawa, and Y. Fujii-Kuriyama, "Structure and Expression of the Ah Receptor Repressor Gene," *J. Biol. Chem.*, vol. 276, no. 35, pp. 33101–33110, Aug. 2001.

[75] T. Hosoya, N. Harada, J. Mimura, H. Motohashi, S. Takahashi, O. Nakajima, M. Morita, S. Kawauchi, M. Yamamoto, and Y. Fujii-Kuriyama, "Inducibility of cytochrome P450 1A1 and chemical carcinogenesis by benzo[a]pyrene in AhR repressor-deficient mice," *Biochem. Biophys. Res. Commun.*, vol. 365, no. 3, pp. 562–567, Jan. 2008.

[76] O. Brandstätter, O. Schanz, J. Vorac, J. König, T. Mori, T. Maruyama, M. Korkowski, T. Haarmann-Stemmann, D. von Smolinski, J. L. Schultze, J. Abel, C. Esser, H. Takeyama, H. Weighardt, and I. Förster, "Balancing intestinal and systemic inflammation through cell type-specific expression of the aryl hydrocarbon receptor repressor," *Sci. Rep.*, vol. 6, p. 26091, May 2016.

[77] M. Frericks, M. Meissner, and C. Esser, "Microarray analysis of the AHR system: Tissue-specific flexibility in signal and target genes," *Toxicol. Appl. Pharmacol.*, vol. 220, no. 3, pp. 320–332, May 2007.

[78] N. T. Nguyen, A. Kimura, T. Nakahama, I. Chinen, K. Masuda, K. Nohara, Y. Fujii-Kuriyama, and T. Kishimoto, "Aryl hydrocarbon receptor negatively regulates dendritic cell immunogenicity via a kynurenine-dependent mechanism," *Proc. Natl. Acad. Sci.*, vol. 107, no. 46, pp. 19961–19966, Nov. 2010.

[79] A. Kimura, T. Naka, T. Nakahama, I. Chinen, K. Masuda, K. Nohara, Y. Fujii-Kuriyama, and T. Kishimoto, "Aryl hydrocarbon receptor in combination with Stat1 regulates LPS-induced inflammatory responses," *J. Exp. Med.*, vol. 206, no. 9, pp. 2027–2035, Aug. 2009.

[80] M. Cella, A. Fuchs, W. Vermi, F. Facchetti, K. Otero, J. K. M. Lennerz, J. M. Doherty, J. C. Mills, and M. Colonna, "A human natural killer cell subset provides an innate source of IL-22 for mucosal immunity," *Nature*, vol. 457, no. 7230, pp. 722–725, Feb. 2009.

[81] E. A. Kiss, C. Vonarbourg, S. Kopfmann, E. Hobeika, D. Finke, C. Esser, and A. Diefenbach, "Natural Aryl Hydrocarbon Receptor Ligands Control Organogenesis of

Intestinal Lymphoid Follicles," *Science (80-.).*, vol. 334, no. 6062, pp. 1561–1565, Dec. 2011.

[82] Y. Li, S. Innocentin, D. R. Withers, N. A. Roberts, A. R. Gallagher, E. F. Grigorieva, C. Wilhelm, and M. Veldhoen, "Exogenous Stimuli Maintain Intraepithelial Lymphocytes via Aryl Hydrocarbon Receptor Activation," *Cell*, vol. 147, no. 3, pp. 629–640, Oct. 2011.

[83] I. Monteleone, T. T. MacDonald, F. Pallone, and G. Monteleone, "The aryl hydrocarbon receptor in inflammatory bowel disease," *Curr. Opin. Gastroenterol.*, vol. 28, no. 4, pp. 310–313, Jul. 2012.

[84] S. Wagage, G. Harms Pritchard, L. Dawson, E. L. Buza, G. F. Sonnenberg, and C. A. Hunter, "The Group 3 Innate Lymphoid Cell Defect in Aryl Hydrocarbon Receptor Deficient Mice Is Associated with T Cell Hyperactivation during Intestinal Infection," *PLoS One*, vol. 10, no. 5, p. e0128335, May 2015.

[85] B. Jux, S. Kadow, and C. Esser, "Langerhans Cell Maturation and Contact Hypersensitivity Are Impaired in Aryl Hydrocarbon Receptor-Null Mice," *J. Immunol.*, vol. 182, no. 11, pp. 6709–6717, Jun. 2009.

[86] S. Kadow, B. Jux, S. P. Zahner, B. Wingerath, S. Chmill, B. E. Clausen, J. Hengstler, and C. Esser, "Aryl Hydrocarbon Receptor Is Critical for Homeostasis of Invariant T Cells in the Murine Epidermis," *J. Immunol.*, vol. 187, no. 6, pp. 3104–3110, Sep. 2011.

[87] M. Tauchi, A. Hida, T. Negishi, F. Katsuoka, S. Noda, J. Mimura, T. Hosoya, A. Yanaka, H. Aburatani, Y. Fujii-Kuriyama, H. Motohashi, and M. Yamamoto, "Constitutive Expression of Aryl Hydrocarbon Receptor in Keratinocytes Causes Inflammatory Skin Lesions," *Mol. Cell. Biol.*, vol. 25, no. 21, pp. 9360–9368, Nov. 2005.

[88] J. M. Carvajal-Gonzalez, A. C. Roman, M. I. Cerezo-Guisado, E. M. Rico-Leo, G. Martin-Partido, and P. M. Fernandez-Salguero, "Loss of dioxin-receptor expression accelerates wound healing in vivo by a mechanism involving TGF," *J. Cell Sci.*, vol. 122, no. 11, pp. 1823–1833, Jun. 2009.

[89] B. Platzer, S. Richter, D. Kneidinger, D. Waltenberger, M. Woisetschlager, and H. Strobl, “Aryl Hydrocarbon Receptor Activation Inhibits In Vitro Differentiation of Human Monocytes and Langerhans Dendritic Cells,” *J. Immunol.*, vol. 183, no. 1, pp. 66–74, Jul. 2009.

[90] A. Kimura, T. Naka, K. Nohara, Y. Fujii-Kuriyama, and T. Kishimoto, “Aryl hydrocarbon receptor regulates Stat1 activation and participates in the development of Th17 cells,” *Proc. Natl. Acad. Sci.*, vol. 105, no. 28, pp. 9721–9726, Jul. 2008.

[91] M. Veldhoen, K. Hirota, A. M. Westendorf, J. Buer, L. Dumoutier, J.-C. Renauld, and B. Stockinger, “The aryl hydrocarbon receptor links TH17-cell-mediated autoimmunity to environmental toxins,” *Nature*, vol. 453, no. 7191, pp. 106–109, May 2008.

[92] J. Qiu, J. J. Heller, X. Guo, Z. E. Chen, K. Fish, Y.-X. Fu, and L. Zhou, “The Aryl Hydrocarbon Receptor Regulates Gut Immunity through Modulation of Innate Lymphoid Cells,” *Immunity*, vol. 36, no. 1, pp. 92–104, Jan. 2012.

[93] M. Veldhoen, K. Hirota, J. Christensen, A. O’Garra, and B. Stockinger, “Natural agonists for aryl hydrocarbon receptor in culture medium are essential for optimal differentiation of Th17 T cells.,” *J. Exp. Med.*, vol. 206, no. 1, pp. 43–9, 2009.

[94] F. J. Quintana, A. S. Basso, A. H. Iglesias, T. Korn, M. F. Farez, E. Bettelli, M. Caccamo, M. Oukka, and H. L. Weiner, “Control of Treg and TH17 cell differentiation by the aryl hydrocarbon receptor,” *Nature*, vol. 453, no. 7191, pp. 65–71, May 2008.

[95] R. Gandhi, D. Kumar, E. J. Burns, M. Nadeau, B. Dake, A. Laroni, D. Kozoriz, H. L. Weiner, and F. J. Quintana, “Activation of the aryl hydrocarbon receptor induces human type 1 regulatory T cell–like and Foxp3+ regulatory T cells,” *Nat. Immunol.*, vol. 11, no. 9, pp. 846–853, Sep. 2010.

[96] L. Apetoh, F. J. Quintana, C. Pot, N. Joller, S. Xiao, D. Kumar, E. J. Burns, D. H. Sherr, H. L. Weiner, and V. K. Kuchroo, “The aryl hydrocarbon receptor interacts with c-Maf to promote the differentiation of type 1 regulatory T cells induced by IL-27,” *Nat. Immunol.*, vol. 11, no. 9, pp. 854–861, Sep. 2010.

[97] I. D. Mascanfroni, M. C. Takenaka, A. Yeste, B. Patel, Y. Wu, J. E. Kenison, S. Siddiqui, A. S. Basso, L. E. Otterbein, D. M. Pardoll, F. Pan, A. Priel, C. B. Clish, S. C. Robson, and F. J. Quintana, "Metabolic control of type 1 regulatory T cell differentiation by AHR and HIF1-α," *Nat. Med.*, vol. 21, no. 6, pp. 638–646, May 2015.

[98] N. I. Kerkvliet, "Recent advances in understanding the mechanisms of TCDD immunotoxicity.," *Int. Immunopharmacol.*, vol. 2, no. 2–3, pp. 277–91, Feb. 2002.

[99] H. Lu, R. B. Crawford, J. E. Suarez-Martinez, B. L. F. Kaplan, and N. E. Kaminski, "Induction of the Aryl Hydrocarbon Receptor-Responsive Genes and Modulation of the Immunoglobulin M Response by 2,3,7,8-Tetrachlorodibenzo-p-Dioxin in Primary Human B Cells," *Toxicol. Sci.*, vol. 118, no. 1, pp. 86–97, Nov. 2010.

[100] H. Sekine, J. Mimura, M. Oshima, H. Okawa, J. Kanno, K. Igarashi, F. J. Gonzalez, T. Ikuta, K. Kawajiri, and Y. Fujii-Kuriyama, "Hypersensitivity of Aryl Hydrocarbon Receptor-Deficient Mice to Lipopolysaccharide-Induced Septic Shock," *Mol. Cell. Biol.*, vol. 29, no. 24, pp. 6391–6400, Dec. 2009.

[101] K. Furumatsu, S. Nishiumi, Y. Kawano, M. Ooi, T. Yoshie, Y. Shiomi, H. Kutsumi, H. Ashida, Y. Fujii-Kuriyama, T. Azuma, and M. Yoshida, "A Role of the Aryl Hydrocarbon Receptor in Attenuation of Colitis," *Dig. Dis. Sci.*, vol. 56, no. 9, pp. 2532–2544, Sep. 2011.

[102] T. Takamura, D. Harama, S. Matsuoka, N. Shimokawa, Y. Nakamura, K. Okumura, H. Ogawa, M. Kitamura, and A. Nakao, "Activation of the aryl hydrocarbon receptor pathway may ameliorate dextran sodium sulfate-induced colitis in mice," *Immunol. Cell Biol.*, vol. 88, no. 6, pp. 685–689, Aug. 2010.

[103] N. A. Molodecky, I. S. Soon, D. M. Rabi, W. A. Ghali, M. Ferris, G. Chernoff, E. I. Benchimol, R. Panaccione, S. Ghosh, H. W. Barkema, and G. G. Kaplan, "Increasing Incidence and Prevalence of the Inflammatory Bowel Diseases With Time, Based on Systematic Review," *Gastroenterology*, vol. 142, no. 1, p. 46–54.e42, Jan. 2012.

[104] R. J. Xavier and D. K. Podolsky, "Unravelling the pathogenesis of inflammatory bowel disease," *Nature*, vol. 448, no. 7152, pp. 427–434, Jul. 2007.

[105] C. G. Mayne and C. B. Williams, “Induced and Natural Regulatory T Cells in the Development of Inflammatory Bowel Disease,” *Inflamm. Bowel Dis.*, vol. 19, no. 8, pp. 1772–1788, Jul. 2013.

[106] I. J. Fuss, M. Neurath, M. Boirivant, J. S. Klein, C. de la Motte, S. A. Strong, C. Fiocchi, and W. Strober, “Disparate CD4+ lamina propria (LP) lymphokine secretion profiles in inflammatory bowel disease. Crohn’s disease LP cells manifest increased secretion of IFN-gamma, whereas ulcerative colitis LP cells manifest increased secretion of IL-5.,” *J. Immunol.*, vol. 157, no. 3, pp. 1261–70, Aug. 1996.

[107] J. P. Hugot, M. Chamaillard, H. Zouali, S. Lesage, J. P. Cézard, J. Belaiche, S. Almer, C. Tysk, C. A. O’Morain, M. Gassull, V. Binder, Y. Finkel, A. Cortot, R. Modigliani, P. Laurent-Puig, C. Gower-Rousseau, J. Macry, J. F. Colombel, M. Sahbatou, and G. Thomas, “Association of NOD2 leucine-rich repeat variants with susceptibility to Crohn’s disease.,” *Nature*, vol. 411, no. 6837, pp. 599–603, May 2001.

[108] Y. Ogura, D. K. Bonen, N. Inohara, D. L. Nicolae, F. F. Chen, R. Ramos, H. Britton, T. Moran, R. Karaliuskas, R. H. Duerr, J. P. Achkar, S. R. Brant, T. M. Bayless, B. S. Kirschner, S. B. Hanauer, G. Nuñez, and J. H. Cho, “A frameshift mutation in NOD2 associated with susceptibility to Crohn’s disease.,” *Nature*, vol. 411, no. 6837, pp. 603–6, May 2001.

[109] L. Sutherland, J. Singleton, J. Sessions, S. Hanauer, E. Krawitt, G. Rankin, R. Summers, H. Mekhjian, N. Greenberger, and M. Kelly, “Double blind, placebo controlled trial of metronidazole in Crohn’s disease.,” *Gut*, vol. 32, no. 9, pp. 1071–5, Sep. 1991.

[110] J. Cosnes, “Tobacco and IBD: relevance in the understanding of disease mechanisms and clinical practice,” *Best Pract. Res. Clin. Gastroenterol.*, vol. 18, no. 3, pp. 481–496, Jun. 2004.

[111] S. M. Lesko, D. W. Kaufman, L. Rosenberg, S. P. Helmrich, D. R. Miller, P. D. Stolley, and S. Shapiro, “Evidence for an increased risk of Crohn’s disease in oral contraceptive users.,” *Gastroenterology*, vol. 89, no. 5, pp. 1046–9, Nov. 1985.

[112] B. J. Geerling, P. C. Dagnelie, A. Badart-Smook, M. G. Russel, R. W. Stockbrugger, and R.-J. M. Brummer, “Diet as a risk factor for the development of ulcerative

colitis," *Am. J. Gastroenterol.*, vol. 95, no. 4, pp. 1008–1013, Apr. 2000.

[113] S. L. Jowett, "Influence of dietary factors on the clinical course of ulcerative colitis: a prospective cohort study," *Gut*, vol. 53, no. 10, pp. 1479–1484, Oct. 2004.

[114] H. Tilg, "Diet and Intestinal Immunity," *N. Engl. J. Med.*, vol. 366, no. 2, pp. 181–183, Jan. 2012.

[115] J. Flegr, J. Prandota, M. Sovičková, and Z. H. Israili, "Toxoplasmosis – A Global Threat. Correlation of Latent Toxoplasmosis with Specific Disease Burden in a Set of 88 Countries," *PLoS One*, vol. 9, no. 3, p. e90203, Mar. 2014.

[116] S. K. Halonen and L. M. Weiss, "Toxoplasmosis," in *Handbook of Clinical Neurology*, 2013, pp. 125–145.

[117] M. W. Benenson, E. T. Takafuji, S. M. Lemon, R. L. Greenup, and A. J. Sulzer, "Oocyst-Transmitted Toxoplasmosis Associated with Ingestion of Contaminated Water," *N. Engl. J. Med.*, vol. 307, no. 11, pp. 666–669, Sep. 1982.

[118] G. Desmonts and J. Couvreur, "Congenital Toxoplasmosis," *N. Engl. J. Med.*, vol. 290, no. 20, pp. 1110–1116, May 1974.

[119] F. Robert-Gangneux and M.-L. Darde, "Epidemiology of and Diagnostic Strategies for Toxoplasmosis," *Clin. Microbiol. Rev.*, vol. 25, no. 2, pp. 264–296, Apr. 2012.

[120] J. P. Dubey, D. S. Lindsay, and C. A. Speer, "Structures of Toxoplasma gondii tachyzoites, bradyzoites, and sporozoites and biology and development of tissue cysts.," *Clin. Microbiol. Rev.*, vol. 11, no. 2, pp. 267–99, Apr. 1998.

[121] D. G. Mordue, S. Håkansson, I. Niesman, and L. D. Sibley, "Toxoplasma gondii resides in a vacuole that avoids fusion with host cell endocytic and exocytic vesicular trafficking pathways.," *Exp. Parasitol.*, vol. 92, no. 2, pp. 87–99, Jun. 1999.

[122] M. W. Black and J. C. Boothroyd, "Lytic Cycle of Toxoplasma gondii," *Microbiol. Mol. Biol. Rev.*, vol. 64, no. 3, pp. 607–623, Sep. 2000.

[123] D. J. Ferguson and W. M. Hutchison, "The host-parasite relationship of Toxoplasma gondii in the brains of chronically infected mice.," *Virchows Arch. A. Pathol. Anat. Histopathol.*, vol. 411, no. 1, pp. 39–43, 1987.

[124] D. K. Howe, S. Honore, F. Derouin, and L. D. Sibley, “Determination of genotypes of Toxoplasma gondii strains isolated from patients with Determination of Genotypes of Toxoplasma gondii Strains Isolated from Patients with Toxoplasmosis,” *J. Clin. Microbiol.*, vol. 35, no. 6, pp. 1411–1414, 1997.

[125] L. D. Sibley and J. C. Boothroyd, “Virulent strains of Toxoplasma gondii comprise a single clonal lineage,” *Nature*, vol. 359, no. 6390, pp. 82–85, Sep. 1992.

[126] J. Ruskin and J. S. Remington, “Resistance to intracellular infection in mice immunized with Toxoplasma vaccine and adjuvant.,” *J. Reticuloendothel. Soc.*, vol. 9, no. 5, pp. 465–79, May 1971.

[127] L. D. Sibley, D. G. Mordue, C. Su, P. M. Robben, and D. K. Howe, “Genetic approaches to studying virulence and pathogenesis in Toxoplasma gondii.,” *Philos. Trans. R. Soc. Lond. B. Biol. Sci.*, vol. 357, no. 1417, pp. 81–8, Jan. 2002.

[128] U. Gross, W. Bohne, M. Soête, and J. F. Dubremetz, “Developmental differentiation between tachyzoites and bradyzoites of Toxoplasma gondii.,” *Parasitol. Today*, vol. 12, no. 1, pp. 30–3, Jan. 1996.

[129] O. Liesenfeld, “Oral Infection of C57BL/6 Mice with Toxoplasma gondii: A New Model of Inflammatory Bowel Disease?,” *J. Infect. Dis.*, vol. 185, no. s1, pp. S96–S101, Feb. 2002.

[130] F. Yarovinsky, “Innate immunity to Toxoplasma gondii infection,” *Nat. Rev. Immunol.*, vol. 14, no. 2, pp. 109–121, Jan. 2014.

[131] Y. M. Ling, M. H. Shaw, C. Ayala, I. Coppens, G. A. Taylor, D. J. P. Ferguson, and G. S. Yap, “Vacuolar and plasma membrane stripping and autophagic elimination of Toxoplasma gondii in primed effector macrophages,” *J. Exp. Med.*, vol. 203, no. 9, pp. 2063–2071, Sep. 2006.

[132] E. R. Pfefferkorn, “Interferon gamma blocks the growth of Toxoplasma gondii in human fibroblasts by inducing the host cells to degrade tryptophan.,” *Proc. Natl. Acad. Sci. U. S. A.*, vol. 81, no. 3, pp. 908–12, Feb. 1984.

[133] C. Fleischmann, A. Scherag, N. K. J. Adhikari, C. S. Hartog, T. Tsaganos, P. Schlattmann, D. C. Angus, and K. Reinhart, “Assessment of Global Incidence and

Mortality of Hospital-treated Sepsis. Current Estimates and Limitations," *Am. J. Respir. Crit. Care Med.*, vol. 193, no. 3, pp. 259–272, Feb. 2016.

[134] R. C. Bone, "Sir Isaac Newton, sepsis, SIRS, and CARS.," *Crit. Care Med.*, vol. 24, no. 7, pp. 1125–8, Jul. 1996.

[135] J. A. Buras, B. Holzmann, and M. Sitkovsky, "Model organisms: Animal Models of sepsis: setting the stage," *Nat. Rev. Drug Discov.*, vol. 4, no. 10, pp. 854–865, Oct. 2005.

[136] A. M. Binkowska, G. Michalak, and R. Słotwiński, "Review paper Current views on the mechanisms of immune responses to trauma and infection," *Cent. Eur. J. Immunol.*, vol. 2, pp. 206–216, 2015.

[137] F. A. Moore, A. Sauaia, E. E. Moore, J. B. Haenel, J. M. Burch, and D. C. Lezotte, "Postinjury Multiple Organ Failure," *J. Trauma Inj. Infect. Crit. Care*, vol. 40, no. 4, pp. 501–512, Apr. 1996.

[138] M. Wichmann, D. C. Borgstrom, and N. R. Caron, *Rural Surgery: Challenges and Solutions for the Rural Surgeon*. 2011.

[139] E. A. Deitch, "Animal models of sepsis and shock: a review and lessons learned.," *Shock*, vol. 9, no. 1, pp. 1–11, Jan. 1998.

[140] S. E. Greisman, "Mechsnisms of endotoxin tolerance: IV. Specificity of the pyrogenic refractory state during continous intravenous infusions of endotoxin," *J. Exp. Med.*, vol. 124, no. 5, pp. 983–1000, Nov. 1966.

[141] M. a Dobrovolskaia, A. E. Medvedev, K. E. Thomas, N. Cuesta, V. Toshchakov, T. Ren, M. J. Cody, S. M. Michalek, N. R. Rice, and S. N. Vogel, "Induction of in vitro reprogramming by Toll-like receptor (TLR)2 and TLR4 agonists in murine macrophages: effects of TLR 'homotolerance' versus 'heterotolerance' on NF-kappa B signaling pathway components.," *J. Immunol.*, vol. 170, no. 1, pp. 508–519, 2003.

[142] L. M. Sly, M. J. Rauh, J. Kalesnikoff, C. H. Song, and G. Krystal, "LPS-induced upregulation of SHIP is essential for endotoxin tolerance," *Immunity*, vol. 21, no. 2, pp. 227–239, 2004.

[143] M. D. Lehner, S. Morath, K. S. Michelsen, R. R. Schumann, and T. Hartung, "Induction of cross-tolerance by lipopolysaccharide and highly purified lipoteichoic acid via different Toll-like receptors independent of paracrine mediators.," *J. Immunol.*, vol. 166, no. 8, pp. 5161–5167, 2001.

[144] B. Poltorak, A.; He, X.; Smirnova, I.; Liu, M.; Van Huffel, C.; Du, X.; Birdwell, D.; Alejos, E.; Silva, M.; Galanos, C.; Freudenberg, M.; Ricciardi-Castagnoli, P.; Layton, B.; Beutler, "Defective LPS Signaling in C3H/HeJ and C57BL/10ScCr Mice: Mutations in Tlr4 Gene," *Science (80-.).*, vol. 282, no. 5396, pp. 2085–2088, Dec. 1998.

[145] Y. Nagai, S. Akashi, M. Nagafuku, M. Ogata, Y. Iwakura, S. Akira, T. Kitamura, A. Kosugi, M. Kimoto, and K. Miyake, "Essential role of MD-2 in LPS responsiveness and TLR4 distribution," *Nat. Immunol.*, Jun. 2002.

[146] M. Fujihara, M. Muroi, K. Tanamoto, T. Suzuki, H. Azuma, and H. Ikeda, "Molecular mechanisms of macrophage activation and deactivation by lipopolysaccharide: roles of the receptor complex.," *Pharmacol. Ther.*, vol. 100, no. 2, pp. 171–94, Nov. 2003.

[147] R. J. Beutler, B.; Hoebe, K.; Du, X.; Ulevitch, "How we detect microbes and respond to them: the Toll-like receptors and their transducers," *J. Leukoc. Biol.*, vol. 74, no. 4, pp. 479–485, Jul. 2003.

[148] W.-J. Lin and W.-C. Yeh, "Implication of Toll-like receptor and tumor necrosis factor alpha signaling in septic shock.," *Shock*, vol. 24, no. 3, pp. 206–9, Sep. 2005.

[149] R. Salomao, M. K. C. Brunialti, M. M. Rapozo, G. L. Baggio-Zappia, C. Galanos, and M. Freudenberg, "Bacterial Sensing, Cell Signaling, and Modulation of the Immune Response During Sepsis," *Shock*, vol. 38, no. 3, pp. 227–242, Aug. 2012.

[150] A. M. T. da Silva, H. C. Kaulbach, F. S. Chuidian, D. R. Lambert, A. F. Suffredini, and R. L. Danner, "Shock and Multiple-Organ Dysfunction after Self-Administration of Salmonella Endotoxin," *N. Engl. J. Med.*, vol. 328, no. 20, pp. 1457–1460, May 1993.

[151] N. C. Riedemann, R.-F. Guo, and P. A. Ward, "The enigma of sepsis," *J. Clin. Invest.*, vol. 112, no. 4, pp. 460–467, Aug. 2003.

[152] N. Zantl, A. Uebe, B. Neumann, H. Wagner, J. R. Siewert, B. Holzmann, C. D. Heidecke, and K. Pfeffer, “Essential role of gamma interferon in survival of colon ascendens stent peritonitis, a novel murine model of abdominal sepsis.,” *Infect. Immun.*, vol. 66, no. 5, pp. 2300–9, May 1998.

[153] S. Maier, T. Traeger, M. Entleutner, A. Westerholt, B. Kleist, N. Hüser, B. Holzmann, A. Stier, K. Pfeffer, and C.-D. Heidecke, “Cecal ligation and puncture versus colon ascendens stent peritonitis: two distinct animal models for polymicrobial sepsis.,” *Shock*, vol. 21, no. 6, pp. 505–11, Jun. 2004.

[154] T. Traeger, P. Koerner, W. Kessler, K. Cziupka, S. Diedrich, A. Busemann, C.-D. Heidecke, and S. Maier, “Colon Ascendens Stent Peritonitis (CASP) - a Standardized Model for Polymicrobial Abdominal Sepsis,” *J. Vis. Exp.*, no. 46, Dec. 2010.

[155] H. Karasuyama and F. Melchers, “Establishment of mouse cell lines which constitutively secrete large quantities of interleukin 2, 3, 4 or 5, using modified cDNA expression vectors,” *Eur. J. Immunol.*, vol. 18, no. 1, pp. 97–104, Jan. 1988.

[156] I. Reiter-Owona, M. Sahm, and H. M. Seitz, “Nonimmunological factors affecting the release of excreted/secreted antigens from Toxoplasma gondii cysts.,” *Zentralbl. Bakteriol.*, vol. 284, no. 2–3, pp. 378–89, Jul. 1996.

[157] C. Jost, I. Reiter-Owona, and O. Liesenfeld, “The timing of sulfadiazine therapy impacts the reactivation of latent Toxoplasma infection in IRF-8−/− mice,” *Parasitol. Res.*, vol. 101, no. 6, pp. 1603–1609, Oct. 2007.

[158] J. V Schmidt, G. H. Su, J. K. Reddy, M. C. Simon, and C. a Bradfield, “Characterization of a murine Ahr null allele: involvement of the Ah receptor in hepatic growth and development.,” *Proc. Natl. Acad. Sci. U. S. A.*, vol. 93, no. 13, pp. 6731–6736, 1996.

[159] W. T. Golde, P. Gollobin, and L. L. Rodriguez, “A rapid, simple, and humane method for submandibular bleeding of mice using a lancet,” *Lab Anim. (NY).*, vol. 34, no. 9, pp. 39–43, Oct. 2005.

[160] U. Erben, C. Loddenkemper, K. Doerfel, S. Spieckermann, D. Haller, M. Heimesaat, M. Zeitz, B. Siegmund, and A. A. Kühl, “A guide to histomorphological evaluation of

intestinal inflammation in mouse models," *Int. J. Clin. Exp. Pathol.*, vol. 7, no. 8, pp. 4557–4576, 2014.

[161] A. Bessede, M. Gargaro, M. T. Pallotta, D. Matino, G. Servillo, C. Brunacci, S. Bicciato, E. M. C. Mazza, A. Macchiarulo, C. Vacca, R. Iannitti, L. Tissi, C. Volpi, M. L. Belladonna, C. Orabona, R. Bianchi, T. V. Lanz, M. Platten, M. A. Della Fazia, D. Piobbico, T. Zelante, H. Funakoshi, T. Nakamura, D. Gilot, M. S. Denison, G. J. Guillemin, J. B. DuHadaway, G. C. Prendergast, R. Metz, M. Geffard, L. Boon, M. Pirro, A. Iorio, B. Veyret, L. Romani, U. Grohmann, F. Fallarino, and P. Puccetti, "Aryl hydrocarbon receptor control of a disease tolerance defence pathway," *Nature*, vol. 511, no. 7508, pp. 184–190, Jul. 2014.

[162] L. Zhou, "AHR Function in Lymphocytes: Emerging Concepts," *Trends Immunol.*, vol. 37, no. 1, pp. 17–31, Jan. 2016.

[163] N. Baba, M. Rubio, L. Kenins, C. Regairaz, M. Woisetschlager, J. M. Carballido, and M. Sarfati, "The aryl hydrocarbon receptor (AhR) ligand VAF347 selectively acts on monocytes and naïve CD4(+) Th cells to promote the development of IL-22-secreting Th cells.," *Hum. Immunol.*, vol. 73, no. 8, pp. 795–800, Aug. 2012.

[164] E. V. Dang, J. Barbi, H.-Y. Yang, D. Jinasena, H. Yu, Y. Zheng, Z. Bordman, J. Fu, Y. Kim, H.-R. Yen, W. Luo, K. Zeller, L. Shimoda, S. L. Topalian, G. L. Semenza, C. V. Dang, D. M. Pardoll, and F. Pan, "Control of TH17/Treg Balance by Hypoxia-Inducible Factor 1," *Cell*, vol. 146, no. 5, pp. 772–784, Sep. 2011.

[165] G. L. Semenza, "Hypoxia-Inducible Factor 1 (HIF-1) Pathway," *Sci. STKE*, vol. 2007, no. 407, p. cm8-cm8, Oct. 2007.

[166] M. Grazia Roncarolo, S. Gregori, M. Battaglia, R. Bacchetta, K. Fleischhauer, and M. K. Levings, "Interleukin-10-secreting type 1 regulatory T cells in rodents and humans," *Immunol. Rev.*, vol. 212, no. 1, pp. 28–50, Aug. 2006.

[167] M. M. Heimesaat, S. Bereswill, A. Fischer, D. Fuchs, D. Struck, J. Niebergall, H.-K. Jahn, I. R. Dunay, A. Moter, D. M. Gescher, R. R. Schumann, U. B. Gobel, and O. Liesenfeld, "Gram-negative bacteria aggravate murine small intestinal Th1-type immunopathology following oral infection with Toxoplasma gondii.," *J. Immunol.*, vol. 177, no. 12, pp. 8785–8795, 2006.

[168] F. J. D. Mennechet, L. H. Kasper, N. Rachinel, W. Li, A. Vandewalle, and D. Buzoni-Gatel, “Lamina propria CD4+ T lymphocytes synergize with murine intestinal epithelial cells to enhance proinflammatory response against an intracellular pathogen.,” *J. Immunol.*, vol. 168, no. 6, pp. 2988–96, Mar. 2002.

[169] M. Muñoz, M. M. Heimesaat, K. Danker, D. Struck, U. Lohmann, R. Plickert, S. Bereswill, A. Fischer, I. R. Dunay, K. Wolk, C. Loddenkemper, H.-W. Krell, C. Libert, L. R. Lund, O. Frey, C. Hölscher, Y. Iwakura, N. Ghilardi, W. Ouyang, T. Kamradt, R. Sabat, and O. Liesenfeld, “Interleukin (IL)-23 mediates Toxoplasma gondii –induced immunopathology in the gut via matrixmetalloproteinase-2 and IL-22 but independent of IL-17,” *J. Exp. Med.*, vol. 206, no. 13, pp. 3047–3059, Dec. 2009.

[170] A. Vossenkämper, D. Struck, C. Alvarado-Esquivel, T. Went, K. Takeda, S. Akira, K. Pfeffer, G. Alber, M. Lochner, I. Förster, and O. Liesenfeld, “Both IL-12 and IL-18 contribute to small intestinal Th1-type immunopathology following oral infection with Toxoplasma gondii , but IL-12 is dominant over IL-18 in parasite control,” *Eur. J. Immunol.*, vol. 34, no. 11, pp. 3197–3207, Nov. 2004.

[171] S. Fujino, A. Andoh, S. Bamba, A. Ogawa, K. Hata, Y. Araki, T. Bamba, and Y. Fujiyama, “Increased expression of interleukin 17 in inflammatory bowel disease.,” *Gut*, vol. 52, no. 1, pp. 65–70, Jan. 2003.

[172] G. S. Baird, D. A. Zacharias, and R. Y. Tsien, “Biochemistry, mutagenesis, and oligomerization of DsRed, a red fluorescent protein from coral,” *Proc. Natl. Acad. Sci.*, vol. 97, no. 22, pp. 11984–11989, Oct. 2000.

[173] M. E. Hahn, S. I. Karchner, M. A. Shapiro, and S. A. Perera, “Molecular evolution of two vertebrate aryl hydrocarbon (dioxin) receptors (AHR1 and AHR2) and the PAS family.,” *Proc. Natl. Acad. Sci. U. S. A.*, vol. 94, no. 25, pp. 13743–8, Dec. 1997.

[174] O. Brandstätter, “Expression und Funktion des Arylhydrocarbon Rezeptor Repressors (AhRR) im darmassoziierten Immunsystem,” *Diss. Rheinische Friedrich-Wilhelms Univ. Bonn*, 2015.

[175] R. Basu, D. B. O’Quinn, D. J. Silberger, T. R. Schoeb, L. Fouser, W. Ouyang, R. D. Hatton, and C. T. Weaver, “Th22 Cells Are an Important Source of IL-22 for Host Protection against Enteropathogenic Bacteria,” *Immunity*, vol. 37, no. 6, pp. 1061–

1075, Dec. 2012.

[176] N. Gagliani, M. C. A. Vesely, A. Iseppon, L. Brockmann, H. Xu, N. W. Palm, M. R. de Zoete, P. Licona-Limón, R. S. Paiva, T. Ching, C. Weaver, X. Zi, X. Pan, R. Fan, L. X. Garmire, M. J. Cotton, Y. Drier, B. Bernstein, J. Geginat, B. Stockinger, E. Esplugues, S. Huber, and R. A. Flavell, "Th17 cells transdifferentiate into regulatory T cells during resolution of inflammation," *Nature*, vol. 523, no. 7559, pp. 221–225, Apr. 2015.

[177] Y. M. Shah, "The role of hypoxia in intestinal inflammation," *Mol. Cell. Pediatr.*, vol. 3, no. 1, p. 1, Dec. 2016.

[178] D. K. Podolsky, "Inflammatory Bowel Disease," *N. Engl. J. Med.*, vol. 347, no. 6, pp. 417–429, Aug. 2002.

[179] Y. Suzuki, M. Orellana, R. Schreiber, and J. Remington, "Interferon-gamma: the major mediator of resistance against Toxoplasma gondii," *Science (80-.).*, vol. 240, no. 4851, pp. 516–518, Apr. 1988.

[180] C. R. Sturge and F. Yarovinsky, "Complex Immune Cell Interplay in the Gamma Interferon Response during Toxoplasma gondii Infection," *Infect. Immun.*, vol. 82, no. 8, pp. 3090–3097, Aug. 2014.

[181] C. Reis e Sousa, S. Hieny, T. Scharton-Kersten, D. Jankovic, H. Charest, R. N. Germain, and A. Sher, "In vivo microbial stimulation induces rapid CD40 ligand-independent production of interleukin 12 by dendritic cells and their redistribution to T cell areas.," *J. Exp. Med.*, vol. 186, no. 11, pp. 1819–29, Dec. 1997.

[182] T. M. Scharton-Kersten, T. A. Wynn, E. Y. Denkers, S. Bala, E. Grunvald, S. Hieny, R. T. Gazzinelli, and A. Sher, "In the absence of endogenous IFN-gamma, mice develop unimpaired IL-12 responses to Toxoplasma gondii while failing to control acute infection.," *J. Immunol.*, vol. 157, no. 9, pp. 4045–54, Nov. 1996.

[183] Y. Lee, A. Awasthi, N. Yosef, F. J. Quintana, S. Xiao, A. Peters, C. Wu, M. Kleinewietfeld, S. Kunder, D. A. Hafler, R. A. Sobel, A. Regev, and V. K. Kuchroo, "Induction and molecular signature of pathogenic TH17 cells," *Nat. Immunol.*, vol. 13, no. 10, pp. 991–999, Sep. 2012.

[184] S. Wu, K.-J. Rhee, E. Albesiano, S. Rabizadeh, X. Wu, H.-R. Yen, D. L. Huso, F. L. Brancati, E. Wick, F. McAllister, F. Housseau, D. M. Pardoll, and C. L. Sears, "A human colonic commensal promotes colon tumorigenesis via activation of T helper type 17 T cell responses," *Nat. Med.*, vol. 15, no. 9, pp. 1016–1022, Sep. 2009.

[185] R. Guiton, V. Vasseur, S. Charron, M. T. Arias, N. Van Langendonck, D. Buzoni-Gatel, B. Ryffel, and I. Dimier-Poisson, "Interleukin 17 Receptor Signaling Is Deleterious during Toxoplasma gondii Infection in Susceptible BL6 Mice," *J. Infect. Dis.*, vol. 202, no. 3, pp. 427–435, Aug. 2010.

[186] G. Cui, X. Qin, L. Wu, Y. Zhang, X. Sheng, Q. Yu, H. Sheng, B. Xi, J. Z. Zhang, and Y. Q. Zang, "Liver X receptor (LXR) mediates negative regulation of mouse and human Th17 differentiation," *J. Clin. Invest.*, vol. 121, no. 2, pp. 658–670, Feb. 2011.

[187] J. S. Stumhofer, A. Laurence, E. H. Wilson, E. Huang, C. M. Tato, L. M. Johnson, A. V Villarino, Q. Huang, A. Yoshimura, D. Sehy, C. J. M. Saris, J. J. O'Shea, L. Hennighausen, M. Ernst, and C. A. Hunter, "Interleukin 27 negatively regulates the development of interleukin 17–producing T helper cells during chronic inflammation of the central nervous system," *Nat. Immunol.*, vol. 7, no. 9, pp. 937–945, Sep. 2006.

[188] C. J. Kim, A. Nazli, O. L. Rojas, D. Chege, Z. Alidina, S. Huibner, S. Mujib, E. Benko, C. Kovacs, L. Y. Y. Shin, A. Grin, G. Kandel, M. Loutfy, M. Ostrowski, J. L. Gommerman, C. Kaushic, and R. Kaul, "A role for mucosal IL-22 production and Th22 cells in HIV-associated mucosal immunopathogenesis," *Mucosal Immunol.*, vol. 5, no. 6, pp. 670–680, Nov. 2012.

[189] N. Ota, K. Wong, P. A. Valdez, Y. Zheng, N. K. Crellin, L. Diehl, and W. Ouyang, "IL-22 bridges the lymphotoxin pathway with the maintenance of colonic lymphoid structures during infection with Citrobacter rodentium," *Nat. Immunol.*, vol. 12, no. 10, pp. 941–948, Aug. 2011.

[190] J. H. Bernink, C. P. Peters, M. Munneke, A. A. te Velde, S. L. Meijer, K. Weijer, H. S. Hreggvidsdottir, S. E. Heinsbroek, N. Legrand, C. J. Buskens, W. A. Bemelman, J. M. Mjösberg, and H. Spits, "Human type 1 innate lymphoid cells accumulate in inflamed mucosal tissues," *Nat. Immunol.*, vol. 14, no. 3, pp. 221–229, Jan. 2013.

[191] C. S. N. Klose, M. Flach, L. Möhle, L. Rogell, T. Hoyler, K. Ebert, C. Fabiunke, D. Pfeifer, V. Sexl, D. Fonseca-Pereira, R. G. Domingues, H. Veiga-Fernandes, S. J. Arnold, M. Busslinger, I. R. Dunay, Y. Tanriver, and A. Diefenbach, "Differentiation of Type 1 ILCs from a Common Progenitor to All Helper-like Innate Lymphoid Cell Lineages," *Cell*, vol. 157, no. 2, pp. 340–356, Apr. 2014.

[192] S. Wagage, B. John, B. L. Krock, A. O. Hall, L. M. Randall, C. L. Karp, M. C. Simon, and C. A. Hunter, "The Aryl Hydrocarbon Receptor Promotes IL-10 Production by NK Cells," *J. Immunol.*, vol. 192, no. 4, pp. 1661–1670, Feb. 2014.

[193] R. Zellweger, M. W. Wichmann, A. Ayala, S. Stein, C. M. DeMaso, and I. H. Chaudry, "Females in proestrus state maintain splenic immune functions and tolerate sepsis better than males.," *Crit. Care Med.*, vol. 25, no. 1, pp. 106–10, Jan. 1997.

[194] P. J. Offner, E. E. Moore, and W. L. Biffl, "Male gender is a risk factor for major infections after surgery.," *Arch. Surg.*, vol. 134, no. 9, pp. 935-8-40, Sep. 1999.

[195] J. E. McGowan, M. W. Barnes, and M. Finland, "Bacteremia at Boston City Hospital: Occurrence and mortality during 12 selected years (1935-1972), with special reference to hospital-acquired cases.," *J. Infect. Dis.*, vol. 132, no. 3, pp. 316–35, Sep. 1975.

[196] J. Liu, G. Mankani, X. Shi, M. Meyer, S. Cunningham-Runddles, X. Ma, and Z. S. Sun, "The Circadian Clock Period 2 Gene Regulates Gamma Interferon Production of NK Cells in Host Response to Lipopolysaccharide-Induced Endotoxic Shock," *Infect. Immun.*, vol. 74, no. 8, pp. 4750–4756, Aug. 2006.

I. List of abbreviations

3MC	3-Methylcholanthrene
ACT	Tris-buffered ammonium chloride
AhR	Aryl hydrocarbon Receptor
AhRR	Aryl hydrocarbon Receptor Repressor
AIP	Aryl hydrocarbon Receptor-interacting protein
AMP	Antimicrobial peptides
ARNT	Aryl hydrocarbon receptor nuclear translocator
APC	Antigen presenting cell
APC	Allophycocyanin
APS	Ammoniumpersulfat
bHLH	Basic helis-loop-helix
BCR	B cell receptor
BMDC	Bome marrow-derived dendritic cell
BMMϕ	Bone marrow-derived macrophage
BSA	Bovine serum albumin
CARS	Compensatory anti-inflammatory responses
CASP	Colon ascendens stent peritonitis
CD	Cluster of differentiation
CLP	Common lymphoid progenitor
CMP	Common myeloid progenitor
CO_2	Carbon dioxide
CP	Cryptopatches
Cy7	Cyanine 7
d	Day
DABCO	Triethylendiamin
DAMP	Danger associated molecular pattern
DAPI	4,6-diamidino-2-phenylindole
DC	Dendritic cell
DMSO	Dimethyl sulfoxide
DNA	Desoxyribonucleic acid
dNTP	deoxynucleotides

ds	Double stranded
DSS	Dextran sulfate sodium
DTT	Dithiothreitol
EAE	Experimental autoimmune encephalomyelitis
EDTA	Ethylene-diaminetetraacetic acid
EGFP	Enhanced green fluorescent protein
EHEC	Enterohaemorrhagic *Esherichia coli*
ELISA	Enzyme-linked Immunosorbent Assay
ES	Embryonic stem
EtOH	Ethanol
FA	Formaldehyde
FACS	Fluorescence activated cell sorting
FAE	Follicle-associated epithelium
FCS	Fetal calf serum
FICZ	6-formylindolo(3,2-b)carbazole
FITC	Fluorescein isothiocyanate
FMO	Fluorescent minus one
FoxP3	Forkhead box P3
FSC	Forward scatter
g	gram
GAPDH	Glyceraldehyde 3 phosphate dehydrogenase
GALT	Gut-associated lymphoid tissue
GC	Germinal center
GM-CSF	Granulocyte macrophage colony stimulating factor
GMP	Granulocyte/macrophage progenitor
h	hour
HAH	Halogenated aromatic hydrocarbons
HEPES	4-(2-hydroxyethyl)-1-piperazineethanesulfonic acid
H&E	Hematoxylin and eosin
HCl	Hydrogen chloride
HIF	Hypoxia inducible factor
HRP	Horse radish peroxidase
HSC	Hematopoietic stem cell
Hsp90	Heat shock protein 90
I3C	Indol-3-carbinol
IBD	Inflammatory bowel disease

IDO	Induce indoleamine 2,3-dioxygenase
IEL	Intraepithelial lymphocytes
IFN	Interferon
Ig	Immunglobulin
IL	Interleukin
ILC	Innate lymphoid cells
ILF	Innate lymphoid follicle
i.p.	Intraperitoneal
IVC	Individually ventilated cages
kb	Kilobase pair
KC	Keratinocyte
KCl	Potassium chloride
kg	Kilogram
Kyn	Kynurenine
LC	Langerhans cells
LD	Lethal dose
LN	Lymph node
LP	Lamina propria
LPS	Lipopolysaccharide
LTi	Lymphoid tissue inducer
mg	Milligram
µm	micrometer
mm	millimeter
mM	Millimolar
M	Molar
MACS	Magnetic cell seperation
MALT	Mucosa-associated lymphoid tissue
M-CSF	Macrophage colony stimulating factor
MD-2	Myeloid differentiation factor
MEP	Megakaryocyte/erythroid progenitor
MFI	Median fluorescence intensity
MHC-I	Major histocompatibility complex class I
MHC-II	Major histocompatibility complex class II
min	Minute
ml	Milliliter
mLN	Mesenteric lymph node
MyD88	Myeloid differentiation primary response gene 88
NaCl	Sodium chloride
NaOH	Sodium hydroxide solution

NF-κB	Nuclear factor-κB
NK	Natural killer cell
NLR	NOD-like receptors
NOD	nucleotide-binding oligomerization domain
O_2	Oxygen
o.n.	Over night
OVA	Ovalbumin
p23	Glutathione-dependent prostaglandin E synthase 3
PAH	Polycyclic aromatic hydrocarbons
PAMP	Pathogen associated molecular pattern
PAS	Per-Arnt-Sim
PBS	Phosphate buffered saline
PCB	Polychlorinated biphenyl
PCDD	Polychlorinated dibenzo-p-dioxins
PCR	Polymerase chain reaction
PE	Phycoerythrin
PerCP	Peridinin chlorophyll protein
PFA	Paraformaldehyde
PMA	Phorbol 12-myristate 13-acetate
PP	Peyer's Patch
PRR	Pattern recognition receptor
PV	Parasitophorous vacuole
RFP	Red fluorescent protein
RIG	retinoic acid-inducible gene
RLR	RIG-like receptors
RNA	Ribonucleic acid
RORγt	RAR-related orphan receptor gamma thymus
ROS	Reactive oxygen species
SDS	Sodium dodecyl sulfate
sec	Seconds
SEM	Standard error of the mean
SIRS	Systemic inflammatory response
SSC	Sideward scatter
TAE	Tris-acetate EDTA
TBS	Tris-buffered saline
TCDD	2,3,7,8-tetrachlorodibenzo-p-dioxin
TCR	T cell receptor

TEMED	Tetramethyl-ethylenediamine
TGF	Transforming growth factor
T_h	T helper
TLR	Toll-like receptor
TNF	Tumor necrose factor
T_r1	Type 1 regulatory T cell
T_{reg}	Regulatory T cell
TRIF	TIR domain-containing adapter-inducing interferon-β
V	Volt
WB	Western blot
WT	Wild-type
XRE	Xenobiotic response elements

II. Figure index

III. Table index

IV. Summary

The Aryl hydrocarbon Receptor (AhR) is a ligand-activated transcription factor that regulates the detoxification of environmental toxins by the induction of metabolizing enzymes. Initially, the AhR was described as a receptor for TCDD, but it could also be identified as a sensor of endogenous ligands, such as tryptophan derivatives, polyphenols and dietary ligands. The activity of the AhR is regulated by the AhR repressor (AhRR), which is an AhR target gene, but its exact function is still largely unknown.

In this thesis, the AhRR/EGFP mouse strain generated in our group, which express green fluorescent protein under the control of the *ahrr* promotor, were analyzed in parasitic and polymicrobial infections. The examination of different *in vitro* differentiated helper T cell populations, isolated from naive splenic $CD4^+$ T cells and differentiated using a combination of different cytokines and antibodies in T_h1, T_h2, T_h17, T_h22, T_r1 and T_{reg} cell populations, showed that the AhRR had no intrinsic effect on the helper T cell differentiation. AhRR/EGFP was expressed in T_h17, T_h22, T_r1 and T_{reg} cells, but not in T_h1 and T_h2 cells. In an Ileitis model, caused by oral infection with the parasite *Toxoplasma gondii*, it was shown that AhRR-deficient mice own a markedly increased sensitivity compared to wild-type littermate control mice. This result was supported by a stronger pathology as well as decreased IFNγ production in the ileum of AhRR-deficient mice. Using the CASP model, which induces polymicrobial peritonitis, it was shown that AhRR-deficient mice exhibited an increased survival rate compared to wild-type mice. Furthermore, the establishment of endotoxin tolerance in AhRR-deficient as well as AhR-deficient mice was analyzed. A tolerance indicated by decreased TNF production could be determined in wild-type, AhR and AhRR-deficient macrophages *in vitro* as well as in AhR- and AhRR-deficient and wild-type mice. Furthermore, AhR-deficient and wild-type mice were also able to establish an endotoxin tolerance after endotoxin priming *in vivo*.

In the course of this work, it became evident of the AhRR has an influence in the intestinal and systemic immune system, which indicate an important role of the AhR/AhRR system in the regulation of immune responses.

V. Zusammenfassung

Der Arylhydrokarbonrezeptor (AhR) ist ein Liganden-aktivierter Transkriptionsfaktor, der die Detoxifikation von Umweltgiften durch die Induktion metabolisierender Enzyme reguliert. Ursprünglich wurde der AhR als Rezeptor für exogene Chemikalien, wie TCDD beschrieben, jedoch konnte er auch als Sensor endogener Liganden, wie Tryptophanderivaten, Polyphenolen und Nahrungsinhaltsstoffen identifiziert werden. Die Aktivität des AhR wird durch den AhR-Repressor (AhRR) reguliert, der ein Zielgen des AhR ist, dessen genaue Funktion jedoch noch größtenteils unbekannt ist.

In der hier vorgelegten Dissertation wurde die in unserer Arbeitsgruppe generierte AhRR/EGFP-Mauslinie, die grün fluoreszierendes Protein unter der Kontrolle des *ahrr* Promotors exprimieren, in parasitären und polymikrobiellen Infektionen untersucht. Die Analyse verschiedener T Helfer Zell Populationen, welche *in vitro* aus naiven Milz $CD4^+$ T Zellen mithilfe einer Kombination aus verschiedenen Zytokinen und Antikörpern in T_h1, T_h2, T_h17, T_h22, T_r1 und T_{reg} Zellpopulationen differenziert wurden, zeigte, dass der AhRR keinen intrinsischen Effekt auf deren Differenzierung hat, allerdings in T_h17, T_h22, T_r1 und T_{reg} Zellen, jedoch nicht in T_h1 und T_h2 Zellen exprimiert wird. In einem Ileitis Modell, verursacht durch orale Infektion mit dem Parasiten *Toxoplasma gondii*, konnte gezeigt werden, dass AhRR-defizienten Mäuse im Vergleich zu Wildtyp-Wurfgeschwistern eine deutlich erhöhte Empfindlichkeit aufweisen. Dieses Ergebnis wurde durch eine stärkere Gewebszerstörung sowie geringere Produktion von IFNγ im Ileum von AhRR-defiziente Mäusen unterstützt. Mittels des CASP Modells, welches eine polymikrobielle Peritonitis induziert, konnte gezeigt werden, dass AhRR-defiziente Mäuse im Vergleich zu Wildtyp-Mäusen geschützt waren. Weiterhin wurde die Etablierung einer Endotoxin-Toleranz in AhRR-defizienten als auch in AhR-defizienten Mäusen analysiert. Dabei konnte sowohl in Wildtyp-, AhR- als auch in AhRR-defizienten Makrophagen *in vitro*, als auch bei AhR- und AhRR-defizienten und Wildtyp-Mäusen die Induktion einer Endotoxin-Toleranz durch eine geringere Produktion von TNF nachgewiesen werden. Auch *in vivo* konnte eine Toleranz bei AhR-defizienten und Wildtyp-Mäusen nach Vorbehandlung mit Endotoxin festgestellt werden.

In dieser Arbeit wurden klare Hinweise auf einen Einfluss des AhRR auf das darmassoziierte, sowie systemischen Immunsystem gefunden, welche auf eine wichtige Rolle des AhR/AhRR-System bei der Regulation von Immunantworten bei Infektionen hindeuten.

VI. Acknowledgements

First and foremost, I would like to express my sincere gratitude to Prof. Dr. Irmgard Förster and PD Dr. Heike Weighardt for giving me the opportunity to complete my thesis in their working group and of course for the help and assistance throughout the project. I am very grateful for the continuous support, patience, encouragement and immense knowledge. Especially, I would like to thank Heike for the guidance, inspiring conversations and the very amusing, witty anecdotes. Her joy and enthusiasm was contagious and very motivational.

Besides my supervisors, I would like to thank Prof. Dr. Johannes Hegemann for mentoring me and the co-correction of my thesis.

My sincere thanks also go to Julia Vorac, Sonja Fassbender and Christiane Stuke for the proof-reading and their insightful comments.

I would like to acknowledge the help of the other working groups of the LIMES institute for their permission to use their technical equipment and the Institute of Medical Microbiology, University of Düsseldorf, especially Prof. Dr. Klaus Pfeffer, PD Dr. Daniel Degrandi and Julia Hartmann for helping me with my initial Toxoplasma-infection experiments.

My deep appreciation goes to the members of the Förster/Weighardt working group; Pauli, Rieke, Julia, Nina, Philippa, Sonja, Anna, Philip, Björn, Lorenz, Oli and Fabi, which have contributed immensely to my personal and professional time. They have been a source of friendship, help and good advice. Special thanks go to Philip for his endless support during all my projects, the entertaining and humorous conversations and just for having a good time at work. And I would like to particularly thank Julia for helping me in various projects, providing valuable advice and knowledge, joining me on my trips to Düsseldorf and becoming a dear friend.

I am thankful to my friends, who have always listened to my never-ending monologues about my work and problems. Thanks for forgiving me that I more or less vanished from the face of the earth and needed forever to reply to messages or sometimes even forgot to reply at all. I am very lucky to have so many special people in my life.

Words cannot express how grateful and thankful am to my family and my husband for all the sacrifices they have made for me and for always standing by my side. I am forever in debt.

This work was supported by the Jürgen Manchot foundation and the MOI graduate school.